Abstract

The objective of this work is to provide a new concept of FT reactor that can ensure a flexible control of hydrocarbons distribution. This is accounted through the in-situ alternation of hydrogen to carbon monoxide molar ratio based on the fact that water or carbon dioxide removal by integrating a tubular membrane can provoke a disequilibrium in the reversible water gas shift reaction favoring the production of carbon monoxide or hydrogen. First, an ideal permeselectivity is considered to quantify the effect of water and carbon dioxide removal on the evolution of hydrocarbons selectivity using two concepts of membrane reactors. Next, the nonideal permeselectivity is processed to include the real case, in which the permeation of other FT components is accounted for. This investigation will provide a clear measurement of how important can be the effect of real-world permeation on hydrocarbons distribution. Our findings show that the water permselective membrane can boost the formation of C_3-C_5 olefin compounds, whereas the separation of carbon dioxide can enhance the formation of paraffins. Based on the second approach, It was found that the total permeation could be governed by the surface diffusion model since the contribution of this mechanism is dominant. Our results show that the permeation factors of different permeates were proportional to the operating pressure. Hydrocarbons with low molecular weight diffuse greater than long-chain hydrocarbons. It can be also highlighted that the permeate amounts have no important effect on the product distribution. So the assumption that considers the separation of CO_2 without assuming other components permeation is well supported.

Keywords: Fischer-Tropsch synthesis, Hydrcarbons distribution control, membrane reactor, in-situ purification.

Resumé

L'objectif de ce travail est de proposer un nouveau concept de réacteur FT capable d'assurer un contrôle flexible de la distribution des hydrocarbures. Cela s'explique par l'alternance in situ du rapport molaire hydrogène / monoxyde de carbone basé sur le fait que l'élimination de l'eau ou du dioxyde de carbone par l'intégration d'une membrane tubulaire peut provoquer un déséquilibre dans la réaction réversible de décalage eau-gaz favorisant la production de monoxyde de carbone ou d'hydrogène . Premièrement, une permésélectivité idéale est considérée pour quantifier l'effet de l'élimination de l'eau et du dioxyde de carbone sur l'évolution de la sélectivité des hydrocarbures en utilisant deux concepts de réacteurs à membrane. Ensuite, la permésélectivité non idéale est traitée pour inclure le cas réel, dans lequel la perméation d'autres composants FT est prise en compte. Cette étude fournira une mesure claire de l'importance de l'effet de la perméation du monde réel sur la distribution des hydrocarbures. Nos résultats montrent que la membrane permsélective à l'eau peut stimuler la formation de composés oléfiniques en C_3-C_5, tandis que la séparation du dioxyde de carbone peut améliorer la formation de paraffines. Sur la base de la deuxième approche, il a été constaté que la perméation totale pouvait être régie par le modèle de diffusion de surface puisque la contribution de ce mécanisme est dominante. Nos résultats montrent que les facteurs de perméation des différents perméats étaient proportionnels à la pression de service. Les hydrocarbures à faible poids moléculaire diffusent plus que les hydrocarbures à longue chaîne. On peut également souligner que les quantités de perméat n'ont pas d'effet important sur la distribution du produit. L'hypothèse qui considère la séparation du CO_2 sans supposer la perméation d'autres composants est donc bien étayée.

Mots clées: Synthese de Fischer-Tropsch, Control distribution des hydrocarbures, reacteur membranaire, purification in-situ.

ملخص

الهدف من هذا العمل هو تقديم مفهوم جديد لمفاعل FT يمكن أن يضمن تحكمًا مرنًا في توزيع الهيدروكربونات. يتم حساب ذلك من خلال التناوب في الموقع بين نسبة الهيدروجين إلى أول أكسيد الكربون المولي استنادًا إلى حقيقة أن إزالة الماء أو ثاني أكسيد الكربون من خلال دمج غشاء أنبوبي يمكن أن يؤدي إلى عدم توازن في تفاعل تحويل غاز الماء القابل للانعكاس لصالح إنتاج أول أكسيد الكربون أو الهيدروجين . أولاً ، تعتبر النفاذية المثالية لقياس تأثير إزالة الماء وثاني أكسيد الكربون على تطور انتقائية الهيدروكربونات باستخدام مفهومين للمفاعلات الغشائية. بعد ذلك ، تتم معالجة النفاذية غير المثالية لتشمل الحالة الحقيقية ، والتي يتم فيها حساب تغلغل مكونات FT الأخرى. سيوفر هذا البحث قياسًا واضحًا لمدى أهمية تأثير التخلل في العالم الحقيقي على توزيع الهيدروكربونات. تظهر النتائج التي توصلنا إليها أن الغشاء الانتقائي للماء يمكن أن يعزز تكوين مركبات الأوليفين C_3-C_5 ، في حين أن فصل ثاني أكسيد الكربون يمكن أن يعزز تكوين البارافينات. بناءً على الطريقة الثانية ، وجد أن الاختراق الكلي يمكن أن يحكمه نموذج الانتشار السطحي لأن مساهمة هذه الآلية هي السائدة. تظهر نتائجنا أن عوامل التخلل لمختلف النفاذية كانت متناسبة مع ضغط التشغيل. تنتشر الهيدروكربونات ذات الوزن الجزيئي المنخفض بشكل أكبر من الهيدروكربونات طويلة السلسلة. يمكن أيضًا إبراز أن الكميات المتخللة ليس لها تأثير مهم على توزيع المنتج. لذا فإن الافتراض الذي يأخذ في الاعتبار فصل ثاني أكسيد الكربون دون افتراض تخلل المكونات الأخرى مدعوم جيدًا.

كلمات مفتاحية: تفاعل فيشار- تروبش، التحكم في توزيع الهيدروكربونات، مفاعل غشائي، التنقية الأنية.

“The joy of discovery is certainly the liveliest that the mind of man can ever feel”

- Claude Bernard -

Acknowledgments

First of all, I would like to thank the almighty ALLAH, my creator, who provided me with the ultra necessary strength and knowledge along the past three years to complete my Ph.D. research.

I would like to thank my supervisor, Prof. Lemnouer CHIBANE for all your guidance and support during this work. I have also enjoyed long hours of discussions with him on various technical and non-technical topics. I look forward to collaborating with him in the future as well. Further, the head of the Laboratory of Chemical Processes Engineering (LGPC), Prof. Saci NACEF is acknowledged for accepting the invitation to be the president of the jury. I am also grateful to him for hosting me at the Lab.

On the same note, I would like to thank the members of my oral examination (PhD Defense) committee for the examination of my thesis and I am highly open and honored to be directed by their expertise in the field of interest for future research. I want to mention Prof. Messaoud GUELLAL, Associate Prof. Ammar FADEL and Associate Prof. Amel AIDI in this regard.

Special thanks to my mother, my father, my two brothers Seif Eddine and Zakaria for cheering me up. I am very grateful to have such an inspirative and supportive family. You are the Best! My lovely mother, Thanks for always being there at the delicate moments and for giving me the confidence to pursue my dreams! You mean a lot to me! I wish to thank my father, for its wise counsel and sympathetic ear. You mean a lot to me!

List of Papers

This thesis is based on the following three papers:

I. A new concept for control and orientation of the distribution of clean hydrocarbons produced by Fischer–Tropsch synthesis over an industrial iron catalyst

Abdelmalek Bellal and Lemnouer Chibane
Reaction Kinetics, Mechanisms and Catalysis, (2020) 129, 725–742.

II. Fischer-Tropsch reaction mixture permeation through a silicalite-1 membrane reactor and its effect on the produced hydrocarbons distribution

Abdelmalek Bellal and Lemnouer Chibane
International Journal of Chemical Reactor Engineering, 18(9), 20200062.

III. On the Effect of the Inlet Hydrogen Amount on Hydrocarbons Distribution Produced via Fischer-Tropsch Synthesis

Abdelmalek Bellal and Lemnouer Chibane
ISSH2 2019: Advances in Renewable Hydrogen and Other Sustainable Energy Carriers, Springer, pp. 451–458.

Nomenclature

A	Cross-section (m^2)
B	Perimeter of cross-section (m)
C_p	Specific heat at constant pressure (J $mol^{-1}K^{-1}$)
C_{pg}	Specific heat of gaseous mixture at constant pressure (J $mol^{-1}K^{-1}$)
d_p	Diameter of catalyst particle (m)
D_C	Diameter of cooling tube (m)
$Đ(\theta_\xi)$	Diffusivity of component ξ (m^2s^{-1})
$Đ(\theta_i)$	Diffusivity of component i (m^2s^{-1})
$Đ_{0,\xi}$	Diffusivity of component ξ at zero loadings and infinite temperature (m^2s^{-1})
$Đ_{0,i}$	Diffusivity of component i at zero loadings and infinite temperature (m^2s^{-1})
$Đ_{\Theta_\xi=0}$	Diffusivity of component ξ at zero loadings (m^2s^{-1})
$Đ_{\Theta_i=0}$	Diffusivity of component i at zero loadings (m^2s^{-1})
E_5	Activation energy for paraffin formation (J mol^{-1})
$E_{5,M}$	Activation energy for methane formation (J mol^{-1})
E_6	Activation energy for olefin formation (J mol^{-1})
E_v	Activation energy for WGS reaction (J mol^{-1})
$E_{dif,\xi}$	Diffusivity activation energy of component ξ (J mol^{-1})
$E_{dif,i}$	Diffusivity activation energy of component i (kJ mol^{-1})
F_i	Molar flow rate of hydrocarbon i (mol s^{-1})
F_i^{reac}	Reaction flux of components i (mol s^{-1})
F_i^{perm}	Permeate flux of components i (mol s^{-1})

F_i^{res}	Residual flux of components i (mol s^{-1})
F_T	Total molar flow rate (mol s^{-1})
F_T^0	Initial molar flow rate (mol s^{-1})
F_{IN}	Molar flow rate of inert gases (mol s^{-1})
$GHSV$	Gas hourly space velocity (h^{-1})
I_{index}	Fraction of inert gas
J_ξ	Permeation flux of component ξ (mol $m^{-2}s^{-1}$)
k_1	Rate constant of CO adsorption (mol $kg^{-1}s^{-1}bar^{-1}$)
k_5	Rate constant of paraffin formation (mol $kg^{-1}s^{-1}bar^{-1}$)
$k_{5,0}$	Preexponenetial factor of rate constant of paraffin formation (mol $kg^{-1}s^{-1}bar^{-1}$)
k_{5M}	Rate constant of methane formation (mol $kg^{-1}s^{-1}bar^{-1}$)
$k_{5M,0}$	Pre-exponential factor of rate constant of methane formation (mol $kg^{-1}s^{-1}bar^{-1}$)
k_6	Rate constant of olefin desorption reaction (mol $kg^{-1}s^{-1}$)
$k_{6,0}$	Pre-exponential factor of rate constant of olefin desorption reaction (mol $kg^{-1}s^{-1}$)
k_{-6}	Rate constant of olefin re-adsorption reaction (mol $kg^{-1}s^{-1}bar^{-1}$)
k_v	Rate constant of CO_2 formation (mol $kg^{-1}s^{-1}bar^{-1.5}$)
$k_{v,0}$	Pre-exponential factor of rate constant of CO_2 formation (mol $kg^{-1}s^{-1}bar^{-1.5}$)
K_2	Equilibrium constant of CH intermediate formation
K_3	Equilibrium constant of CH_2 intermediate formation
K_4	Equilibrium constant of CH_3 alkyl formation
K_v	Group of constants in WGS reaction
K_ξ	Adsorption equilibrium constant of component ξ (bar^{-1})

$K_{\xi,0}$	Adsorption equilibrium constant of component ξ at infinite temperature (bar^{-1})
K_i	Adsorption equilibrium constant of component i (bar^{-1})
$K_{i,0}$	Adsorption equilibrium constant of component i at infinite temperature (bar^{-1})
K_{WGS}	Equilibrium constant of WGS reaction
L	Reactor length (m)
l	Dimensionless reactor length
M	Inlet molar flow ratio between hydrogen and carbon monoxide
O/P	Olefin over paraffin selectivity ratio
P_i	Partial pressure of hydrocarbon$i$ (bar)
P_{IN}	Partial pressure of inert gas (bar)
P_{perm}	Partial pressure in permeate side (bar)
$P_{perm,tot}$	Total pressure in permeate side (bar)
P_{reac}	Partial pressure in reaction side (bar)
P_T	Total pressure in reaction side (bar)
P_T^0	Initial total pressure in reaction side (bar)
P_ξ	Partial pressure of component ξ (bar)
q_ξ	Amount adsorbed of component ξ ($\mathrm{mol\ kg^{-1}}$)
q_ξ^{sat}	Saturation amount adsorbed of component ξ ($\mathrm{mol\ kg^{-1}}$)
q_i	Amount adsorbed of component i ($\mathrm{mol\ kg^{-1}}$)
q_i^{sat}	Saturation amount adsorbed of component i ($\mathrm{mol\ kg^{-1}}$)
R	Universal gas constant (8.314 $\mathrm{J\ mol^{-1}K^{-1}}$)
R_j	Rate of reaction$j$ ($\mathrm{mol\ kg^{-1}s^{-1}}$)
$R_{C_nH_{2n+2}}$	Paraffin reaction rate ($\mathrm{mol\ kg^{-1}s^{-1}}$)

$R_{C_nH_{2n}}$	Olefin reaction rate (mol $kg^{-1}s^{-1}$)
R_{WGS}	Water-gas shift reaction rate (mol $kg^{-1}s^{-1}$)
S_i	Hydrocarbonsselectivity (%)
T	Temperature (K)
T_{sh}	Shell temperature (K)
T_{ref}	Reference temperature (K)
U_{sh}	Heat transfer coefficient shell-gases (W m^{-2} K^{-1})
v	Gas linear velocity (m s^{-1})
x	Membrane coordinate
y	Molar fraction
z	Axial reactor coordinate
c	Probability of diffusion in the right direction

Greek letters

ε	Porosity of catalytic bed
ε_m	Porosity of membrane-support layer
ρ	Catalyst density(kg m^{-3})
ρ_g	Gas density (kg m^{-3})
ρ_m	Membrane density (kg m^{-3})
υ_{ij}	Stoichiometric coefficient of hydrocarbon i in reaction j
μ	Gas dynamic viscosity (bar s)
δ	Membrane thickness (m)
λ	Diffusional length (m)
θ_ξ	Fractional sites occupancy for component ξ
θ_i	Fractional sites occupancy for component i
ΔH_{R_j}	Enthalpy of reaction j (J mol^{-1})

$\Delta H_{ads,\xi}$	Adsorption enthalpy of component ξ (J mol^{-1})
$\Delta H_{ads,i}$	Adsorption enthalpy of component i (kJ mol^{-1})
$\Delta S_{ads,i}$	Adsorption entropy of component i (kJ mol^{-1})

Subscripts

g	Gas-phase
i	Index indicating FT components
IN	Inert gases
j	Index indicating reactions
m	Membrane
n	Chain length of hydrocarbons
0	Inlet reactor

Abbreviations

BTL	Biomass To Liquid
CTL	Coal To Liquid
CR	Conventional reactor
FT	Fischer-Tropsch
GTL	Gas To Liquid
GD	Gaseous diffusion
HC	Hydrocarbons
MRC	Membrane reactor for carbon dioxide removal
MRW	Membrane reactor for water removal
PF	Permeation factor
SD	Surface diffusion
SP	Selective permeation
WGS	Water-gas-shift

Table of Contents

Abstract i

Acknowledgments iii

List of Papers iv

Nomenclature v

Lites of Figures xii

Liste of Tables xiv

General Introduction 1

CHAPTER I: General Concept of Fischer-Tropsch Synthesis

I.1. General considerations on Fischer-Tropsch synthesis 4

I.2. Fischer-Tropsch reaction kinetics and micro-kinetics 8

I.2.1. Iron catalysts 12

I.2.2. Cobalt catalysts 17

I.3. Reactors used in FT 21

I.3.1. Fixed bed reactor 21

I.3.2. Fluidized bed reactor 26

I.3.3. Slurry bubble column reactor 28

I.3.4. Membrane reactor 32

I.4. Aims and Outline of this Thesis 35

CHAPTER II: Membrane Reactor Simulation Model

II.1. Concept of membrane reactor for ideal permeselectivity 36

II.1.1. Simulation concept 36

II.1.2. Membrane reactor description 38

II.1.3. Reactor model 41

II.1.4. Kinetic model 44

II.1.5. Permeation model 46

II.2. Concept of membrane reactor for non-ideal CO_2 permeselectivity 50

CHAPTER III: Control of Hydrocarbons Distribution Using Membrane Reactor

III.1. In-situ H_2O and CO_2 removal 56

III.2. Effect of permeation on hydrocarbons distribution 56

III.2.1. Inlet H_2/CO ratio alternation 57

III.2.2. Inert gas fraction alternation 65

CHAPTER IV: Effect of Non-ideal Permeselectivity on Hydrocarbons Distribution

IV.1. Diffusion process 70

VI.2. Predominant mechanism under FT reaction conditions 71

IV.3. Pressure effect on CO_2 permeselectivity 73

References 88

Lites of Figures

Figure I.1: reactions scheme for FT synthesis 4

Figure I.2: Mechanisms of FT synthesis: (a) CH_2 insertion, (b) CO_2 insertion, (c) enol 11

Figure I.3: Concentration and temperature profile in multi-tubular Fischer-Tropsch reactor 24

Figure I.4: multitubular fixed bed reactor 25

Figure I.5: (a) Circulating fluidized bed reactor, (b) fixed Fluidized bed reactor 27

Figure I.6: FT slurry bubble column reactor 29

Figure I.7: Homogeneous and churn-turbulent regime in a slurry bubble column reactor 31

Figure II.1: Schematic diagram of FT membrane reactor, (a): Conventional reactor (CR), (b): Membrane reactor for water removal (MRW), (c): Membrane reactor for CO2 removal (MRC). 40

Figure II.2: Scheme of the FT membrane reactor 52

Figure III.1: Effect of the inlet H_2/CO ratio on hydrocarbons selectivity a: $(H_2/CO)^0=1$, b: $(H_2/CO)^0=1.5$, c: $(H_2/CO)^0=2$ and d: $(H_2/CO)^0=2.5$. Conditions: T= 533K, P=20bar and GHSV= $4000h^{-1}$ 61

Figure III.2: WGS reaction rates evolution in the reactors configurations a:$(H_2/CO)^0=1$, b:$(H_2/CO)^0=2.5$. Conditions: T= 533K, P=20bar and GHSV= $4000h^{-1}$ 62

Figure III.3: Evolution of H_2/CO ratio along the reactor at different initial values a: $(H_2/CO)^0=1$, b: $(H_2/CO)^0=1.5$, c: $(H_2/CO)^0=2$ and d: $(H_2/CO)^0=2.5$ Conditions: T= 533K, P=20bar and GHSV= $4000h^{-1}$ 64

Figure III.4: Effect of the inert gas fraction in the permeate side on hydrocarbons selectivity for different $Iindex$. a: $Iindex = 3$, b: $Iindex = 6$, c: $Iindex = 9$, d: $Iindex = 12$. Conditions: $(H_2/CO)^0$=2.5, T=533 K, P= 20bar, GHSV=4000h^{-1}..... 66

Figure III.5: Effect of the inert gas fraction on the permeation flux of carbon dioxide (a) and water (b). Conditions: T= 533K, P=20bar and GHSV= 4000h^{-1}. 68

Figure III.6: Evolution of H_2/CO ratio along the reactor for different $Iindex$ a: $Iindex = 3$, b: $Iindex = 6$, c: $Iindex = 9$ and d: $Iindex = 12$ Conditions: T= 533K, P=20bar and GHSV= 4000h^{-1}. 68

Figure IV.1: Contribution of surface diffusion (SD) and gaseous diffusion (GD) on the total permeation under simultaneous variation of initial temperature and total pressure. 73

Figure IV.2: Evolution of reaction flux (solid), permeate flux (dash) and residual flux (dot) along the reactor at an initial pressure of 11bar. 75

Figure IV.3: Evolution of reaction flux (solid), permeate flux (dash) and residual flux (dot) along the reactor at an initial pressure of 14bar. 79

Figure IV.4: Evolution of reaction flux (solid), permeate flux (dash) and residual flux (dot) along the reactor at an initial pressure of 17bar. 80

Figure IV.5: Evolution of reaction flux (solid), permeate flux (dash) and residual flux (dot) along the reactor at an initial pressure of 20bar. 82

Figure IV.6: Variation of the permeation factor as a function of initial pressure. 84

Figure IV.7: Variation of the CO_2 selective permeation as a function of initial pressure. 85

Liste of Tables

Table I.1: Micro-kinetic expression For methane on iron and cobalt catalysts. 20

Table II.1: Catalyst and gas proprieties..... 37

Table II.2: Reactor dimensions and operating conditions..... 38

Table II.3: Kinetic constants and activation energy for FT and WGS reactions. 45

Table II.4: Water and carbon dioxide adsorption and diffusion parameters..... 50

Table II.5: Adsorption parameters for the permeates..... 54

Table II.6: Diffusion parameters of permeate species..... 55

Table III.1: Measured O/P ratios in the reactor exit for different $(H_2/CO)^0$ ratios. 65

Table III.2: Measured O/P ratios in the reactor exit for different fractions of inert gas ($Iindex$)..... 69

General Introduction

Currently, a promising topic in the energy industry is the obtention of environmentally clean fuels from the transformation of remote abundant sources. The Fischer-Tropsch (FT) synthesis can convert synthesis gas into a multicomponent mixture of predominantly hydrocarbons. Synthesis gas, a mixture of predominantly CO and H_2, obtained from either coal, biomass or natural gas. Fuels produced with the FT process are of a high quality due to very low aromaticity and absence of sulfur. These fuels are valuable for further industrial transformation such as blending stocks for transportation fuels derived from crude oil or directly used as an upgraded combination of low cost and effective source of energy that respond to the environmental policies. This technology can deliver a direct control of hydrocarbons composition, which constitutes another benefit to achieve the desired distribution of paraffin and olefins. This involves a deep optimization of reactor parameters such as the inlet H_2/CO molar ratio, the nature of the used catalyst, and the running temperature. In this context, the increase in the H_2/CO ratio will favor the production of paraffin. The partial pressure of carbon monoxide and hydrogen can be managed by water elimination, whereas the equilibrium of the secondary water gas shift (WGS) reaction shifted toward the formation of reactants ($CO+H_2O$) or products (H_2+CO_2).

A critical literature review on the general concept of FT synthesis, the kinetic mechanisms and models and the applied industrial configuration of reactors is given in Chapter I. The kinetic mechanisms for CO consumption to hydrocarbons present some uncertainties and do not fully provide a uniform picture of hydrocarbons distribution. Most of the devoted works on FT kinetic are aiming to better understand the reaction mechanism under a restricted range of conditions. Many authors derived Langmuir-Hinshelwood-Hougen-Watson (LHHW) or Eley-Rideal type of rate expressions for

reactant consumption. In most cases, the formation of the building block or monomer, methylene, is assumed to be the rate-determining step. Due to now, none of the available literature models can fully describe the reaction pathway and obtains enough details to predict the product spectrum as a function of operating conditions.

For performing the theoretical investigation of ideal and non-ideal permeation effect on hydrocarbons distribution, a new membrane reactor configuration that deals with water separation or carbon dioxide separation from the reaction zone is proposed in Chapter II. The procedure of analysis is based on building a mathematical model with MATLAB software that can describe the variation of hydrocarbons selectivities at the reactor outlet associated with separate integration of permeselctive membranes to carbon dioxide and water.

Chapter III discusses the proven possibility of applying a new concept of the FT reactor to ensure a more flexible and readily way of controlling and managing the main distribution of hydrocarbons. The particular enhancement of the production yield of desirable product composition can be granted by integrating a tubular membrane to the conventional fixed-bed reactor. The developed configuration will give a big dash to the industry of FT synthesis as valuable production is needed to cover the additional cost of process installation and operation and thus achieving a higher profit rate. The findings were reviewed and compared to the case where the configuration of a conventional fixed bed reactor is applied. Further investigation is done by quantifying the effect of specific operating parameters such as inlet molar ratio (H_2/CO) and inert gas fraction on the distribution of final products. The results of this study will help with structuring the orientation of hydrocarbons composition as a function of the corresponding equilibrium

of the water gas shift reaction. This includes the impact of *in-situ* water and carbon dioxide separation on the evolution of the H_2/CO ratio and water gas shift reaction rate.

In the previous chapter, the permeation through the silicalite-1 membrane is considered only to carbon dioxide, therefore, assuming other components diffusion is required for the generalization of the model. Non-ideal carbon dioxide permeselectivity is investigated in Chapter IV. Up to now, few works deal with the permeation of wide range hydrocarbons and syngas through silicalite-1 type membranes. Some literature works suggest that the permeation model of the investigated range of hydrocarbons and other gases can be described by a combination of surface diffusion and gaseous diffusion. At now day, the available information does not cover high processing pressures, at which is operated FT synthesis. To be able to predict the permeation effect of such components, a deep investigation of membrane permeselectivity is required. To do this, a variation of total permeation as a function of the initial pressure and temperature is studied for two separate models: surface diffusion and gaseous diffusion. The model which has a major attribution to the permeation process is used for a comparative investigation of different components permeance and pressure effect on the membrane efficiency and the selective separation of CO_2. Also, the consideration of the permeation process can deliver a significant accuracy about reactor performance and the tendency of hydrocarbons composition. So, the outlet olefin to paraffin ratio is recommended to confirm the real magnitude of the assumption of negligible permeation of hydrocarbons, and its impact on the final distribution.

CHAPTER I

General Concept of Fischer-Tropsch Synthesis

I.1. General considerations on Fischer-Tropsch synthesis

Fischer-Tropsch synthesis is defined as an alternative technology that can cover the sharp depletion in the reserve of traditional fossil fuels [1,2]. For the last decades, it is known as the most promising way to reduce the dependency of the industry on the uncontrollable and large fluctuation in the price of drilled oil. This may present a perfect representation of the economic situation worldwide and remote the production of a wide range of hydrocarbons with higher quality and minimal impact on the environment [3]. This configuration can deliver a selective formation of wax materials and even an accountable portion of oxygenates (Figure I.1). By using abundant resources such as coal and biomass, the benefit will be very higher and this may attract more companies to invest in the predominant production of syngas for further application as feedstock to the FT process. The main technologies used for converting natural gas, coal and biomass are known as gas to liquid (GTL), coal to liquid (CTL) and biomass to liquid (BTL), respectively [4].

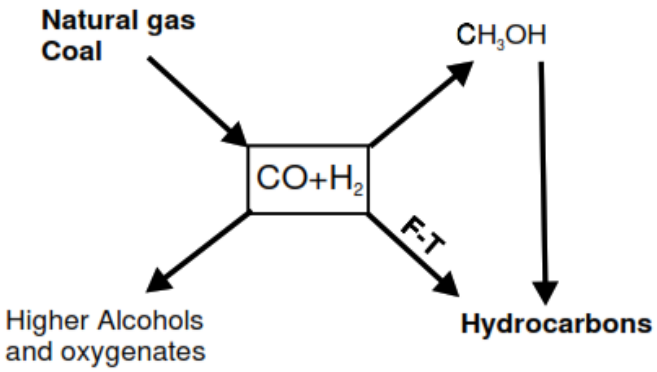


Figure I.1: reactions scheme for FT synthesis [5].

The principle of transformation is based on the gasification of biomass to syngas or either partial oxidation and steam reforming of natural gas and coal [6]. The biomass feedstock fr gasification process is composed of different biomass heavy dry residues such as straw,

energy crops [7]. The main set of FT synthesis is classified as desirable and undesirable reactions, where the formation of paraffin and olefins is considered to be the selective interaction on the catalyst surface. It consists of CO hydrogenation to a wide range of hydrocarbons (HC) and water (Eq.I.1 and I.2).

For paraffin formation:

$$nCO + (2n + 1)H_2 \rightarrow C_nH_{2n+2} + nH_2O \quad \text{(I.1)}$$

For olefins formation:

$$nCO + 2nH_2 \rightarrow C_nH_{2n} + nH_2O \quad \text{(I.2)}$$

As a side reaction, the formed water during the production of hydrocarbons will react with adsorbed carbon monoxide to generate carbon dioxide and hydrogen species. This will increase the molar ratio of syngas and consequently a change in the distribution of hydrocarbons. Also, this reaction is considered as a secondary parasite step, in which the formation of carbon dioxide will harm the environment and reduce the activity of the catalyst by noncontrollable occupancy of the active site. This can lead to competitive adsorption between the syngas and the carbon dioxide resulting in a sharp decline in the reaction rate of FT synthesis. After all, this process can claim the advantage of eliminating the produced water from the reaction area to avoid catalyst permanent deactivation. In fact, the iron catalyst is more sensitive to water than the cobalt catalyst and the high activity of water gas shift reaction (Eq.I.3) on the Fe_2O_3 phase can prevent catalyst poisoning through the oxidation process. Furthermore, the feed composition of syngas must be clan from any metallic effluents especially plomb that can change the catalyst structure by forming a bond with reducted iron sites Fe-Pb. On the other hand, cobalt

catalyst has a more stable form but this is not a full indication that is not exposed to the possible oxidation caused by the presence of water. However, there are some studies reported a positive effect of water formation on the reaction rate of FT reaction over cobalt catalysts. This abnormal trend is not completely understood and according to other studies, a nonactive spinal phase is formed on the surface of the cobalt catalyst due to the assisted oxidation by water. For this purpose, the partial pressure ratio of water over hydrogen P_{H_2O}/P_{H_2} must be maintained lower than a specific threshold equal to 0,6. CoO and Co_3O_4 are the general forms for cobalt deactivation under FT operating conditions. The production of hydrocarbons is followed by side formation of oxygenates such as alcohol, ketones organic acids with minor quantity (Eq.I.4).

$$CO + H_2O \leftrightarrow H_2 + CO_2 \quad \text{(I.3)}$$

$$nCO + 2nH_2 \rightarrow C_nH_{2n}O + (n-1)H_2O \quad \text{(I.4)}$$

FT process involves three main units including syngas production through usual resources conversion, feedstock pretreatment and FT synthesis. The FT section constitutes higher interest and it is basically composed of a large-scale reactor, syngas purification from carbon monoxide and a compression unit for recycling the unconverted part of the final products. However, operating at high selective distribution requires additional parametrization of the gasification unit, in which the syngas molar ratio is adjusted according to the drawn plans for FT cuts. In general, the syngas produced from biomass has much higher carbon monoxide content compared to hydrogen. This is not seen for natural gas transformation because of the low molecular weight of reactants. A predefinition of syngas composition is also important to determine the appropriate catalyst for the conversion. In contrast to iron, cobalt catalyst activity is restricted to a

narrow range of variation in the molar ratio of the syngas H_2/CO [8,9]. As we discussed above, the water gas shift reaction can alter the composition of syngas towards an increase in the molar ratio. This is can be beneficial for both industrial types of catalysts, but with a higher specification to cobalt, in which more hydrogen content is required. Chemical and physical promoters are usually blended to the iron catalyst in order to increase its activity to FT reaction and enhance the selectivity towards the production of heavier hydrocarbons [10–12]. For cobalt the addition of promoters can elevate more the cost of the catalyst and thus increasing the exposition of the active phase on the surface of the catalyst will generate a large area of contact with just using support materials either than promoters [13,14]. After hydrocarbons production, a large set of the conventional refining process is used to enhance the quality of products and gaining some advantages through multiple transformations of crude oil to more valuable cuts that can be sold directly for further treatment or delivered to associated units for general purposes. From a general perspective, the fuels produced by FT synthesis are clean of nocive material to the environment such as benzene and sulfur [15,16]. In fact, the emission of carbon dioxide can also be reduced to a factor of 15% through the combustion of synthesis fuels [17]. This will reduce the need for treatment steps and address any problem related to the presence of these undesirable components in the conventional type of fuels. Actually, the produced diesel by FT synthesis has a high cetane number resulting in better ignition properties. In general, the acceptable cetane number for commercial diesel is about 55 which is much less than the offered number by synthesis diesel (70). The diesel obtained from BTL can be borderline competitive to the derived diesel from crude oil at a large scale of comparison including the price and the quality [18]. Also, BTL can offer high-

quality jet fuel compared to the conventional one which requires additional treatment for certified use.

I.2. Fischer-Tropsch reaction kinetics and micro-kinetics

Considerable researches were devoted to developing a more comprehensive mechanistic scheme for describing the reaction at the microscopic level [19–21]. The kinetic of FT is referred to be general when the representative model does not scoop the variation of product distribution. This kind of kinetic can be used only to oversimplify the evolution of syngas conversion and it is based on empirical correlations that describe the total variation in reaction rate related to syngas consumption [22]. The reaction rate of FT synthesis is expressed by power-law kinetics derived from Langmuir-Hieshelwood-Hougen-Watson (LHHW) and Rideal mechanisms [23,24]. Different theoretical sets of elementary reactions were builts to predict the reaction pathway on the catalyst surface. Most of these kinetics expressions fit with the experimental investigations at a narrow range of reaction conditions [25]. However, the weak interaction between the syngas and the catalyst surface will result in lower occupancy. This behavior constitutes a major concept of the applied Eley-Redial model. The LHHW kinetic expression is mainly taken for describing the whole process by only one rate-determining step via either the monomer formation or reaction termination [26]. The elementary reactions are defined by bonding formation with active sites or other molecules [27]. Anywhere, the contribution of a large number of products that are engaged in the FT reaction to the reaction rate must not be neglected for the sake of reducing the size of the investigation. This may create a non based explanation of observed alteration in the final distribution of products. Anderson Schulz Flory (ASF) model is well known as a complete model that can predict the distribution of hydrocarbons. According to the ASF model, the final

composition of hydrocarbons is determined by the spatial architecture that surrounds the active site of chain growth [28]. The change in the selectivity of hydrocarbons is related to the rate of desorption at which methyl addition can be substituted by hydrogen or double bond formation for producing paraffin or olefins, respectively. In general, the desorption probability of olefins is quite higher than that of paraffin because the desorption of paraffin is more likely to be inhibited by the propagation process. But for instance, any change in the spatial constraints by raising the feed molar ratio H_2/CO can provoke competitive adsorption on the surface of the catalyst and thus unexpected tendency towards the formation of saturated hydrocarbons will take place. But this model assumes a linear distribution of hydrocarbons along the chain length, for instance, the production yield of ethane is regressive to the production yield methane. This model is weak for predicting the real distribution, which lies in the changes that can be generated through the variation in the surface coverage or the catalyst activity. However, the ASF model implies that less selective production is obtained for long hydrocarbons chains. In other words, the desorption rate of hydrocarbons decreases along with the carbon number. By assuming constant chain growth probability, the ASF model does not predict the influence of products on final distribution [22]. For this purpose, a detailed kinetic model came to the surface to deal with integrating a logical construction that can describe all possible deviation through a separate prediction of hydrocarbons distribution. In general, the micro-kinetic model of the FT reaction is essential for the prediction of the real reaction pathway that can be executed consistently to match the obtained conversion of syngas and hydrocarbons selectivity. However, These detailed kinetic models were developed by applying different mechanisms that were proposed to present an accurate evolution of product distribution. Far away, three mechanisms have been widely

accepted. This includes CH_2 insertion, CO insertion and enol mechanisms (Figure I.2). There is a sequence in the intermediate reactions that lie mainly on hydrogen dissociative adsorption followed by a combination with the adsorbed molecules of carbon monoxide. Based on the way of which hydrogen will react with carbon monoxide, two plausible interactions can be wrapped up including hydrogen bonding with carbon after carbon monoxide dissociation or direct insertion of hydrogen on the nondissociated carbon monoxide. The first approach conducts to the direct formation of CH_2 intermediates as known by the carbide mechanism, where hydrocarbons are built through the successive insertion of hydrogen on the formed phase with carbon atom (Fe_3C_5) [27]. The originality of this proposed mechanism back to Fischer and Tropsch, in which they have implied that hydrocarbons chains growth is granted through the successive addition of CH_2 formed on the catalyst surface to the adsorbed R-C radicals [22,28]. This mechanism can generate linear alkanes, linear alkenes and branched 1-alkenes through three estimated reaction pathways [22]. This theory was primarily discarded due to the nonexistence of the carbide phase on the surface of cobalt and nickel catalysts [28]. Anywhere, updated researches on the predicted model have proven through the utilization of spectroscopic methods the reactivity of carbon with hydrogen for the formation of methyl intermediates [22]. Isotropic-tracer techniques are used to identify the presence of methyl on the surface of the Fe/Al_2O_3 catalyst [29]. Also, the activation of CO dissociation by hydrogen assistance has prevailed CH_2 insertion mechanism to be valid on cobalt [22]. A recent study has shown that the direct carbon monoxide dissociation is expected to be more difficult than H-assisted carbon monoxide dissociation [30]. Storch and his team are the first who proposed a mechanism that is based on this approach for the apparent explanation of oxygenates formation during FT synthesis [28]. However, even there are fewer shreds of

evidence on the formation of a carbonic surface on cobalt its seems that the reaction pathways follow the carbide mechanism. The carbide mechanism is more appropriate for describing the micro-kinetic of FT synthesis.

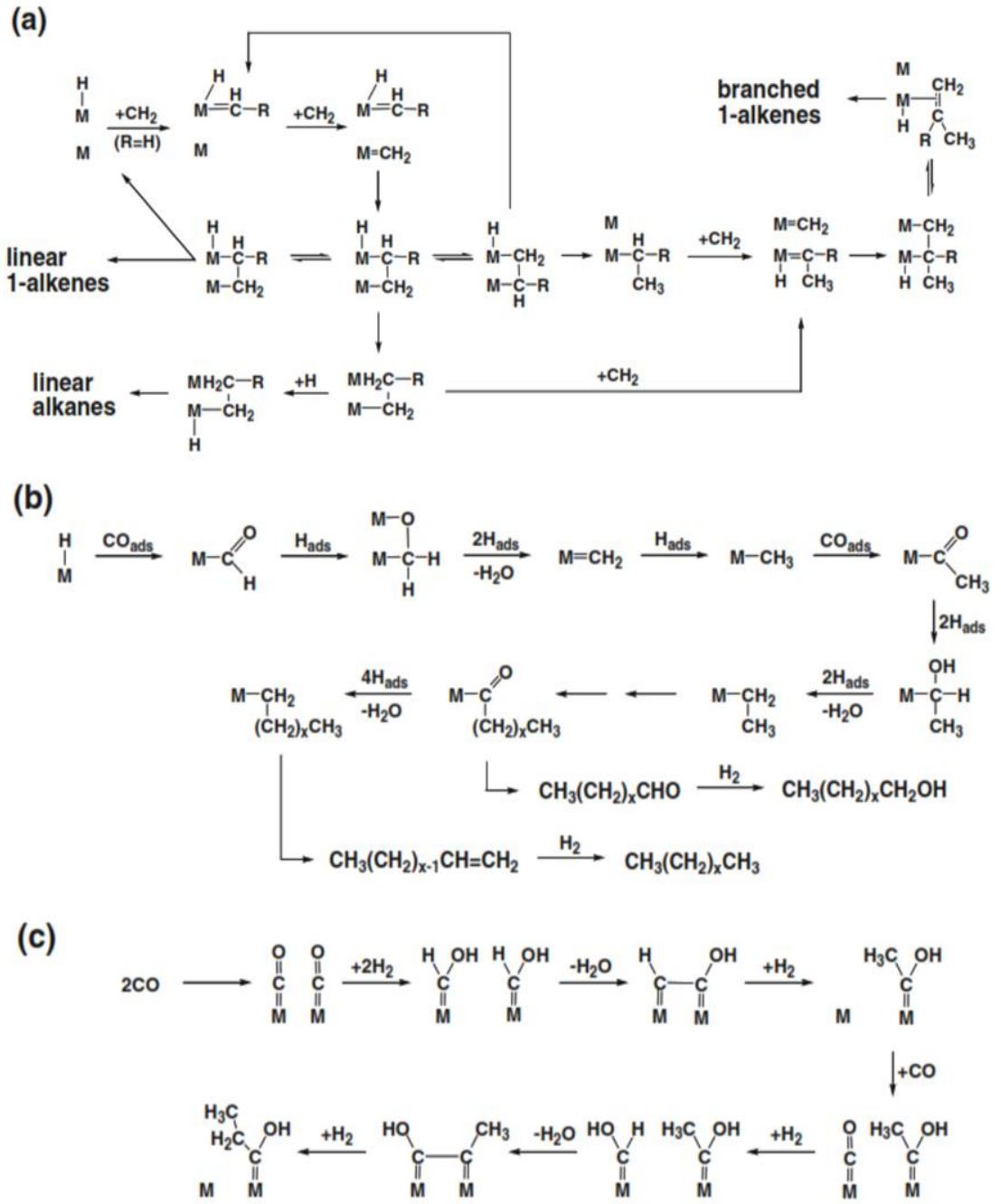


Figure I.2: Mechanisms of FT synthesis: (a) CH_2 insertion, (b) CO_2 insertion, (c) enol [22].

The CO insertion mechanism is also used to describe the formation of oxymethylene on the catalyst surface. The enol mechanism is still not ruled because of the contradiction that was found during the experiment of injecting alcohol with syngas as a feed mixture. The results indicate that the alcohol was clung to the propagated hydrocarbons chain by the liberation of oxygen molecules instead of reacting with adsorbed carbon monoxide [28]. Thus, the postulated carbon monoxide insertion is not supported to describe the pathway of the FT reaction. A wide range of transition metals was tested on the FT reaction. But only cobalt and iron catalysts were commercialized since Rh, Ir, and Pt metals have poor catalytic activity, Ni generates excessive production of methane and Ru is too expensive [13,18,22,31]. Ideally, reaction conditions, as well as catalyst type, determine the convenient combination of the reaction rate. Kinetic models of iron and cobalt catalysts will be be reviewed in more detail. The rate-determining step can be attached to carbon monoxide consumption or reaction termination through hydrocarbon desorption.

I.2.1. Iron catalysts

The iron catalyst was the first material tested on FT synthesis [28]. The cost of iron-based FT catalyst is lower than that of cobalt and it was estimated at the range of 10-40$/bbl [2]. In contract to cobalt, the activity of iron catalysts towards the production of light hydrocarbons is less influenced by temperature gradient. Even at high operating temperatures the selective synthesis of heavy hydrocarbons still favored [28]. In most cases, the alkali promoters are added to the active phase to enrich the acidic character of the catalytic surface by chemical structuration or physical dispersion of the phase on the support. In reality, the production of light or heavy hydrocarbons can be directed through the applied method for iron preparation [28]. We can distinguish that the reduction of

natural magnetite can result in high production of gases while a synthetic method using precipitation of iron sales leads to a more accurate selection of the liquid phase. Along with that, it can be said that the second method is favored regarding the goals of FT synthesis for large production of useful petroleum cuts such as gasoline and diesel. A set of reaction rates for iron catalyst were reviewed by Lox and Froment [27] and Van der Laan and Bennackers [26]. At low conversions, the reaction rate is reported to be expressed in terms of the first-order power-law expression dependency where carbon monoxide partial pressure has no contribution to the reaction rate [6,7]. In his study, Anderson found that the inhibition effect of formed water must be included for higher operating temperatures and syngas conversion (60%). Here, site occupancy is considered and assumed to be strongly defined by carbon monoxide and water adsorption [32]:

$$R_{FT} = \frac{k_0 P_{CO} P_{H_2}}{P_{CO} + a P_{H_2O}} \quad \text{(I.5)}$$

Dry has explored this effect by using the carbonyl mechanism as a derivative source beyond the strong formation of water molecules [33]. His incorporation of the Langmuir-Hinshelhood-Hougen-Waston (LHHW) approach was conducted to the formulation of Anderson's equation. Huff and Satterfield indicate that the adsorption term a depends on syngas composition as it decrease with increasing the partial pressure of hydrogen [34]. Based on this observation he derived another reaction rate equation that describes more accurately the relative variation of adsorption to the presence of hydrogen, where the constant a is substituted by:

$$a = \frac{b}{P_{H_2}} \quad \text{(I.6)}$$

Several studies reported that the utilization of Huff and Satterfield equation for approaching the experimental results has got a reasonable matching. The calculated activation energy of the FT reaction rate corresponds to the range of expectation (between 71 kJ/mol and 105 kJ/mol) [34–39]. Inhibition by CO_2 is generally not considered to be applied to the general law because of its low adsorption on the catalyst surface [36,40]. But the effect may become remarkable when the water gas shift reaction is highly activated by increasing the operating temperature [41]. This reaction will produce a large amount of CO_2 that provokes a reduction in the number of active sites through the adsorption process. Consequently, a decline in the FT reaction rate is expected to happen. A similar equation to that used on water inhibition was proposed for incorporating the CO_2 effect:

$$R_{FT} = \frac{k_0 P_{CO} P_{H_2}}{P_{CO} + a P_{CO_2}} \quad \text{(I.7)}$$

A general kinetic model was developed to consider the difference in generated effect by water gas shift reaction activity [41]:

$$R_{FT} = \frac{k_0 P_{CO} P_{H_2}}{P_{CO} + a P_{H_2} + b P_{CO_2}} \quad \text{(I.8)}$$

All the discussed kinetics were assumed to be valid only if we define the elementary reaction of hydrogen with carbon atoms as a rate-determining step, while all other steps are considered to be at a quasi-equilibrium state [26,42]. As we mentioned in the above section, this kind of kinetic model can not fully characterize the evolution of product formations along the reactor section and does not reply to the intense needs of constructing a deep knowledge about FT kinetic for sharp prediction of selectivities. Some works reported the successful application of power-law expressions in describing

the production rate of hydrocarbons as a function of the partial pressure of carbon monoxide and hydrogen [1,25]:

$$R_{HC} = k_{HC} P_{CO}^{m} P_{H_2}^{n} \quad \text{(I.9)}$$

The model was applied on a specific range of hydrocarbons including CH_4, C_2H_4, C_2H_6, C_3H_8, n-C_4H_{10}, i-C_4H_{10} and C_{5+} paraffin. According to Rahmati's findings, the power of partial pressure of CO is negative for methane and ethane which indicates the low formation of light paraffin at a higher injection flow rate of carbon monoxide [25]. This is in agreement with what was reported by other studies using a distinct form of kinetics. The estimation rate of hydrocarbons by applying empirical correlations of power-aw kinetic has let to good results [43]. For higher chain length the power of carbon monoxide partial pressure increases and thus resulting in less dependency of hydrocarbons formation on hydrogen partial pressure. Mazzone and Fernandes used a polymerization model to define the mass balance for the formed hydrocarbons by assuming that alkyl and alkenyl mechanisms are both acting in FT synthesis [44,45]. A reaction path based on CO consumption to the formation of methyl on the surface of the precipitated iron catalyst (Fe-Cu-K-SiO_2) was used to develop a distinct set of kinetic models [26]. Carbide and enol mechanisms can be perfectly applied to represent the experimental results, where the best model showed that the hydrogen association to nondissociative carbon monoxide is highly recommended to be the rate-determining step. Even old investigation has proven the dissociative adsorption of CO on the iron catalyst through the application of spectroscopic techniques, there is still no clear evidence for the relative rate of carbide formation [46,47]. This can be explained by the diversity in the structure of carbide along with the surface plan of iron [48]. Theoretical investigation of the iron model carried out using DFT calculations has shown that the minimum energy paths are consistent with H-

assisted CO dissociation [49]. Furthermore, Lox and Froment reported that the variation in the partial pressure of hydrogen and carbon monoxide affect similarly the initial pressure of paraffins and olefins. This implicit the formation of paraffin and olefins chains along parallel reaction paths [27]. The formation of hydrocarbons on iron catalysts using carbide mechanisms can be summarized in five essential steps [27]:

- The molecular adsorption of carbon monoxide
- Dissociative adsorption of hydrogen
- Methyl intermediate formation
- Propagation of hydrocarbons building block
- Desorption of hydrocarbons products

The rate equation is developed by applying some assumptions related to the adsorption mechanism. The accuracy of the Langmuir-Freundlich-Hinshelwood model in describing FT synthesis was investigated in a slurry phase bubble column reactor over a wide range of conditions, the results are in very good matching with the experiment [50]. ASF model with two chain growth probability was first proposed by Donnelyet al [51] and it is widely used to describe the observed deviation in the basic model. A study has reported the higher accuracy of the model compared to the experimental results. Also, this model can provide a good interpretation of the non-linear distribution of hydrocarbons. As indicated by the theoretical model, the low apparition of heavy olefins on the FTS hydrocarbons spectrum is a result of the high activation energy [52]. Also, the production rate of hydrocarbons can be described by using fundamental assumptions such as steady-state kinetic [53,54]. By assuming a detailed scheme for the elementary reactions, many researchers were able to derive a complete mechanistic model from polymerization kinetic. Here, the rate of paraffin desorption by hydrogenation is equal to the rate of

methyl intermediate formation [55]. Also, the rate constant is dependent on the chain length at lower molecular weight including the desorption reaction for methane, propane. In general, the formation of hydrocarbons is related to the distribution of adsorbed species on active sites, for instance, paraffin is produced through the reactivity of alkyl chain with the nearby site that carries the monomer and another contains the hydrogen atom for termination reaction. Only limited number of kinetics predict the formation of oxygenates, a study done by Christophe [56] that considers two assumptions where non-dissociative adsorption of carbon monoxide is used for describing the formation of hydrocarbons and global stoichiometric reaction model is applied for defining the formation of alcohol over a precipitated iron catalyst in slurry bubble column reactor [56]. However, secondary reactions such as olefins readsorption were proven to have a higher tendency to occur during FT synthesis. The possibility of getting a secondary reaction of olefins is proposed to be held on a separate hydrogenation site [36]. The developed models show a decrease in olefins to paraffin ratio upon the increase in chain growth. This decrease in olefins content was explained by the excessive readsorption of olefins. However, FTS and WGS reactions are generated on different kinds of active sites and the interaction between these two reactions is ensured via the gas phase [52]. Separate expressions are used to describe the mechanism of the WGS reaction.

I.2.2. Cobalt catalysts

Cobalt has low selectivity towards the formation of oxygenates [22]. This property represents a benefit to the FT industry where a low generation of oxygenic compounds is needed to be established for achieving high production profit. ASF approach for FT reaction rates has shown a linear tendency, except for methane where positive deviation in the chain length probability has been remarked due to the methanation reactions that

are favored over the cobalt catalyst [57]. The readsorption reactions of olefins are also considered by many kinetic approaching types of research [28]. FT synthesis aims to ensure a large production of long hydrocarbons chain length [28]. As a solution for maintaining the formation of methane, a low H_2/CO molar ratio must be put to avoid the valueless light distribution of fuel while heavier compounds are desirable for commercial and energetic benefits [9,28]. In fact, the large diffusion of hydrogen through the cobalt pores will constitute a barrier or as it is called 'egg-shell' that prevents the insertion of methyl intermediates [28]. Also, methane selectivity is highly sensitive to the operational parameters, since the increase in FT temperature can boost its formation. In general, a narrow range of pressure and temperature variation was applied to FT reaction over the cobalt catalyst for limiting the production of light hydrocarbons [13]. Only a few kinetic studies on cobalt catalysts are reported in the literature. The developed kinetics are quite different from that of iron catalyst. It can be noted that theses kinetic expressions include a dual-site surface reaction of the rate-determining step [26]. The inhibition of water is not expressed for cobalt catalysts as well as the inhibition of CO_2 due to less activity of water gas shift reaction [26]. A study shows that methyl formation via the H-assisted CO dissociation is more consistent for describing the FT mechanism on cobalt [49]. Several developed models for expressing the general reaction rate are based on carbide mechanisms and enol/carbide combination mechanism [54]. This involves two rate-determining steps including dissociative adsorption of hydrogen on cobalt surface and carbon intermediate formation. Assuming other elementary reactions as a determining step has conducted to new forms of kinetic models. However, the generated models by considering carbon monoxide hydrogenation resulted in large variance with respect to the experiments. An experiment was carried out in a slurry reactor has delivered a well fitting

of kinetic measurements with Langmuir-Hinshlwood model for the bimolecular surface reaction [58]:

$$R_{FT} = \frac{kP_{CO}P_{H_2}}{(1+K_1P_{CO})^2} \quad \text{(I.10)}$$

Literature investigations have correlated the rate of syngas consumption to the kinetics used on the iron catalyst and the best fit was achieved [59]. In comparison to iron, FT kinetic over cobalt is not associated with the formation of water and carbon dioxide and is controlled through one type of catalytic site. Detailed LHHW equations that describe the reaction rate are widely accepted models for approaching a good representation of the production rate of hydrocarbons. Similarly to the iron catalyst, the secondary reaction was also considered as a basis for building the kinetic model. The increase in the reabsorption rate was due to the higher physisorption of longer olefins chains. Besides, the readsorption coefficient of ethene is larger than that of olefins. Lox and Froment developed kinetic models for multiple rate-determining steps including the desorption of products and the adsorption of carbon monoxide [27]. Their prediction for constant olefins to paraffin ratio does not cover the observed deviation in product distribution.

Table I.1: Micro-kinetic expression For methane on iron and cobalt catalysts.

Catalyst	Reactor type	Operating conditions			kinetic expression	Reference
		T (C°)	*P (MPa)*	*H_2/CO*		
Fe-Cu-La-Si	Continuous spinning basket	290	1.7	1	$R_{CH_4} = k_6 K_1 K_2 K_3 K_9 \frac{P_{H_2}^3 P_{CO}}{P_{H_2O}} \theta_*$	[64]
Fe-Mn	Continuous spinning basket	260-300	1-1.99	15.8-25.5	$R_{CH_4} = k_{9,1} K_1 K_4 K_7 K_8 P_{H_2}^2 P_{CO} \theta_*^2$	[65]
Fe-Mn	Continuous spinning basket	270-300	1.67-2.6	1	$R_{CH_4} = k_{11,1} K_1 K_2 \alpha_T P_{H_2} P_{CO} \theta_*^2$	[66]
Fe-Cu-K	Continuous spinning basket	250	1.1-2.5	0.8-2	$R_{CH_4} = k_{4,M} K_2 \alpha_1 P_{H_2} \theta_*^2$	[67]
Co/Al_2O_3	Fixed-bed microreactor	230-250	2-2.5	2.1	$R_{CH_4} = k_{7M} K_4 K_6 K'_3 \frac{P_{H_2}^3 P_{CO}}{P_{H_2O}} \theta_*^2$	[68,69]
Co-Ni/HZSM-5	Fixed-bed	200-240	1-2.5	1-2.5	$R_{CH_4} = \frac{k_6 K_4 P_{H_2}}{1 + \frac{k_6 K_4^{0.5} P_{H_2O}}{k_5 K_1 K_2 K_3 P_{CO} P_{H_2}^{1.5}}} \theta_*^2$	[70]
$Ru-Co-ZrP/SiO_2$	Fixed-bed	210-240	1-2.5	1-2	$R_{CH_4} = k_{CH_4} \gamma_1 \gamma_H \theta_*^2$	[31]

I.3. Reactors used in FT

Commercial FT reactors were developed before and during World War II for increasing the potential production of fuels at large scale. After passing this period, the interest in FT synthesis has declined due to the high cost of process installation and operation. Recently, the conversion of remote natural gas to hydrocarbons has revived the interest in implanting more advanced technologies in the commercialized reactors. This has been conducted to large production capacities with economical benefit. The main type of reactors that are mostly used by the industry of FT synthesis described in the following section. More advanced concepts of reactors belong to the classes of a fixed bed, fluidized bed and slurry reactors.

I.3.1. Fixed bed reactor

A fixed bed reactor is mostly the preferred conception for large scale production of hydrocarbons, where finite specification on the composition purity is not required [67]. For minimizing the pressure drop along the catalytic bed, a large diameter of particles is used for packing the reaction section. This will mainly conduct intraparticle diffusion issues and consequently a sharp reduction in the reaction rate is expected. Considering the low inclusion of the external mass transfer effect, it is proven through the experiment that the deposit of hydrocarbons interior the porous media of particles creates a liquid-film or interface that has resistance to the diffusion of reactants molecules through the active sites. This represents a determining factor in the diffusivity process of hydrogen into filled pores of heavy hydrocarbons [68]. In fact, the intraparticle diffusion starts to take place if the diameter of the catalyst is superior to 0.5 mm. So, this factor plays an impediment role in the modest integration of a fixed bed reactor in the FT industry. The nature of the FT reaction is exothermic isothermal conception is needed for maintaining

the initial temperature. By considering these thermic restrictions multi tubes are implanted inside the reactor shell for ensuring desirable convection and therefore flexible control of exothermic FT reactions. Many reactor configurations were put in use for industrial applications. The radial transport of heat can also cause bad distribution problems and poor conductivity of tubes walls can generate some rise in the temperature profile along with the radial dispersion. The presence of temperature fluctuations is hardly seen in the sable operating regions and must be avoided as it can cause a decline in the catalyst performances including selectivity shifting and activity decrease. Besides the choice of reactor diameter, the catalyst particle size and the gas velocity can determine the trend of heat transfer inside the catalytic bed. Research has investigated the relation between heat transport and bulk flow regime, the results indicate that the heat conductivity and the transfer coefficient tends to increase upon Reynolds number raise. This confirms the assumption that higher particle size generates less flow resistance or pressure drop and thus higher fluid velocity is resulted in conducting the heat transfer in both radial and axial directions of reactant flow [68]. This proportionality can be inversed by applying a larger catalyst size. The implantation of a single tubular reactor, in which the cooling fluid circulates inside the catalytic section can guarantee high heat elimination through overall convection of the bulk and thus better control of the reaction conditions [28,69]. A spray of oil is fed to the upper section of the reactor to remove the heat generated by the catalytic reaction and thus achieving better control of temperature [70]. A variety of fixed bed tubular reactors are widely used in the industry of FT, the reactor may constitute of a large-sized tube filled with a set of parallel fine tubes that carry the catalytic bed. The heat transfer is ensured through injecting a cooling fluid water/steam in the outer section of the reaction tubes. Other reactor designs include the arrangement

of catalyst particles in a shell system, where the cooling fluid flows in the area inside the tube. This type of reactor is used by the Sasol oil company [70]. Since the heat transfer in the axial direction is relatively low in the case of long tubes are installed, temperature profiles present nonequal distribution of temperature along with the reactor length. The difference in temperature between the bulk region and the walls of the tubes is huge at a large scale of measurement. Figure I.3 shows a strong dependency of temperature on the radial distance at the reactor inlet. This was explained by the high reaction rate due to the important partial pressure of reactants. For longer distances, the radial profile becomes less observable due to the decrease in reaction rates as the reactants are more consumed. It is also relevant that the reactor was designed with an extended variation in the diameter. This is not responding to the suggested requirement for reducing the temperature gradient. To maintain the operating temperature unconverted portion of the feed gas is recycled [70]. Building a higher number of concentric catalytic tubes is beneficial in terms of reducing FT exothermicity but this implies a longer period to operate a replacement of the deactivated catalysts [56]. An adiabatic fixed bed with a single bed is based on circulating the hot fluid in the external cooling system [68]. This type of reactor has a limited scale of conversion with a capacity of 15bbl/day. Also, heat transfer requires large recycling steams and this will result in a higher drop in pressure and intense consumption of energy. These limiting factors let the adiabatic fixed-bed reactor not be considered in further applications for syngas conversion [68]. Multitubular fixed bed reactor with gas recycling has got increasingly interested utilization due to its large scale of treatment of 400bbl/day (Figure I.4). The reaction rate profile along with the reactor length is incredibly higher than that of the nonrecycled reactor and the enhanced flow rate conducts to greater elimination of heat from the circulating fluid.

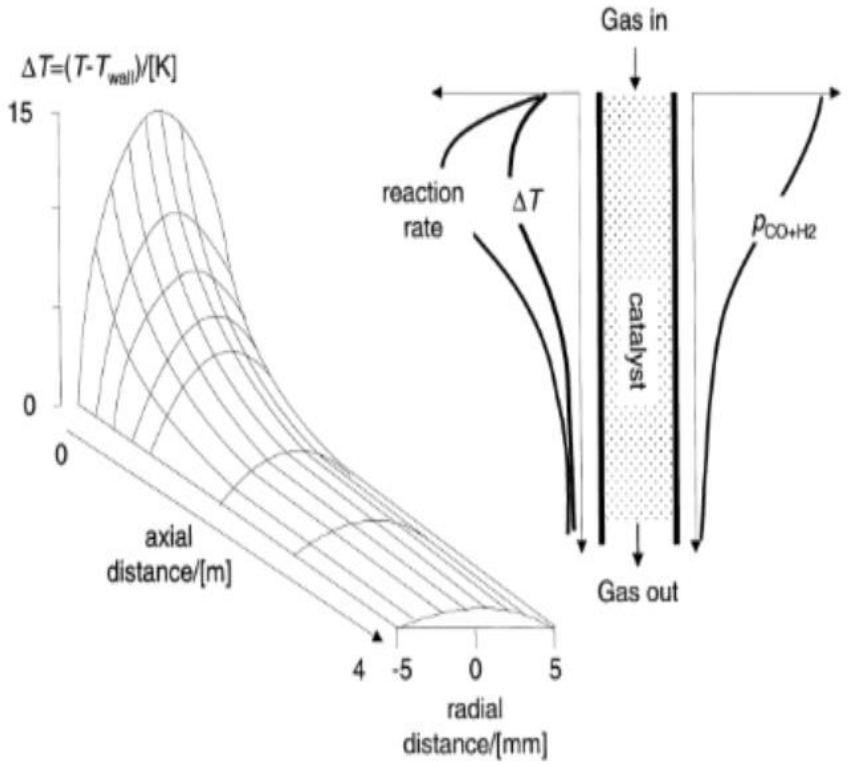


Figure I.3: Concentration and temperature profile in multi-tubular Fischer-Tropsch reactor [68].

This process was installed by Sasol company at Sasolburg in South Africa [68]. Moreover, the concentration profile is affected by flow resistance in the axial direction, strictly speaking, a small value of conversion can be achieved at the reactor outlet. This is way unconverted fluid is highly recommended to be recycled. To gain some heat transfer in one hand and increase the linear velocity of reactants in the other hand. This combination of temperature control and through gas recycling will lead to higher production capacity, lower cooling area and reasonable reduction in packed catalyst quantity. A multitubular reactor has been applied for the transformation of syngas in heavy and waxy FT hydrocarbons with a special design of catalyst structure and reactor capacity [71]. This has improved the production rate compared to the conventional one with 3000bbl of daily conversion capacity. The high packed amount of catalysts in the

multitubular reactor makes it not an attractive process due to the repetitive loading and unloading operations, which require a shut-in production for long period. In contrast to the fluidized bed reactor and slurry bubble column reactor, the multitubular reactor does not need an integrated unit that works on the separation of catalyst from the reaction phase. This part of the process may require advanced technology for ensuring effective filtration of the small part of the catalyst particles that can be generated from the attrition problem. This will affect the estimated benefit and can introduce additional costs to the operating plant. The scaling up for multi-tubular rig is done in an easy manner where the principal in laboratory application is identical to the industrial field.

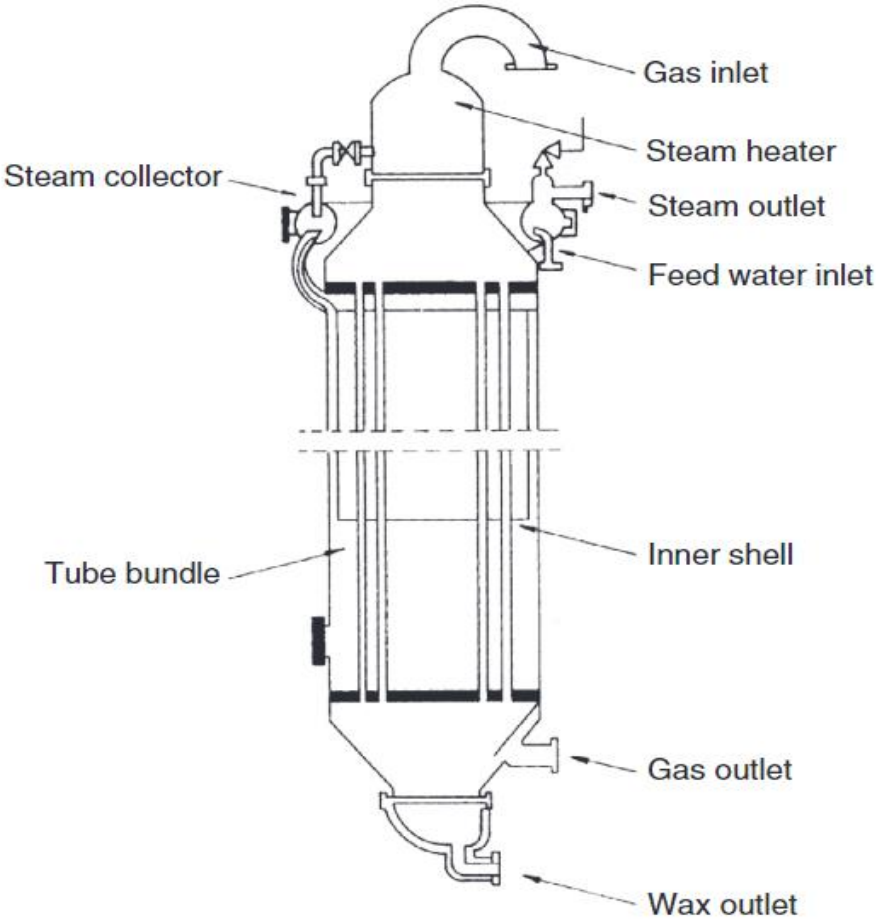


Figure I.4: multitubular fixed bed reactor [72].

I.3.2. Fluidized bed reactor

FT synthesis is characterized by high exothermicity, which can provoke bad distribution of reaction rate and syngas conversion due to the apparition of hot spots along the catalytic bed. Fluidized bed reactors are known for their smooth elimination of the generated excess in heat through phases mixing. This characteristic has attracted many industries to apply such kinds of reactors. As we discussed above, the fixed bed reactor is performed over large-sized catalysts which results in intraparticle diffusion limitations. By using a Fluidized-bed catalyst lower diffusion limitation is expected because of the small size of catalyst particles ($100\mu m$). However, the small size of particles can cause a serious problem by creating a possible agglomeration and thus inhibit the flow of fluids. The commercialized fluidized bed reactor is operated at relatively high temperature and moderate pressure, which leads to the large production of light hydrocarbons [68]. In fact, the conditions must be kept as it is otherwise the heavier chain of hydrocarbons will inevitably condensate on the surface of the catalyst and ruling out the possibility of having chain growth probability higher than 0.71. The only chance to have a heavier composition of products is to add a liquid phase to the gas and solid phase in the reaction area. By this attempt, when the temperature reaches the dew point, the hydrocarbons will condensate in the liquid phase rather than coating the catalyst particles. Several studies are devoted to developing the existing versions of circulating fluidized bed reactors [70]. The major problems of fixed fluid bed reactors are inspected to cover the degradation of the catalyst due to attrition as well as the readily decline in the amount of catalyst in the reaction zone [70]. Sasol company was able to adapt the circulating fluid bed reactor to its high-temperature FT plant [70]. A three-phase fluidized bed reactor is referred to as a fluid circulation process in which the catalyst bed is expanded by a concurrent flow of oil and

gas [68]. The configured reactor has not been commercialized and the only lab-scale reactor was built and tested [73].

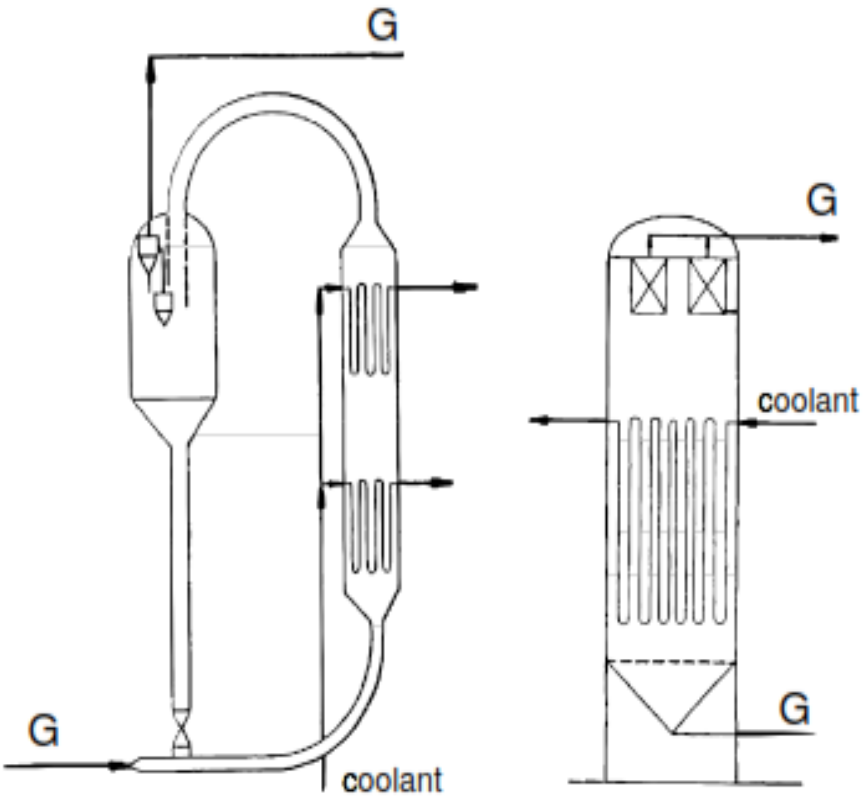


Figure I.5: (a) Circulating fluidized bed reactor, (b) fixed Fluidized bed reactor [5].

A bubbling regime was performed on a fluidized bed reactor for producing gasoline, where the reaction heat is eliminated using immersed bindles of pipings [74]. This process has been constructed in Brownsville but it was abandoned later on due to technical problems [68]. The first commercial version of a fixed fluidized bed reactor has been implemented in Sasolburg [75]. This has got a successful application with regards to the circulating fluid bed scale due to its compact form, less catalytic attrition and readily maintenance. These advantages reduced the operating cost of the process and thus resulting in higher utilization of a fixed fluidized bed reactor was achieved. The reaction rate of FT synthesis is related to catalyst density, for more compact reactors, syngas

conversion reaches its optimum state. The substitution of deactivated catalyst is easier in a fluidized bed reactor, where it can be accomplished at a higher time rate without any interruptive shut in the production. The high operating temperature of the circulating fluidized-bed reactors (Figure I.5(a)) results in product distribution with lower molecular weight. Due to the limitations of this problem and other unsolved problems Sasol company has substituted the circulating bed reactor by fixed fluidized-bed reactor. Currently, no additional plants were put under construction using this technology [2].

I.3.3. Slurry bubble column reactor

The syngas is initially in a gas state and it will partially be converted to a liquid phase if heavier hydrocarbons take part at the production stage this may lead to bad heat transfer along the reactor length and especially at the reactor inlet where the reaction rate is significant. By adding an initial composition that includes a portion of the liquid phase, the whole parts of the reactor will be subjected to the same velocity and therefore similar profile associated with reactants concentration and heat exchange is leveled up. Here it comes the idea of developing a new concept of reactor that can process a slurry combination of phases. This kind of reactor conveys a particular emphasis on production efficiency. The variation in hydrocarbons yield is fully controllable through additional parameters such as the flow rate of injected gases and the contact surface. Moreover, the smaller catalyst size is a milestone advantage to achieve a higher reaction rate by reducing the external and internal diffusion limitations. However, the capacity per train is limited and the delicate separation of catalyst particles from the reaction mixture in addition to the catalytic attrition during the reaction process and transportation for regeneration represents the main challenging drawbacks that have limited the commercialization of SBC [57]. According to recent researches, the slurry bubble column reactor is the most

required technology for the selective production of diesel [76]. This plant has been designed using a reasonable configuration (Figure I.6).

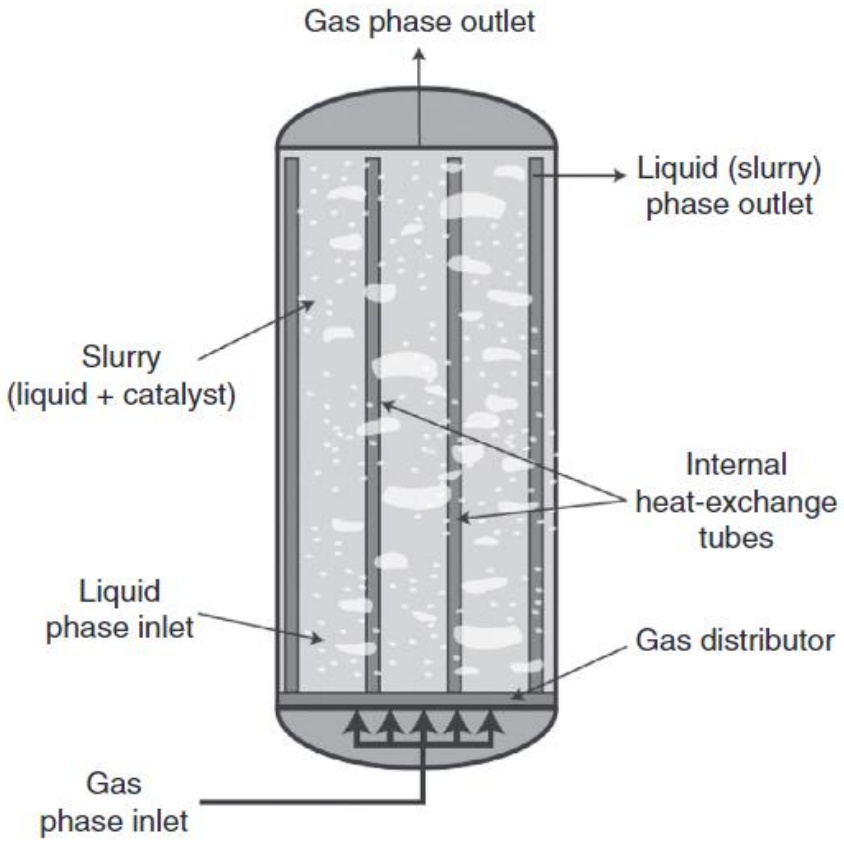


Figure I.6: FT slurry bubble column reactor [77].

To address the catalyst attrition problem, a precipitated iron catalyst was sintered at elevated temperatures. A large amount of collaborative work between *IFP Energies Nouvelles* and *ENI technology* was devoted to scaling up the slurry bubble column reactor with complementary tools [56]. They were able to increase the capacity per train by investigating the hydrodynamics of the slurry reactor on different scales and optimizing the operating conditions for achieving higher catalytic activity. The configuration of the reactor is associated with the catalyst type and size. The performed catalyst on the slurry

bubble column reactor is in powder form with a mean grain diameter of $50\,\mu m$. The reactor is constructed with a principal vessel that ensures the contact between three different phases: the solid catalyst is put in the suspension of the liquid products and the gas reactants are injected from the bottom of the reactor. This configuration has many advantages including a homogenous system for concentration and heat exchange and easy catalyst regeneration [56]. However, the complexity of design has routed many difficulties for unit installation and operation. Some earlier concept of slurry bubble column reactors is based on immersing cooling pipes in the slurry phase for removing the generated heat by the reaction. High carbon monoxide conversion of about 90% was achieved by using this same configuration at a superficial gas velocity of 0.1m/s [68]. Exxon has developed a lab-scale internal cooling system for slurry reactors and the predicted capacity for large scale applications is about 200bbl/day [78]. Sasol used the same concept to develop a reactor with a higher production capacity that can substitute the operated multitubular version of reactors. We can differentiate two kinds of flow regimes involving the bubbly flow regime and the churn turbulent regime. The bubbly flow regime is also known as the homogenous regime, which is consists of small size bubbles generated at a low linear gas velocity [68]. The velocity corresponds to the injection rate of gas reactants and by increasing the level of mixing above a predefined threshold the bubbles will compress to form a larger set of bubbles. This situation is similar to the caused one by churn turbulent regime, where a heterogenous rise in velocity will take place in the fluid mixture. Usually, a homogeneous regime is more preferable for laboratory applications, since that heterogeneous regime will cause many numbers of problems related to the fluid flow in small tested vessels (Figure I.7). By the way, the large productivity requires an additional raise in feed gas velocity to reach at least a

heterogeneous flow regime. Also, a high concentration of the catalyst is needed for achieving better activity and thus enhancing the total conversion. A study has shown that the increase in catalyst packing will boost the formation of larger bubbles in the solution from an effective destroy of initial small size bubbles [79]. However, the claimed advantage of the heterogeneous flow regime is ensuring perfect heat exchange by applying larger enhancement in the heat transfer coefficient.

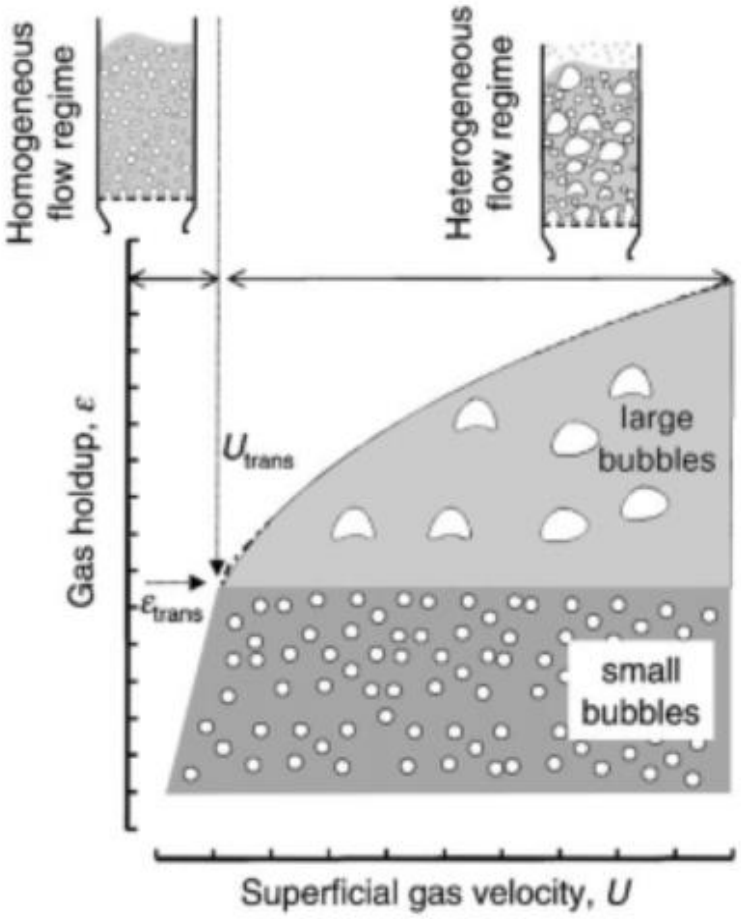


Figure I.7: Homogeneous and churn-turbulent regime in a slurry bubble column reactor [68].

On the other side, performing at a homogeneous regime can cause mass transfer limitation as the diffusion of gas in the liquid phase is relatively lente and the area of contact between

the two interfaces is considered as impediment factor for its bigger contribution. This situation can also be provoked by the increase in productivity. For the higher concentration of the catalyst, the larger activity will play a role in creating an improving the reaction rate and therefore gas-liquid mass transfer will become a rate-determining step. The real quantification of the mass transfer effect was done by conducting some experimental comparative tests between the heterogeneous and homogeneous case of the regime [80]. The results show that applying a heterogeneous regime has led to a greater mass transfer rate, which is an obvious indication of the low contribution of the mass transfer limitation in the overall FT reaction rate. The hydrodynamic plays a vital role in scaling up the slurry reactor as the laboratory experiments are projected under low flow velocities. So, considering other parameters that can alter the flow regime, more risk is taken for designing the appropriate reactor scale with maintaining the first defined regime using a pilot plant. The dispersion of the liquid phase is roughly related to the reactor size. The commercial plant is more expected to have a high mixing regime. The separation of the gas phase from the final solution can present a serious issue as the gas-liquid interface is delicate to be weakened.

I.3.4. Membrane reactor

A membrane reactor can associate the reaction process to the separation step by coupling these two in one single unit. This double role is highly beneficial for the industry as it reduces the extensive installation of the treatment units for separation and recycling purposes and also ensures lower inhibition of the reaction rate by the presence of undesirable components thought separating them from the reaction mixture. This allows the production at a higher rate in line with low effective cost. A study done by Alihellal [81] has proven that a water permeselective membrane reactor can deliver the good

potential for anticipating higher syngas conversion compared to the conventional one. Hence, applying such a concept on FT synthesis has got increasingly interested in the last years. Actually, this process can fully substitute the conventional reactors described above in terms of enhancing multiple considerations for the reactor design including the economical state and the quality of final products. Typically, fixed bed membrane reactors have been intensely investigated. But including the membrane concept to other reactors systems such as a fluidized bed reactor has granted a better experience as these types of configurations improve mass and heat transfer along the reactor length [82]. The efficiency of the selected membranes for the separation process is related to the operating parameters and we can distinguish that the zeolitic membranes are more likely to be applied for the case when we deal with exothermic reactions such as FT synthesis. This is because of its higher tendency to resist elevated temperatures. Therefore, thermal stability is the main character of the mineral membranes. Several industrial applications are commonly known for the membrane reactor including hydrogen and biofuel productions [83–85]. The membrane reactor can be integrated for further applications related to the control of the FT reactants' injection rate in the reaction zone, which is basically chosen according to the designated function and configuration. These kinds of membranes are known as distributed feeding membranes and they are used for selective injection of hydrogen and carbon monoxide that control the distribution of reactants. As an advantage, the initial syngas molar ratio can be maintained to have a less anticipated deviation in hydrocarbons selectivity [4]. Since product selectivity is strongly dependent on the H_2/CO ratio and feed distribution control can optimize the production [9]. For instance, the placement of the catalyst within the membrane will generate a different molar flow rate profile of reactants in the reaction area when compared to the external

packing of the catalyst bed, in which higher dispersion of the fluid phase is expected to take place. What was described so far is related to the case of having different configurations, while the function is defined by two modes of separation illustrated in co-feeding control of reactants into the reactor section and in the opposite selective permeation of by-products [86]. By using a permeselective membrane to hydrogen, high dispersion of hydrogen along the reactor can be achieved through multilayers injection and thus conducting a remarkable favoring in the production yield of long hydrocarbons chain. However, the alternation in the hydrocarbons distribution can be reached out using a different concept, in which the indirect control of hydrogen amount in the reaction zone is assisted by provoking disequilibrium in water gas shift reaction rate through removing carbon dioxide or water. Hopefully, this is what will be discussed and proved through this work. The membrane reactor is also more environmentally friendly compared to the conventional reactor as the greenhouse gases will be sharply reduced by the in-situ purification. In literature, only water purification has ben discussed. The accumulation of formed water during the FT process in the gas phase can decrease the partial pressure of the reactants and cause permanent deactivation of the catalyst by reoxidation. The membranes permeselective to water are able to recover the water from the reaction zone and by doing that reaction between water and carbon monoxide will be inhibited to discourage the formation of carbon dioxide by the water gas shift reaction. This effect will boost the consumption of carbon monoxide by the desirable FT reactions resulting in higher production yield of hydrocarbons [81,83]. The integration of mordenite and silica membranes for water separation has led to higher peremeselectivity factors with better-observed performances for the case at which the zeolitic membrane is used [9,83]. Otherwise, the purification of carbon dioxide has not been discussed in the literature. The

ability to control the distribution of hydrocarbons from carbon dioxide removal can make the development of a new technology that is based on the parallel production of a specific range of hydrocarbons more efficiently and cost-effectively. The increase in conversion of formed water via the direct shift of water gas shift reaction can enhance the formation of a large portion of the hydrogen and prevent the catalyst from water poisoning.

I.4. Aims and Outline of this Thesis

The problem to be dealt with in this thesis is the non-accurate control of hydrocarbons distribution through a simple alternation in the operating parameters. To handle this lack in process intensification necessitate a reliable design Fischer-Tropsch reactor that can deliver direct access to the in-situ control of syngas composition along with the reactor length. Therefore, the major aim of this thesis is the development of a product distribution concept based on using the purification of by-products as an advanced advantage to protect the environment and the equipment from damaging and at the same time providing an easy orientation of the system towards the desired type of production. For this purpose, a new model of membrane reactor was developed theoretically to control the distribution of final products assisted by a permeselecitive elimination of water or carbon dioxide from the reaction mixture. This will provoke a disequilibrium in the water gas shift reaction rate and thus resulting in typical favoring of hydrogen or carbon monoxide content in the reaction area. This trend will respond to the final aim of this thesis as the in-situ control of the syngas molar ratio has direct access to the alternation of hydrocarbons distribution towards the production of saturated or non-saturated kind of hydrocarbons at one side and long or short length hydrocarbons at another side.

CHAPTER II

Membrane Reactor Simulation Model

II.1. Concept of membrane reactor for ideal permeselectivity

II.1.1. Simulation concept

To begin the theoretical analysis of the suggested configurations through the established procedure, certain parameters had to be available first before starting to create the reactor model. This includes the initial setting and the predefined constant for the mathematical representation of physical metrics variation, which is associated with mass balance, heat gradient and pressure drop. Catalyst and gas characteristics are shown in Table 1. The reactor and membrane dimensions and operating parameters are summarized in Table 2. These sets of parameters are coherent and reflect the actual configuration of reactor properties at the industrial stage. The idea is to give a realistic approach to the tested simulation. From the mathematical investigation, the molar fluxes of FT compounds have been quantified through in order to correlate the overall production yield with the particular formation of hydrocarbons. Eventually, the *ODE45* function on *MATLAB* is used to solve the generated ordinary differential equations. This function implements a Runge-Kutta method with an elementary step for efficient computation and it is designed to handle the related mathematical problem at a given position. It is beneficial to produce a visual representation of what exactly the evolution of the reactor system represented by highly complicated-looking ordinary differential equations simplified to predict readable measurement. However, *ODE45* is a versatile *ODE* solver and is the first solver you should try for most problems. If the problem is stiff or requires high accuracy, then there are other *ODE* solvers that might be better suited to the problem. Some *ODE* problems exhibit stiffness, or difficulty in evaluation. Stiffness is a term that defines a precise definition, but in general, stiffness occurs when there is a difference in scaling somewhere in the problem. For example, if an *ODE* has two solution components that vary on

drastically different time scales, then the equation might be stiff. You can identify a problem as stiff if nonstiff solvers (such as *ODE45*) are unable to solve the problem or are extremely slow. If you observe that a nonstiff solver is very slow, try using a stiff solver such as *ODE15s* instead. When using a stiff solver, you can improve reliability and efficiency by supplying the Jacobian matrix or its sparsity pattern. In chapter III, FT synthesis was conducted in a conventional fixed-bed reactor and membrane reactor for water or carbon dioxide removal. A reactor simulation using MATLAB software was planned for three different conceptions of reactors: membrane reactor for water removal (MRW), a membrane reactor for carbon dioxide removal (MRC) and a conventional reactor (CR). To measure and to analyze the process performances, the following metrics are used: the outlet selectivity of hydrocarbons and the Olefin to Paraffin ratio (O/P). Besides, the evolution of water gas shift reaction rates and the actual H_2/CO molar ratio are measured and quantified using the persistent command attached to the algorithm.

Table II.1: Catalyst and gas proprieties.

Catalyst density (kg m^{-3})	1290	[81]
Diameter of catalyst particle (m)	2.5×10^{-3}	[81]
GHSV (h^{-1})	4000	[93]
Gas density (kg m^{-3})	13.2	[81]
Gas viscosity (bar s^{-1})	1.8×10^{-10}	[81]

Table II.2: Reactor dimensions and operating conditions.

Reactor length (m)	7.0	[81]
Diameter of cooling tube (m)	10×10^{-3}	-
Diameter of reaction zone (m)	30×10^{-3}	-
Porosity of catalytic bed (-)	0.6	[81]
Bulk density (kg m^{-3})	774	-
Density of Sillicalite-1 membrane (kg m^{-3})	1760	[87]
Thickness of Sillicalite-1 membrane (μm)	$0.5 - 50$	[88]
Density of NaA membrane (kg m^{-3})	1900	[89]
Thickness of NaA membrane (μm)	$3 - 30$	[90,91]
Porosity of membrane-support layer	0.52	[92]
Initial pressure (bar)	20	[93]
Initial temperature (K)	533	[91]
Shell temperature: T_{sh} (K)	508	-
Heat transfer coefficient shell-gas: U_{sh} (W m^{-2} K^{-1})	800	[22]

II.1.2. Membrane reactor description

The reaction section consists of an outlet tube packed with the iron catalyst and an inner tube carrying the cooling water. As shown in Figure II.1, the membrane reactor is made up of two separate sides, in which the walls of the reaction zone are designed by a tubular membrane. This configuration will allow the *in-situ* removal of water or carbon dioxide along the catalyst bed. The injection of sweeping gas in the permeation section is necessary for creating a difference in the partial pressure of the separated components. In order to simplify the reactor calculations, several assumptions are taken into consideration

for the construction of the mathematical model. First, it includes the integration of the ideal plug flow as a dispersion regime by estimating a neglectable variation in the concentration along the transversal direction to the bulk flow due to the infinite homogeneity of fluid's displacement rate along the reactor section [94]. Second, ideal gas law is applied as a general rule for wide utilization that deals with nonexcessive pressure, which can occupy a considerable volume that surpasses the critical point where the interaction between molecules and the volume of particles should be taken into account. Third, for the sake of simplifying the overall calculations, the porosity of the catalytic bed was considered to be invariant for the longitudinal and the axial representation. Fourth, the reaction zone is considered to be a homogeneous phase, in which the solid part is assumed to be mixed with the solution resulting in neglectable interaction between the two phases that is due to the mass and heat transfer interface from the bulk solution to the core of the catalyst. Fifth, for investigating the effect of removing carbon dioxide and water on the distribution of hydrocarbons, permeselective models were applied so far only for the selected components based on the approximation that support a lower diffusion of other reaction species through the chosen kinds of membranes. This assumption does not really reflect the reality but further work has proven was presented in the following chapter has reinforced the correct estimation that can be extended to the negligible permeation of FT mixture compared to the permeation of carbon dioxide and water through Silicalite-1 and NaA membranes, respectively. It is also indicated from the related study that even under some operating conditions the permeation was entirely enhanced, the permeation of targeted species is widely accepted as the determining representation. Models are useful for representing the evolution of any sub variation of the investigated metric in the real reactor, for scale-up and for diagnosing the probable

concept that can provide more satisfactory results that agree well with the real-world measurements. we often try to design real reactors so that their flows approach the ideal model described above.

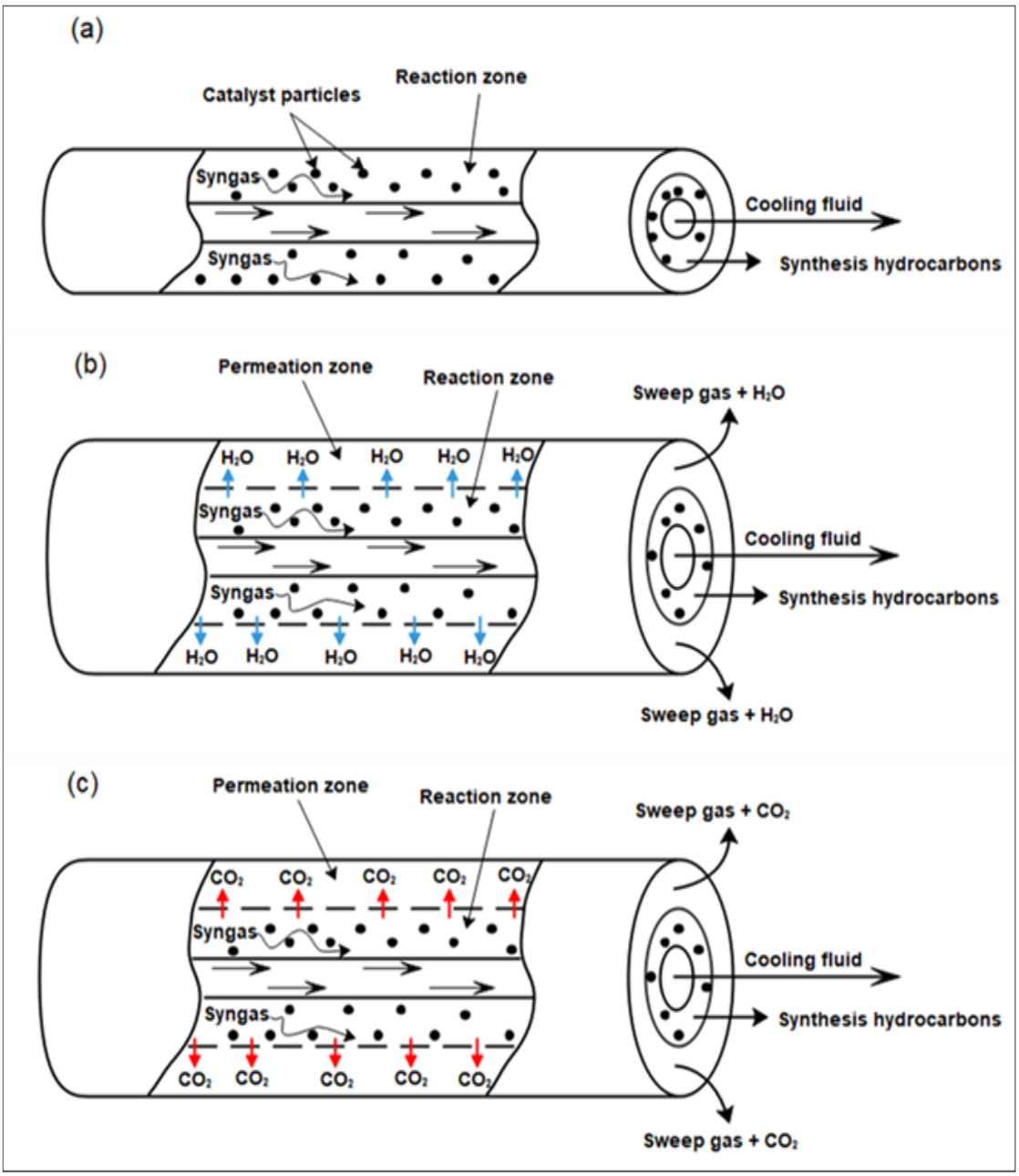


Figure II.1: Schematic diagram of FT membrane reactor, (a): Conventional reactor (CR), (b): Membrane reactor for water removal (MRW), (c): Membrane reactor for CO_2 removal (MRC).

II.1.3. Reactor model

In a plug flow reactor, the composition of the fluid varies from point to point along a flow path; consequently, the material balance for a reaction component must be made for a differential element of volume dV when we deal with homogenous fluid and elementary change in the catalyst mass dm for the heterogeneous system. According to reaction stoichiometry and based on the plug flow assumption, the mass balance in the reaction side is given by:

$$\frac{dF_i}{dz} = \rho A \upsilon_{ij} R_j \tag{II.1}$$

$i = CO, H_2, CH_4, C_2H_6, C_3H_8, C_4H_{10}, C_5H_{12}, C_2H_4, C_3H_6, C_4H_8, C_5H_{10}, CO_2, H_2O$

Where F_i is the molar flow rate of hydrocarbons and it can be written in the function of dimensionless reactor length (l):

$$\frac{dF_i}{dl} = \rho A L \upsilon_{ij} R_j \tag{II.2}$$

L is the reactor length ρ is the bulk density and R_j is the rate of reaction j. For the reactor as a whole, the expression must be integrated. Now reaction rate is certainly dependent on the concentration or conversion of materials. This mass balance equation can be written either in terms of molar flux or conversions. For systems of changing density, it is more convenient to use conversions; however, there is no particular preference for constant density systems. Whatever its form, the principal equation interrelates the rate of reaction, the extent of reaction and the catalyst mass and if anyone of these quantities is unknown it can be found from the other three. Graphical and numerical resolutions of molar flux evolution along with the reactor length can be displayed by using mathematical integration. However, for certain simple kinetic forms, analytic integration is possible and

convenient but at a higher level of complexity, in which the detailed micro-kinetic is applied graphical approach is needed as a possible representative solution. Considering that the synthesis hydrocarbons are the major components of the outlet mixture as water and carbon dioxide formation is largely smaller than the overall production of hydrocarbons, the selectivity of paraffin and olefins can be calculated with the following expression:

$$S_i(\%) = \frac{F_i}{\sum F_i - (F_{H_2} + F_{CO} + F_{CO_2} + F_{H_2O})} \times 100\% \quad \text{(II.3)}$$

The partial pressure of FT compounds is calculated by a simple formula that is referred to as the general law of Dalton:

$$P_i = \frac{F_i}{F_T} P_T \quad \text{(II.4)}$$

Where F_T is the sum of molar flow rates of individual gases along the reactor.

$$F_T = \sum F_i \quad \text{(II.5)}$$

The initial total molar flow rate is expressed by:

$$F_T^0 = F_{CO}^0 \ (1 + M) \quad \text{(II.6)}$$

Where the inlet molar ratio of syngas is defined by the following equation:

$$\mathrm{M} = \frac{F_{H_2}^0}{F_{CO}^0} \quad \text{(II.7)}$$

When there is no flow through the packed bed, the net gravitational force acts downward. When flow begins upward, friction forces act upward and counterbalance the net gravitational force. For a high enough fluid velocity, the friction force is large enough to

lift the particles. This represents the onset of fluidization. The frictional force can be expressed in terms of a friction factor. This leads to an equation describing the flow of a fluid past a collection of particles, which is known as the Ergun equation that can contribute to the understanding pressure drop along the length of the packed bed at a given fluid velocity. Where the pressure drop depends on the packing size, length of the bed, fluid viscosity, fluid density and catalytic bed porosity. It can be written as:

$$\frac{dP_T}{dl} = -\frac{L\nu}{d_p}\left(\frac{1-\varepsilon}{\varepsilon^3}\right)\left(\frac{150(1-\varepsilon)\mu}{d_p} + 1.75\rho_g \nu\right) \quad \text{(II.8)}$$

The linear velocity of reactants can be calculated by ideal gas law:

$$\nu = \frac{F_T^0 R T_0}{P_T^0 A} \quad \text{(II.9)}$$

Heat balance considerations are important in designing and operating a reactor at the optimum temperature. The calculation is related to generated heat from the exothermic FT reactions in the conducted gas flow. The energy balance is given by the following expression [81,95] :

$$\frac{dT}{dl} = \frac{\rho AL}{F_T C_{pg}} \sum_{j=i}^{B} R_j \left(-\Delta H_{R_j}\right) + \frac{L\pi D_C}{F_T C_{pg}} U_{sh}(T_{sh} - T) \quad \text{(II.10)}$$

Where the enthalpy of reaction j is calculated using Kirchhoff law:

$$\Delta H_{R_j} = \left(\Delta H_{R_j}\right)_{298.15} + \int_{298.15}^{T} (\sum \upsilon_{ij} C_{p,product} - \sum \upsilon_{ij} C_{p,reactant}) dT \quad \text{(II.11)}$$

The calculated value of the specific heat of the gaseous mixture (C_{pg}) is necessarily practical for accounting the change gaseous composition in temperature calculations. In this case, the heat capacity for each substance change is correlated to temperature by using

empirical determinations. C_{pg} is the average amount of heat needed for a temperature change of 1 K and it is calculated by the following equation:

$$C_{pg} = y_{H_2} C_{p,H_2} + y_{CO} C_{p,CO} + y_{CO_2} C_{p,CO_2} + y_{H_2O} C_{p,H_2O} + \sum y_i C_{p,i} \qquad \text{(II.12)}$$

$$i = CH_4, C_2H_6, C_3H_8, C_4H_{10}, C_5H_{12}, C_2H_4, C_3H_6, C_4H_8, C_5H_{10}$$

II.1.4. Kinetic model

Different mechanisms approaches including carbide formation, enol formation, and CO insertion were proposed to describe the kinetic model of the FT reaction [64,96–98]. But the carbide mechanism is widely accepted for the iron catalyst as suggested by a spectroscopic demonstration of the dissociative adsorption of carbon monoxide on iron catalyst surface under operating temperatures superior to 350K [22]. This why a similar kinetic model developed for an industrial Fe-Cu-K catalyst [93] was chosen for our study under the range of conditions as follows: temperature of 493-542 K, pressure of 11-40 bar, H_2/CO inlet molar ratio of 1-3. The reaction rates of methane (eq. 13), n-paraffins (eq. 14), and 1-olefins (eq. 15) are given as follow:

For a chain length of $n = 1$:

$$R_{CH_4} = k_{5M} P_{H_2} \alpha_1 / DEN \qquad \text{(II.13)}$$

For a chain length of $n \geq 2$:

$$R_{C_nH_{2n+2}} = k_5 P_{H_2} \prod_{k=1}^{n} \alpha_k / DEN \qquad \text{(II.14)}$$

$$R_{C_nH_{2n}} = k_6 (1 - \beta_n) \prod_{k=1}^{n} \alpha_k / DEN \qquad \text{(II.15)}$$

Where

$$\alpha_1 = \frac{k_1 P_{CO}}{k_1 P_{CO} + k_{5M} P_{H_2}} \quad \text{(II.16)}$$

$$\alpha_A = \frac{k_1 P_{CO}}{k_1 P_{CO} + k_5 P_{H_2} + k_6} \quad \text{(II.17)}$$

$$\alpha_n = \frac{k_1 P_{CO}}{k_1 P_{CO} + k_5 P_{H_2} + k_6 (1 - \beta_n)} \quad \text{(II.18)}$$

$$\beta_n = \frac{k_{-6}}{k_6} \frac{P_{C_n H_{2n}}}{\alpha_A^{n-1} \frac{k_1 P_{CO}}{k_1 P_{CO} + k_5 P_{H_2}} + \frac{k_{-6}}{k_1 P_{CO} + k_5 P_{H_2} + k_6} \sum_{a=2}^{n} \alpha_A^{n-2} P_{C_{(n-a+2)} H_{2(n-a+2)}}} \quad \text{(II.19)}$$

$$DEN = 1 + \left(1 + \frac{1}{K_2 K_3 K_4} \frac{P_{H_2O}}{P_{H_2}^2} + \frac{1}{K_3 K_4 P_{H_2}} + \frac{1}{K_4}\right) \sum_{f=1}^{n} \left(\prod_{k=1}^{f} \alpha_k\right) \quad \text{(II.20)}$$

Table II.3: Kinetic constants and activation energy for FT and WGS reactions [93].

k_1	$2.23\text{x}10^{-2}$	$\text{mol kg}^{-1}\text{s}^{-1}\text{bar}^{-1}$	K_4	0.226	–
$k_{5M,0}$	$4.65\text{x}10^{6}$	$\text{mol kg}^{-1}\text{s}^{-1}\text{bar}^{-1}$	$k_{v,0}$	$15.7\text{x}10^{3}$	$\text{mol kg}^{-1}\text{s}^{-1}\text{bar}^{-1.5}$
$k_{5,0}$	$2.74\text{x}10^{5}$	$\text{mol kg}^{-1}\text{s}^{-1}\text{bar}^{-1}$	K_v	$1.13\text{x}10^{-3}$	$\text{bar}^{-0.5}$
$k_{6,0}$	$2.66\text{x}10^{9}$	$\text{mol kg}^{-1}\text{s}^{-1}$	E_{5M}	$92.89\text{x}10^{3}$	j mol^{-1}
k_{-6}	$2.75\text{x}10^{-2}$	$\text{mol kg}^{-1}\text{s}^{-1}\text{bar}^{-1}$	E_5	$87.01\text{x}10^{3}$	j mol^{-1}
K_2	$1.81\text{x}10^{-2}$	–	E_6	$111.04\text{x}10^{3}$	j mol^{-1}
K_3	$4.68\text{x}10^{-2}$	–	E_v	$45.08\text{x}10^{3}$	j mol^{-1}

The kinetic rate of WGS reaction is given by the following equation [93]:

$$R_{WGS} = \frac{k_v \left(\frac{P_{CO} P_{H_2O}}{P_{H_2}^{0.5}} - \frac{P_{CO_2} P_{H_2}^{0.5}}{K_{WGS}}\right)}{1 + K_v \frac{P_{CO} P_{H_2O}}{P_{H_2}^{0.5}}} \quad \text{(II.21)}$$

k_v is the rate constant of CO_2 formation, and K_v is the group of constant in WGS reaction. The equilibrium constant of WGS reaction can be calculated by the following equation [1,81]:

$$K_{WGS} = \frac{5078.0045}{T} - 5.8972089 + 13.958689 \times 10^{-4}T - 27.592844 \times 10^{-8}T^2 \quad \text{(II.22)}$$

The reaction rate constants are evaluated according to the Arrhenius equation:

$$k(T) = k_0 \exp\left(\frac{-E}{RT}\right) \quad \text{(II.23)}$$

II.1.5. Permeation model

The selection of the suitable zeolitic membrane for water separation depends basically on adsorption affinity. The hydrophilic character of the membrane becomes more important by decreasing the Si/Al ratio and thus result in a high water separation. NaA membrane is characterized by a lower range of Si/Al ratio, which makes it the most required zeolite-type for selective permeation of water from a gas mixture. The application of this membrane for the separation of the binary mixture has led to satisfactory results. Indeed, H_2O/H_2 selectivity surpasses the value of 300 at room temperature [99]. Even the selective separation of water decline upon temperature increase, hydrogen permeation stills barely remarkable compared to water permeation. However, H_2O/H_2 selectivity at the reaction temperature was covered by another experiment where the mordenite membrane was used. The results show that a high separation factor of 37 could be achieved at 531K [83]. Permeates of other species such as hydrocarbons are also negligible compared to water permeation. This maybe will have a minor effect on the final distribution (O/P). A study has shown that the permeation of carbon dioxide in hydrophilic membranes was remarkably decreased in the presence of water [100]. For

assuring low water adsorption and high separation of carbon dioxide, it is necessary to use a hydrophobic membrane such as silicalite-1, but the inconvenience of this kind of membrane is also permeable to other gases. This will create a competitive diffusion through the membrane layer. According to literature investigations, the permeation of CH_4 and H_2 can be neglected compared to CO_2 permeation at ordinary levels of temperature [92,101,102]. The separation of a binary mixture by silicalite-1 has shown higher CO_2/CH_4 selectivity (5.5) at room temperature [103]. Some experiments reported that CO_2/CH_4 selectivity was enhanced with pressure increase [87,103]. Also, it was reported that CO_2/H_2 selectivity decrease from 9.8 to approximately 1 by raising the temperature from 0°C to 100°C [104]. This can be contributed to the change in the mass transport mechanism for H_2 and CH_4 species at high temperatures. In general, the prediction of CH_4 and H_2 permeation follows a combination between surface diffusion and gaseous diffusion mechanisms. A study [92] has shown that even the adsorption of H_2 and CH_4 tends to reach zero loadings at a temperature range superior to 400K and CO_2 adsorption is much less limited to high operating temperature, a decline in the selective permeation of CO_2 is observed. This implicit the activation of gaseous diffusion for H_2 and CH_4 species, which is independent of the molecular adsorption. At high temperatures, the diffusion of CO_2 through the silicalite-1 membrane follows the Henry regime, in which the permeation becomes linearly dependent on the pressure gradient. However, the selective separation of CO_2 through the silicalite-1 membrane is not described in the literature under a similar temperature range to the FT reaction. This leads us to use a mathematical correlation for describing the evolution of CO_2 permeation in the function of temperature. So, the temperature dependence of the diffusivity and the adsorption can be calculated by using the equations described below. Generally, the apparent permeation

of gases in the zeolitic pores is a combination of gaseous diffusion and surface diffusion mechanisms [86]. At high molecular adsorption, which can be found in water separation using NaA membrane and carbon dioxide separation using the Sillicalite-1 membrane, the permeation is described only by surface diffusion [10,91,99]. The permeation flux is expressed by Maxwell-Stefan equation [105,106]:

$$J_\xi = -\varepsilon_m * \rho_m * q_\xi^{sat} * Đ(\theta_\xi) \frac{d\theta_\xi}{dx} \quad \text{(II.24)}$$

J_ξ is the permeation flux through the zeolitic membrane ($\xi = H_2O, CO_2$) and ε_m is the porosity of the membrane-support layer.$\rho_m$is the density of the membrane. The diffusivity Đ (θ_ξ) depends on sites occupancy and it is expressed by Darken equation [107]:

$$Đ\ (\theta_\xi) = Đ_{\theta_\xi=0} \frac{dlnP_\xi}{dlnq_\xi} \quad \text{(II.25)}$$

$Đ_{\theta_\xi=0}$ is the corrected diffusivity, corresponding to the diffusivity at very low loading on the membrane layer. This parameter depends only on temperature:

$$Đ_{\Theta_\xi=0} = Đ_{\xi,0} \exp\left(\frac{-E_{dif,\xi}}{RT}\right) \quad \text{(II.26)}$$

The adsorption is described by Langmuir isotherm:

$$q_\xi = q_\xi^{sat} \theta_\xi \quad \text{(II.27)}$$

$$\theta_\xi = \frac{K_\xi P_\xi}{1+K_\xi P_\xi} \quad \text{(II.28)}$$

q_ξ^{sat} is the saturation amount adsorbed of component ξ. K_ξ is the adsorption equilibrium constant and it can be written as:

$$K_{CO_2} = K_{CO_2,0}\exp\left(\frac{-\Delta H_{ads,CO_2}}{RT}\right) \quad \text{(II.29)}$$

$$K_{H_2O} = K_{H_2O,0}\exp\left(\frac{-\Delta H_{ads,H_2O}}{R}\left(\frac{1}{T} - \frac{1}{363,4}\right)\right) \quad \text{(II.30)}$$

Integration of equation (24) in combination with the Langmuir isotherm (eq. 31), we obtain:

$$J_\xi = \frac{\varepsilon_m \rho_m q_\xi^{sat} Đ_{\theta_{\xi=0}}}{\delta} \ln\left(\frac{1+K_\xi P_{reac,\xi}}{1+K_\xi P_{perm,\xi}}\right) \quad \text{(II.31)}$$

δ is the thickness of the membrane layer. P_{rec} and P_{per} are the partial pressures in the reaction and permeate sides, respectively, with constant total pressure in the permeation zone:

$$P_{perm,tot} = P_{perm,\xi} + P_{IN} \quad \text{(II.31)}$$

The partial pressure of inert gas (P_I) is defined by the following expression:

$$P_{IN} = \frac{F_{IN}}{F_{perm,\xi}+F_{IN}} P_{perm,tot} \quad \text{(II.32)}$$

Where the molar flow rate of inert gas can be calculated using inert fraction (I_{index}):

$$F_{IN} = F_{CO}^0 I_{index} \quad \text{(II.33)}$$

I_{index} is defined as the ratio between the inert gas flow rate to that of the inlet carbon monoxide.

Table II.4: Water and carbon dioxide adsorption and diffusion parameters [87,91].

Parameters	$\mathbf{H_2O}$	$\mathbf{CO_2}$
q_{ξ}^{sat} (mol kg^{-1})	11.4	2.79
$K_{\xi,0}$ (bar^{-1})	1.5×10^{2}	5.62×10^{-5}
$\Delta H_{ads,\xi}$ (J mol^{-1})	-45×10^{3}	-25×10^{3}
$Đ_{\xi,0}$ (m^{2}s^{-1})	4×10^{-12}	1.76×10^{-7}
$E_{dif,\xi}$ (J mol^{-1})	34×10^{3}	15.4×10^{3}

II.2. Concept of membrane reactor for non-ideal CO_2 permeselectivity

The fact that hydrocarbons are permeable through the silicalite-1 membrane can not be avoided and to quantify the real permeation of the different compounds constituting the reaction mixture, the FT reaction was carried out over the same type of catalyst used in investigating the ideal separation of water and carbon dioxide from the reaction mixture. Here, the reactor concept is similar to the described one in the above section with the silicalite-1 membrane is installed for the further investigation that deals with consideration of other FT species diffusion through the membrane (Figure II.2). This refers to non-ideal permselective separation of carbon dioxide from the mixture. So, in this section, the permeation behavior for each specie through the silicalite-1 membrane was described by specific equations and it is coupled to the equations describing the reaction. It should be noted that in the whole system, each component is defined by a molar flow rate generated by the reaction (F^{reac}), a molar flow rate in the permeate side

(F^{perm}) and a residual molar flow rate (F^{res}). The residual molar flow rates along the reactor can be correlated according to the following expression:

$$\frac{dF_i^{res}}{dl} = \frac{dF_i^{reac}}{dl} - \frac{dF_i^{perm}}{dl} \quad \text{(II.34)}$$

$i = CO, H_2, CH_4, C_2H_6, C_3H_8, C_4H_{10}, C_5H_{12}, C_2H_4, C_3H_6, C_4H_8, C_5H_{10}, CO_2, H_2O$ are the different species that supposed could permeate through the membrane. Here, the residual molar flow rates mean that the number of species remaining in the reaction side. The variation of F_i^{reac} as a function of dimensionless reactor length (l) is given by:

$$\frac{dF_i^{reac}}{dl} = \rho A L v_{ij} R_j \quad \text{(II.35)}$$

Here, L is the reactor length ρ is the bulk density and R_j is the rate of reaction j given in the appendix of the present manuscript.

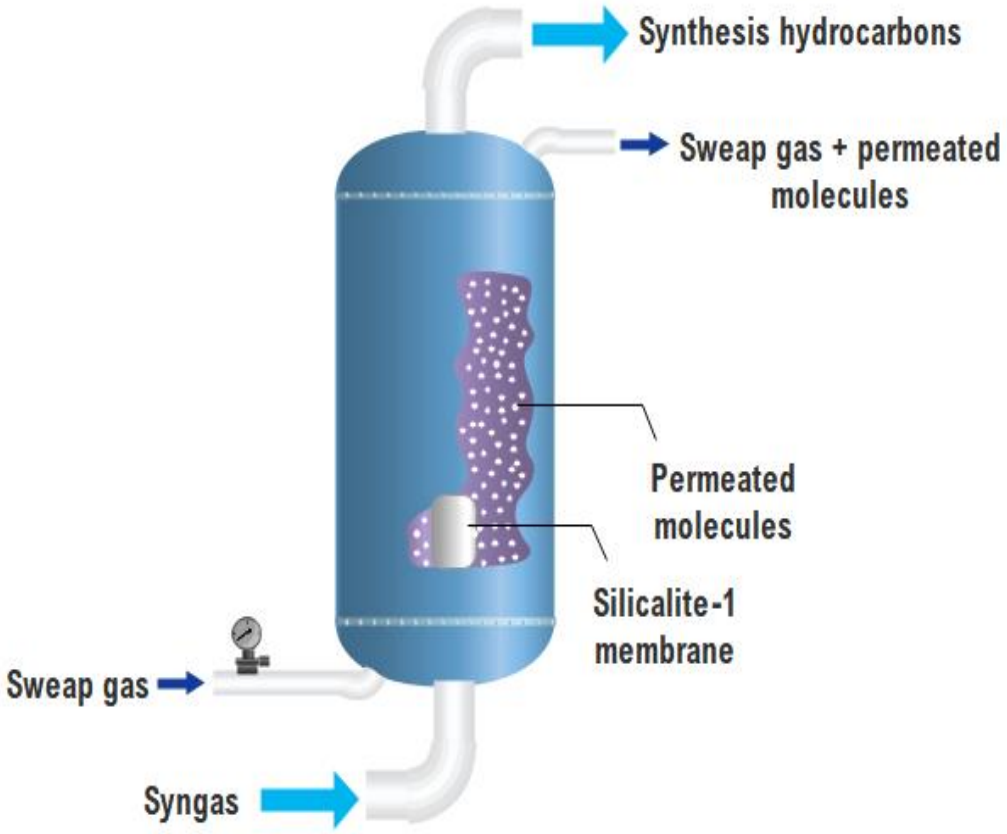


Figure II.2: Scheme of the FT membrane reactor.

In general, the permeate flux is described in terms of surface diffusion and gaseous diffusion. The variation in the contribution of these two pointed mechanisms to the permeation process can be pictured as a function of the predicted deviation of the molecular adsorption. For a mass transport that is based on surface diffusion, high molecular adsorption occurs on the membrane surface. Whenever, the different situations can be discussed at low adsorption, in which the permeation is extended to be more dependent on the gaseous diffusion. It has been reported in the literature that the equilibrium between these two models can be shifted according to the investigated kind of the membrane and the diffused components [107,108]. The gaseous diffusion model is introduced and expressed as:

$$\frac{dF_{GD,i}^{perm}}{dl} = \frac{\varepsilon_m B L}{R T} Đ_{GD,i} \frac{dP_i}{dx} \quad \text{(II.36)}$$

Where, x is the membrane position, ε_m is the porosity of the membrane and B is the perimeter of membrane cross-section. The diffusivity ($Đ_{GD,i}$) is defined by the following equation [92]:

$$Đ_{GD,i} = \frac{\lambda_i}{z} \sqrt{\frac{8 R T}{\pi M}} exp \left(\frac{-E_{GD,i}}{RT}\right) \quad \text{(II.37)}$$

λ_i is the diffusional length, z is the probability of molecule can make a jump in the right direction. This parameter is equal to 1 for Knudsen's regime [30]. By integration of the equation (3) we obtain:

$$\frac{dF_{GD,i}^{perm}}{dl} = \frac{\varepsilon_m B L}{R T \delta} Đ_{GD,i} (P_{reac,i} - P_{perm,i}) \quad \text{(II.38)}$$

δ is the thickness of the membrane layer. All the adsorption and diffusion parameters for each species are summarized in Table II.5 and Table II.6, respectively.

For surface diffusion, the model is described in the above section of ideal permeselectivity using Maxwell-Stefan representation. To describe the process behavior, the permeation factor is used to define the evolution of membrane efficiency.

Actually, this parameter is independent on the reaction flux and it can be calculated by the following expression:

$$PF = \frac{F_i^{perm}}{F_i^{reac}} \quad \text{(II.39)}$$

In addition, the selective permeation of CO_2 from the gas mixture is also used through the following definition [109]:

$$SP = \frac{\left(F_{CO_2}^{Perm}/F_i^{Perm}\right)}{\left(F_{CO_2}^{reac}/F_i^{reac}\right)} \quad \text{(II.40)}$$

Table II.5: Adsorption parameters for the permeates.

Components	q^{sat}	Kx10^{-2}	ΔH_{ads}	ΔS_{ads}	Reference
CH_4	4.5	–	-22.6	-70	[92]
C_2H_6	3	–	-30.4	-74	[92]
C_3H_8	2.4	–	-38.2	-80	[92]
C_4H_{10}	2.2	–	-45.9	-85	[92]
C_5H_{12}	$1.41^{(a)}$	10	-63.5	–	[110–112]
C_2H_4	2.28	0.063	-24	–	[113,114]
C_3H_6	2.27	0.96	-39.98	–	[113,114]
C_4H_8	1.8	1.134	-46.36	–	[111,112]
C_5H_{10}	1.15	94.79	-75	–	[111]
CO	5.1	–	-17.9	-55	[92]
H_2	5.4	–	-5.9	-43	[92]
H_2O	2.8	48.38	-25	–	[109,115]
CO_2	5	–	-24.1	-58	[92]

Table II.6: Diffusion parameters of permeate species.

Components	$Đ_0$ x10^{+8}	E_{dif}	E_{GD}	Reference
CH_4	3.9	8.8	-7.9	[92]
C_2H_6	1.7	10.5	-7.2	[92]
C_3H_8	0.75	12.2	-11.4	[92]
C_4H_{10}	0.4	13.7	-13.1	[92]
C_5H_{12}	0.02	19.24	–	[111,116]
C_2H_4	3.1	3.38	–	[117]
C_3H_6	2.1	6.28	–	[117]
C_4H_8	0.97	16.6	–	[118,119]
C_5H_{10}	0.031	20.5	–	[119]
CO	0.9	7.1	-9.9	[92]
H_2	1.5	2.1	-8.3	[92]
H_2O	0.001	30.3	–	[115]
CO_2	17.6	9.6	-10.3	[87,92]

CHAPTER III

Control of Hydrocarbons Distribution Using Membrane Reactor

III.1. In-situ H_2O and CO_2 removal

The most common way to minimize the concentration of the by-products in the reaction area can be guaranteed by the integration of a permselective membrane, which allows *in-situ* water removal along the catalyst bed [83,86]. The zeolitic membranes are highly recommended for FT synthesis due to their stability at high-temperature levels and for better separation of gaseous mixture [120] and a highly selective permeation of water could be observed through the NaA zeolite membrane [99]. In fact, the high content of aluminum in the NaA structure gives the membrane a hydrophilic character [91]. Also, the hydroxy sodalite SOD membranes can assure ultra-water separation because of their high polarity. On the other hand, the silicalite-1 membrane was preferred for carbon dioxide separation from the gaseous phase [87].

III.2. Effect of permeation on hydrocarbons distribution

FT process has known plenty of actual parametric intensifications in the objective of enhancing the reaction efficiency and thus reaching high fuel quality. In light of the foregoing research, multiple parameters can affect the distribution of hydrocarbons at the conventional stage and this may require a deep optimization of reactor operating parameters including gas hourly space velocity, temperature and initial pressure. Low values of gas hourly space velocity can favor the production of heavier paraffin while unsubstantial levels of pressure will adverse the production of paraffin and swift the overall reaction rate towards the formation of olefins. Despite this remarkable variation in hydrocarbons distribution, the effect of such parameters is complex and thoroughly restricted under a narrow range of investigations, in which implicate delicate control of the process. Hence, the membrane reactor is developed for the purpose of getting more accessibility to the distribution of hydrocarbons by altering the molar ratio of syngas

along with the reactor length. This can provide a manageable control of product composition at any targeted zone of the reactor. Two parameters are mostly considered for parametric influence on the distribution of hydrocarbons in the three constructed models of FT reactor: membrane reactor for water removal (MRW), a membrane reactor for carbon dioxide removal (MRC) and a conventional reactor (CR). This includes the inlet H_2/CO ratio and inert gas fraction effects on the final composition and the in-situ variation of the syngas molar ratio along with the reactor length. If we investigate the usual operating parameters then we will not persuade a good explanation of membrane reactor performances as the temperature and pressure have a lower influence on the permeation properties compared to the chosen parameters.

III.2.1. Inlet H_2/CO ratio alternation

The inlet H_2/CO is known for being one of the parameters that can control the molecular weight of synthesis hydrocarbons and under some consideration, the accurate valuation of this metric must be done at the first applied measurements for installing the FT plant. This includes the good choice of adequate gasification process that can so far deliver the desired composition of syngas. For instance, CTL produces a large amount of carbon monoxide and this will result in a low H_2/CO molar ratio compared to the substituted composition from other processes such as GTL and BTL that can ensure high production of hydrogen. The H_2/CO molar ratio can offer resilient and readily orientation of hydrocarbons distribution as the amount of the injected H_2 in the reactor inlet has a direct influence on FT kinetic, high or low surface recovery can shift FT reaction towards the formation of paraffin or olefins according to the energetic potential of hydrogenation. A study was carried out separately in a Fixed bed reactor to investigate the impact of the injected amount of hydrogen on the production yield and product distribution has led to

the conclusion that the increase in the inlet hydrogen to carbon monoxide molar ratio at a fixed carbon monoxide flow rate ($0.1\ mol\ s^{-1}$) was able to shift the distribution of hydrocarbons towards the production of paraffins [121]. Based on the obtained results, a high H_2/CO ratio favors the production of light-saturated paraffin including methane and ethane with a productive selectivity of 39.61% and 6.23%, respectively; while the overall production of olefins was disfavored by increasing the inlet molar ratio and this effect was clearly seen through the measurement of olefins to paraffins ratio, in which a sharp decline in the ratio was remarked. A significant behavior was attributed to CH_4 and C_2H_6, in which their selectivities were increased from 23.37 to 39.61 and 4.79 to 6.23% respectively, by raising the inlet H_2/CO from 1 to 3. This can be explained by the fact that the excessive insertion of H_2 on the catalyst surface will cause faster desorption of hydrocarbons to smaller chain lengths rather than a continuous propagation for the formation of heavier paraffin. Furthermore, implying that the H_2/CO molar ratio harms the production of hydrocarbons with high molecular weight, the total selectivity of butane and pentane was decreased from 7.3 to 5.42% by increasing the molar ratio from 1 to 3. It is evident that the increase in H_2/CO molar ratios is the adequate requirement for achieving a light mixture of hydrocarbons including CH_4 and C_2H_6, whereas lower molar ratios are desirable for high production of olefins and long-chain paraffin. These opposite trends in hydrocarbons selectivity justify the decrease in olefins to paraffins ratio. O/P ratio tends to reach the minimum value that corresponds to 0.8 at the highest molar ratio due to the great desorption rate of paraffins compared to that of olefins. Also, it can be caused by the secondary hydrogenation that takes place to convert olefins to saturated hydrocarbons. Considering hydrocarbons chain length variation, the decline in O/P ratio was the same for all ranges of hydrocarbons, which indicate that olefins readsorption for

paraffins formation by hydrogenation reactions is independent on carbon number. These results agree well with the proposed kinetic model for FT reactions and with the results that are reported in the literature [9], which exhibits an experimental investigation of the H_2/CO ratio effect on the O/P ratio. Hence, H_2/CO molar ratio is the key parameter to control and manage reactor performances. Besides, the H_2/CO molar ratio incrementation from 1 to 1.5 can conduct to a major improvement in the hydrocarbons yields, whereas the enhancement in hydrocarbons yields is less remarkable at higher molar ratios. Noteworthy, light paraffins are more sensitive to H_2/CO molar ratio change. At least, it can be said that the incorporation of a high initial amount of H_2 at the reactor inlet can shift the hydrocarbons distribution by decreasing the selectivity of olefins and favoring the formation of light paraffins and also it can be a preferential parameter for increasing the hydrocarbons yields and thus resulting in higher fixed bed reactor performances. The investigation of this effect on hydrocarbons distribution was extended to cover the new concept of FT reactors including additional separation of water gas shift reaction effluents. This may explain how could be that the change in initial composition is able to alter the equilibrium state and in which direction the distribution of hydrocarbons will be oriented regarding this effect on the permeation process. Figure III.1(a), 1(b), 1(c) and 1(d) shows the effect of the inlet hydrogen to carbon molar ratio (H_2/CO) on the entire distribution of hydrocarbons in MRW, MRC, and CR reactors. The selectivity of synthesis paraffin and olefins was investigated under an extended range of inlet ratio varied from 1 to 2.5 according to BTL technology requirements. If we do a comparative interpretation of the obtained results at the lowest value of the H_2/CO ratio and we may end up with a clear observation of the difference in the selectivities between the investigated reactor concepts. The selectivity of methane in the CR is about 24.29%,

which is lower than that of MRC and higher than the obtained value in MRW. Similar results were observed for ethane and ethylene but with lower tendency. In the case of carbon dioxide separation, the selectivity of ethane and ethylene was slightly increased, while it was decreased by applying a permselective membrane to water. These reasonable trends are due to the change in the partial pressure of hydrogen along the reactor caused by the alternation that takes place for water gas shift reaction equilibrium. By removing carbon dioxide from the reaction zone, the forward reaction rate of the water-gas shift is favored due to the low concentration of the products on the right side of the reaction. This may implicate a large production of hydrogen through carbon monoxide reaction with formed water. The increase in hydrogen amount leads to an excessive insertion of hydrogen on the catalyst surface, which may reduce the propagation rate of hydrocarbon chains and thus promotes the formation of light hydrocarbons, especially methane. This approach was largely accepted as the most appropriate explanation for the observed deviations in ASF models at high estimated values of the H_2/CO molar ratio. A similar tendency was also remarked when the variation of other reactor parameters such as temperature and gas hourly space velocity have been inspected but this referred to a different explanation of the situation. The selectivity of light hydrocarbons such as methane, propylene, and ethylene is favored by high temperatures as an intense increase in selectivity was observed for methane to reach 19%. This is also contributed to the increase in hydrogen amount due to the expected improvement in the FT reactions rate resulting in a higher formation of water that can react with carbon monoxide to produce hydrogen with relatively higher partial pressure. Hence, a positive effect was observed regarding temperature raise. But the more pronounced effect is associated with the actual modification in the catalyst occupancy by favoring particular dominancy of hydrogen

adsorption through a consistent presence of hydrogen around the catalyst surface, which can be ensured by the integration of permeselective membrane to carbon dioxide. By investigating the reaction rate of water gas shift we can get better prediction and visualization of the effect of selective permeation on the equilibrium state. As presented in Figure III.2(a), reducing the concentration of carbon dioxide in the reaction area will shift the equilibrium of WGS reaction towards the production of hydrogen by increasing the reaction rate from a value of $1.37x10^{-4}$ to $3.83x10^{-4}\, mol\, kg^{-1}\, s^{-1}$.

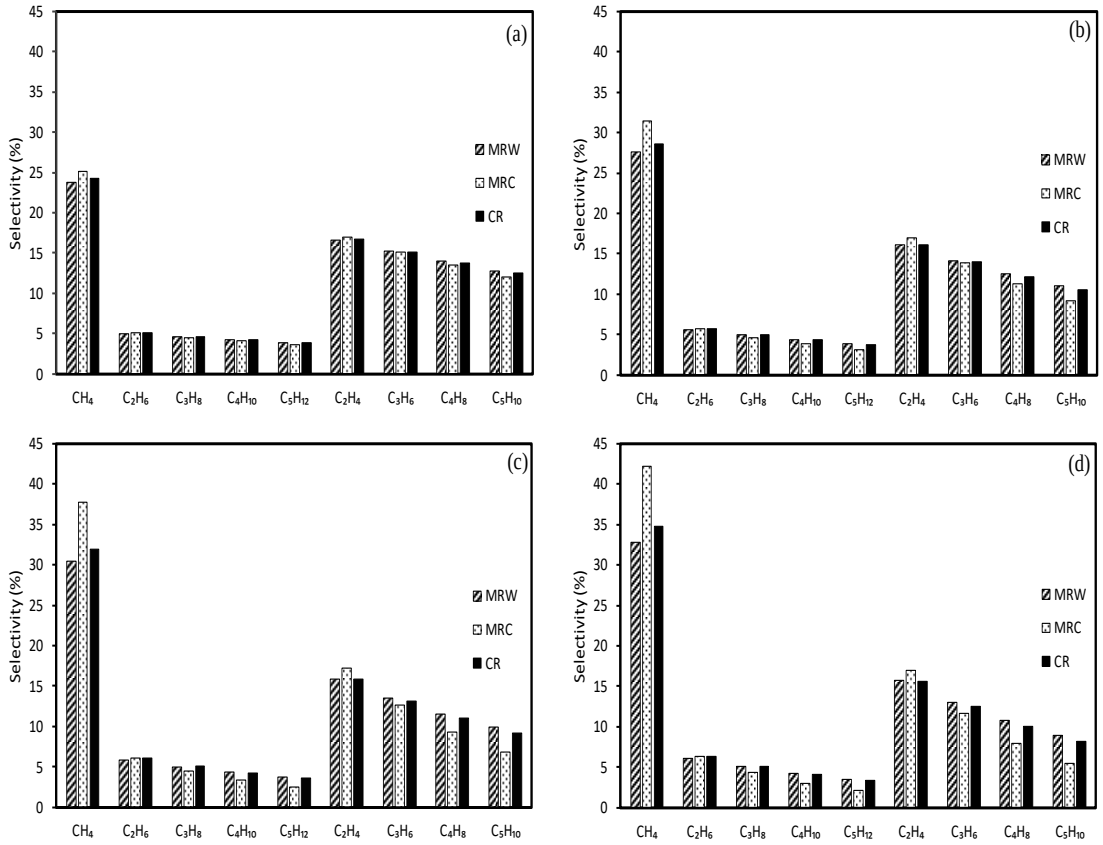


Figure III.1: Effect of the inlet H_2/CO ratio on hydrocarbons selectivity a: $(H_2/CO)^0=1$, b: $(H_2/CO)^0=1.5$, c: $(H_2/CO)^0=2$ and d: $(H_2/CO)^0=2.5$. Conditions: T= 533K, P=20bar and GHSV= $4000h^{-1}$.

If we include a further comparison between only the upper and lower limit for the range of the inlet molar ratio we can find that the effect becomes more remarkable when the highest value is considered. This was clearly illustrated in Figure III.2(b). In contrast, it was subjected that the elimination of water has led to a negative effect on the overall reaction rate of WGS due to the inhibition of the forward reaction rate by the controlled reduction in the partial pressure of water. This will boost the reaction reversibility to reach its equilibrium state again by compensating the occurred shortage in the concentration of the reactants through a relative consumption of the formed compounds including hydrogen and carbon dioxide. This will result in ta higher rate of the reverse water gas shift reaction, which will be substituted from the forward reaction rate. This effect was illustrated using the representative evolution of the in-situ H_2/CO ratio along with the reactor length. It can be seen from Figure III.3(a) that water elimination is responsible for a persistent decrease in the H_2/CO molar ratio since that hydrogen reacts with the formed carbon dioxide for the production of carbon monoxide.

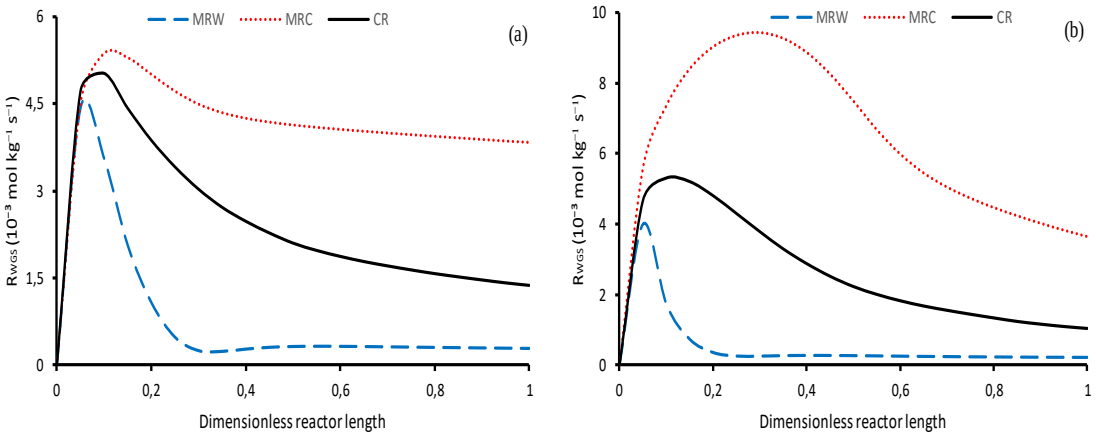


Figure III.2: WGS reaction rates evolution in the reactors configurations a:$(H_2/CO)^0$=1, b:$(H_2/CO)^0$=2.5. Conditions: T= 533K, P=20bar and GHSV= 4000h^{-1}.

This direct alternation in the syngas composition can promote a large variation in the distribution of hydrocarbons as the molecular weight of hydrocarbons is strongly related to the adsorbed amount of carbon monoxide and hydrogen. Such an effect of carbon dioxide removal on the H_2/CO ratio results in high productivity of methane and ethane. At a high value of the inlet H_2/CO molar ratio (2.5), the selectivity of methane and ethane reach 42.2% and 6.37%, respectively, with a growth rate higher than the reported one in MRW and CR. This feature may infer and support the logical assumption that MRC is highly recommended for obtaining light hydrocarbons by favoring the production of water gas shift hydrogen. The selective composition of the remaining hydrocarbon was also investigated regarding its dependency on the H_2/CO ratio. The effect is different from the observed one for methane and ethane. For general observation, the selectivity of propane, butane, and pentane are favored by applying a permeselective membrane to water. Indeed, the increase in the inlet H_2/CO ratio has decreased the overall production of butane and pentane and has shown a dual effect on propane production in the case of MRC. Increasing the inlet molar ratio from 1 to 1.5 can conduct to a slight increase in propane selectivity. But a persistent increase in the molar ratio from 1.5 to 2.5 results in a negative trend. As indicated herein, the termination rate of hydrocarbons is directly related to the concentration of hydrogen in the reaction area. As such a high increase in the molar initial ratio will limit the formation of propane and favor the production of lighter paraffin such as methane and ethane. This can be also related to the high increase in the H_2/CO ratio along the reactor length (Figure III.3(d)). In fact, water elimination maintains the partial pressure small enough to not inhibit the formation of heavier paraffin by increasing the reverse WGS reaction rate. This will conduct a favored consumption of

hydrogen by the WGS reaction and thus higher formation of carbon monoxide is achieved resulting in a lower in-situ syngas molar ratio.

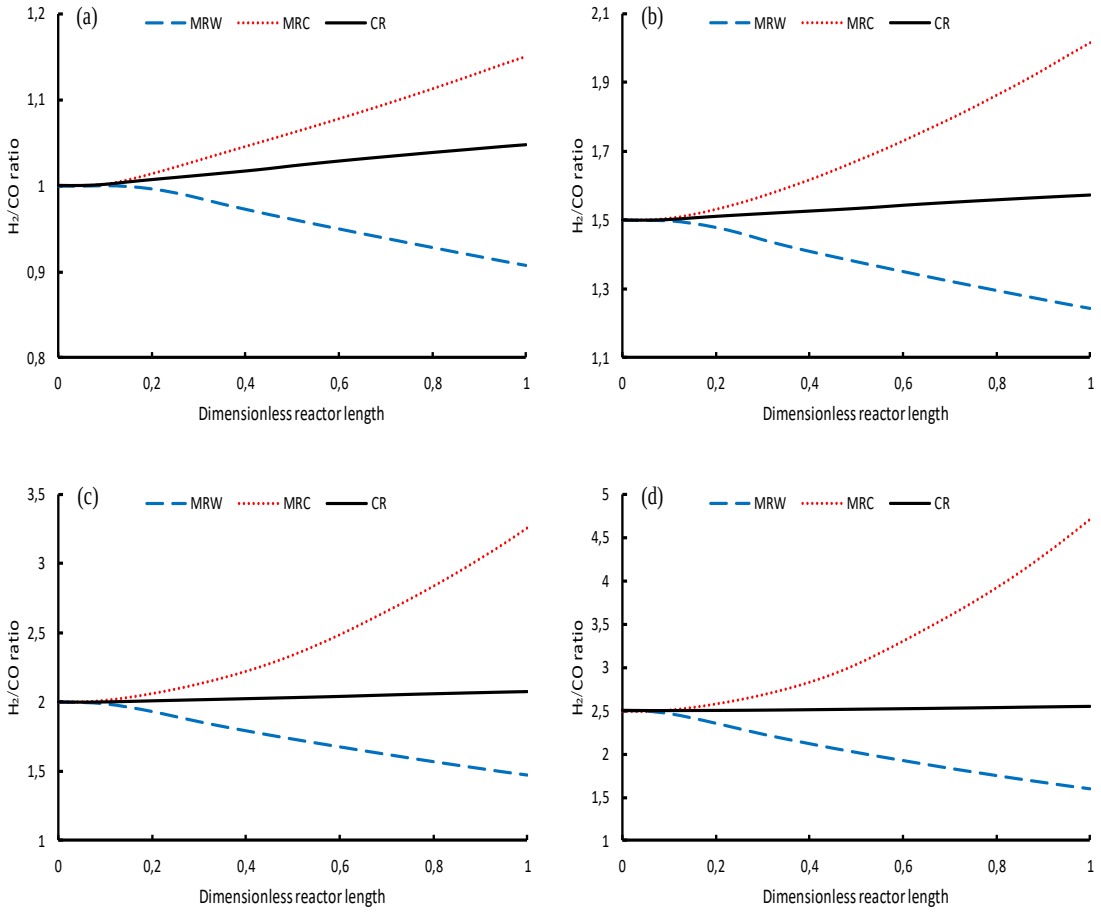


Figure III.3: Evolution of H_2/CO ratio along the reactor at different initial values a: $(H_2/CO)^0$=1, b: $(H_2/CO)^0$=1.5, c: $(H_2/CO)^0$=2 and d: $(H_2/CO)^0$=2.5 Conditions: T= 533K, P=20bar and GHSV= 4000h^{-1}.

Besides, if we look further on the productive deviation of olefins we can notice that the increase in the molar ratio disadvantage the overall production of olefins. This in agreement with what can be expected by the higher presence of hydrogen in the reaction area, which conducts the assisted hydrogenation of olefins to the formation of saturated hydrocarbons. Evidently, increasing the inlet H_2/CO ratio has caused a decrease in the

Olefin to Paraffin (O/P) ratio in all investigated configurations. This was indicted in Table III.1, in which a slight change in the O/P ratio was observed for lower integration of the inlet syngas molar ratio, while higher H_2/CO values will provoke a large difference between the three configurated sets of reactors. The *in-situ* water removal enhances the O/P ratio and the *in-situ* carbon dioxide removal inhibits the formation of olefins. Thus, MRW is referred to be the preferential configuration for achieving high olefins distribution.

Table III.1: Measured O/P ratios in the reactor exit for different $(H_2/CO)^0$ ratios.

$(H_2/CO)^0$ ratio	**Measured O/P ratios**		
	MRW	**MRC**	**CR**
1	1,4138	1,3594	1,3838
1.5	1,1645	1,0542	1,1177
2	1,0278	0,8486	0,9657
2.5	0,9384	0,7228	0,8637

III.2.2. Inert gas fraction alternation

The permeation of water and carbon dioxide through a membrane is ensured by the generated motrice force by the pressure gradient between the reaction and the permeate side. Thus, the fraction of inert gas in the permeate side plays an important role in altering this variation of pressure through increasing it or decreasing it. As the elimination of water and carbon dioxide is strongly related to the partial pressure of these components in the permeation zone, a higher concentration of inert gas will consequently provoke a decrease in the impact of cumulated species permeation on the membrane performances. The increase of the driving force may be caused by the decrease of the partial pressure of the

evacuated gas from the permeate side or an increase in its concentration in the reaction side by improving the production rate. To clearly interpret the first deviation and see how the change in separation efficiency of carbon dioxide and water may alter the final composition of products, an examination of the effect of the inert gas fraction on hydrocarbons distribution was investigated by using arbitrary values and it was limited to a diluted inert gas varied from $I_{index} = 3\ to\ 12$. Figure III.4 shows the effect of the inert gas fraction in the permeate side on hydrocarbons selectivity at a high inlet H_2/CO molar ratio (2.5). It was found that the initial distribution of paraffin and olefin in each reactor remains constant at all ranges of the inert fraction.

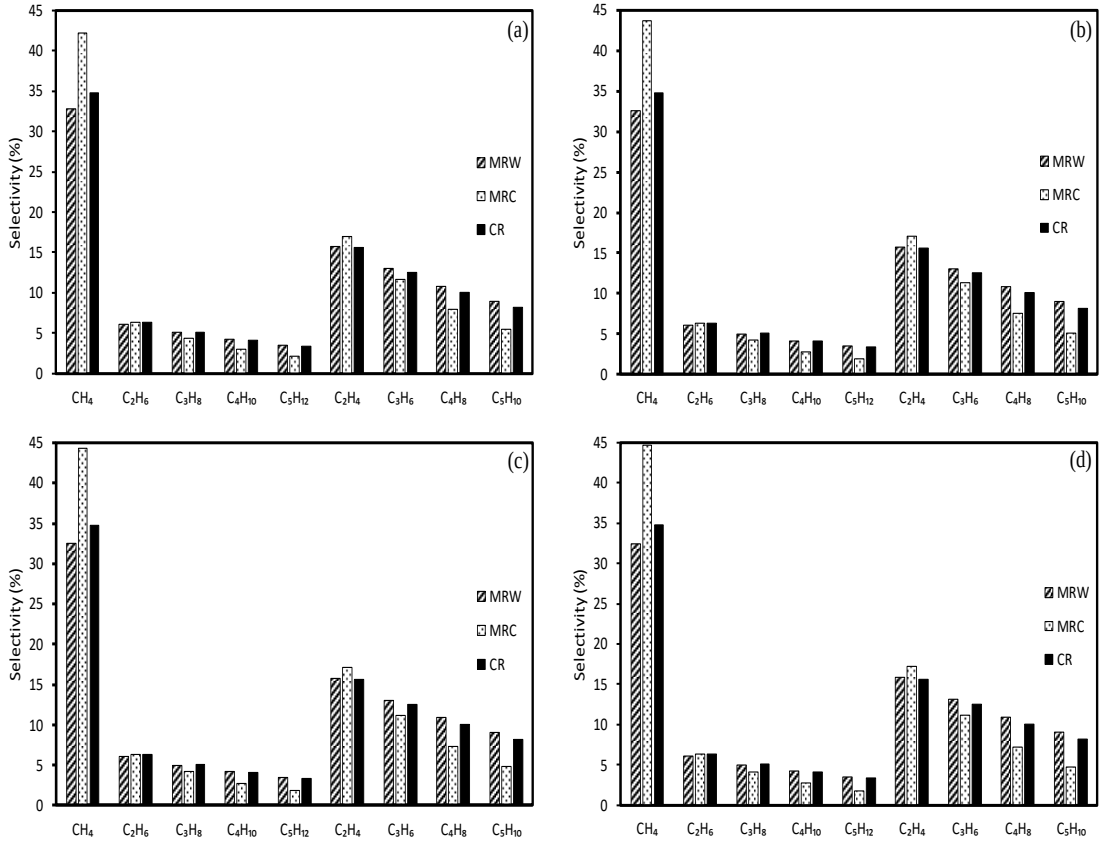


Figure III.4: Effect of the inert gas fraction in the permeate side on hydrocarbons selectivity for different I_{index}. a: $I_{index} = 3$, b: $I_{index} = 6$, c: $I_{index} = 9$, d: $I_{index} = 12$. Conditions: $(H_2/CO)^0$=2.5, T=533 K, P= 20bar, GHSV=4000h^{-1}.

Actually, the increase in the fraction of inert gas has led to a major improvement in the selectivity of dominant components in the hydrocarbon mixture. This reflects a decrease in the selectivity of C_2 to C_5 paraffin in each membrane reactor, whereas, a distinct effect was observed for methane production in MRW compared to other configurations. The selectivity of methane in MRC was significantly increased from 42.2 to 44.75% by increasing the fraction of inert gas (I_{index}) from 3 to 12. In contrast, a decrease in methane selectivity was observed in MRW. The impact can be further explained by the fact that the evolution of water and carbon dioxide permeation along the membrane reactors (Figure III.5(a) and III.5(b)) is an indicator of how high or low membrane separation can change hydrocarbons distribution. It should be noted that at a higher fraction of inert gas in the permeate side, the permeation flux increase towards maximum values of 3.72×10^{-2} $mol.m^{-2}.s^{-1}$ and 2.44×10^{-2} $mol.m^{-2}.s^{-1}$ for carbon dioxide and water, respectively. This leads to a distinct effect on the production rate of hydrogen and carbon monoxide by water gas shift reaction (Figures III.6(a), III.6(b) and III.6(c)). It was found that the high increase in H_2/CO ratio along the reactor can be achieved in MRC at the inert gas fraction of 12 (Figure III.6(d)). In the case of water removal, increasing the inert gas fraction has shown a negative trend in the evolution of H_2/CO. The forced deviation of the molar ratio can be attributed to the change in the equilibrium of the WGS reaction. However, great water separation results in an increase in carbon monoxide formation by the reverse WGS reaction while high carbon dioxide separation favors the production of hydrogen by the forward WGS reaction. According to this change in hydrogen and carbon monoxide amount in the reaction area, it is obvious to see the high production of methane in MRC and an overall decline of the paraffin selectivity in MRW.

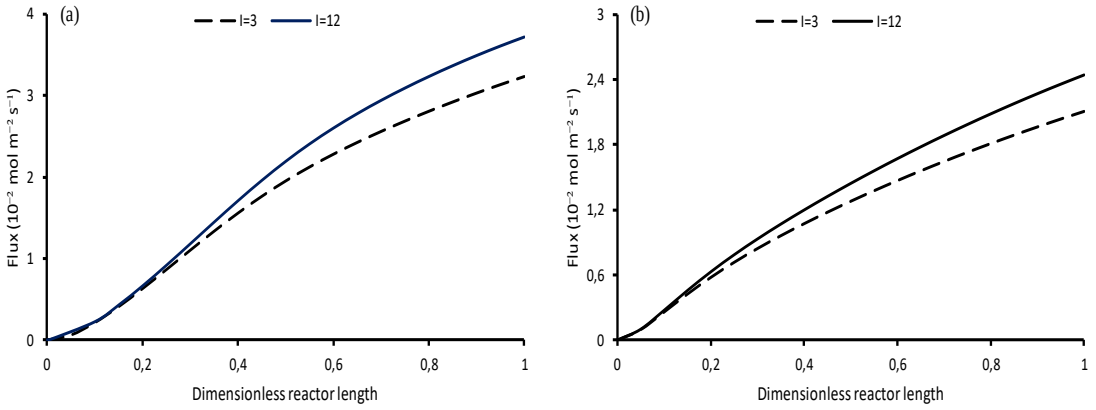


Figure III.5: Effect of the inert gas fraction on the permeation flux of carbon dioxide (a) and water (b). Conditions: T= 533K, P=20bar and GHSV= 4000h^{-1}.

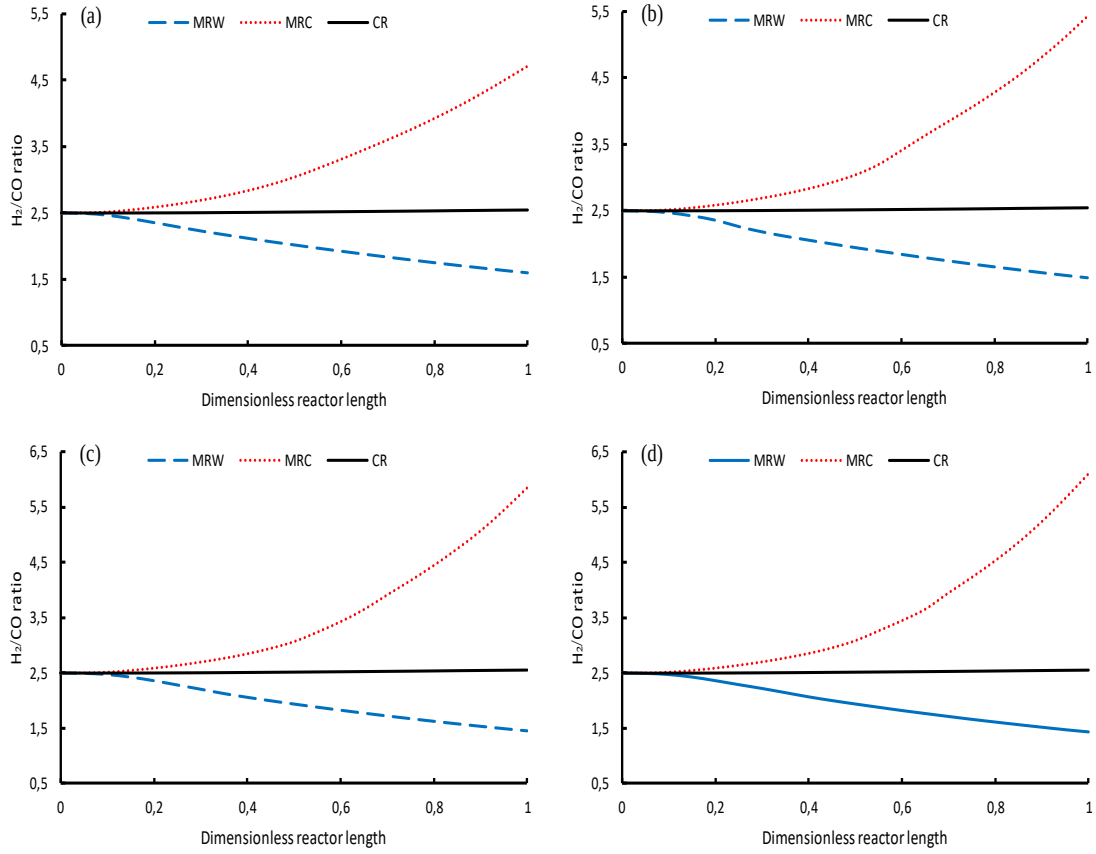


Figure III.6: Evolution of H_2/CO ratio along the reactor for different I_{index} a: $I_{index} = 3$, b: $I_{index} = 6$, c: $I_{index} = 9$ and d: $I_{index} = 12$ Conditions: T= 533K, P=20bar and GHSV= 4000h^{-1}.

Furthermore, a comparative interpretation of olefins selectivity has shown that the increase in the fraction of inert gas enhances the formation of unsaturated hydrocarbons in MRW due to the higher decrease in H_2/CO ratio along the reactor. In addition, the implantation of the perm-selective membrane for carbon dioxide removal favors the formation of ethylene. Otherwise, the selectivity of C_3 to C_5 olefins in MRC can be reduced by increasing the fraction of inert gas with a significant decline reported for the selectivity of pentene, in which present a diminution from 5.48% to 4.73%, measured at a fraction of inert gas (I_{index}) of 3 and 12, respectively. It can be also concluded from results summarized in Table III.2 that any increase in the fraction of inert gas in MRC conducts to moderate hydrogenation of olefins to paraffin as indicated by the diminution of the O/P ratio. At a low range of inert gas fraction (I_{index} from 3 to 6), the decrease in the O/P ratios was more pronounced. Moreover, an increase in the O/P ratios was observed in the MRW due to the hydrogen dilution. This would mean that for higher separations, the composition of hydrocarbons consists basically of methane in MRC and olefins in MRW.

Table III.2: Measured O/P ratios in the reactor exit for different fractions of inert gas (I_{index}).

I_{index}	**Measured O/P ratios**		
	MRW	**MRC**	**CR**
3	0,9384	0,7228	0,8637
6	0,9491	0,6958	0,8637
9	0,9537	0,6834	0,8637
12	0,9562	0,6762	0,8637

CHAPTER IV

Effect of Non-ideal Permeselectivity on Hydrocarbons Distribution

IV.1. Diffusion process

Regarding the required configuration, the integration of a permeselective membrane to the reactor conception can assure selective separation of products from gas mixture or readily orientation of the reactant flow [86]. The MFI membrane has been proposed as one of the recommended types of membranes for the separation and the purification of hydrocarbons mixture from carbon dioxide [106,122,123]. As we concluded from the results of the previous chapter, the utilization of the FT membrane reactor for the *in-situ* removal of carbon dioxide is highly promising in the way that the technology can orientate the distribution of synthesis hydrocarbons without any access to the parameters of the reactor. Besides this major contribution that is obtained from the intensification of FT reactor performances, further assumptions may be envisaged to get closer to reality. Widely known in the literature that the choice of diffusion mechanism to model the permeation of particular species depends on multiple factors that can be shortened to the variation in the surface affinity, the kinetic diameter of the molecules and the size of the porous media. We distinguish two mechanisms that are more covered for explaining the selective separation of species through the zeolitic membrane. This includes the micropores diffusion mechanisms: surface diffusion and gaseous diffusion. The micropore diffusion can be considered as surface diffusion only if the pore size becomes comparable to the molecular size. The activated diffusion which known as gaseous diffusion is strongly related to the molecular size and shape, pores size and the interaction between the pore walls and the gas molecules. Both surface diffusion and gaseous diffusion were introduced to describe the permeation of the studied mixture through the silicalite-1 membrane in the Fischer-Tropsch reactor. As we mentioned in Chapter II that hydrocarbons and other species such as hydrogen are subjected to different permeation

mechanisms. In reality, the contribution of each mechanism to the overall permeation is related to the operational parameter of the reactor. At a more accurate level, we should accomplish the permeation process of surface diffusion by gaseous diffusion through joining the two mechanisms in one descriptive. For defining which mechanism is more predominant at a specific range of variation in the process conditions, analytical quantification of the permeation based on separate modelization using surface diffusion and gaseous diffusion approaches. Due to the limited availability of data in the literature, we applied the gaseous diffusion model only CH_4, C_2H_6, C_3H_8, C_4H_{10}, CO and H_2 species. The contribution of each mechanism was estimated by calculating the overall permeation of the FT mixture.

VI.2. Predominant mechanism under FT reaction conditions

By investigating the evolution of permeation as a function of temperature and pressure simultaneously in Figure IV.1, it can be seen that the utilization of the gaseous diffusion model has generated a negligible amount of permeation compared to the surface diffusion model. The permeate flux of the surface diffusion is higher than the permeate flux of gaseous diffusion by a magnitude of 17 times under the investigated range of initial pressure and temperature. The larger difference was observed at 533 K and 20 bar with total permeate flux equal to 0.1819mol s^{-1} and 0.02125mol s^{-1}, for surface diffusion and gaseous diffusion; respectively. These results indicate that the permeation is not only dependent on pressure gradient, which is the case of gaseous diffusion; instead, molecular adsorption has a higher contribution to the overall permeation through the silicalite-1 membrane. It is also illustrated that the surface diffusion contrary to the gaseous diffusion has a nonremarkable variation with temperature. The flux is defined as velocity times density, so, at high temperature, the diffusion becomes dependable only on the velocity

as the density is negligible due to the desorption process. This trend is in agreement with the literature, where a slight decrease in the permeate flux of several hydrocarbons was observed at the same investigated range of temperature [92]. In fact, the surface diffusion becomes less influenced by the molecular adsorption at high operating temperatures and this will result in a minor change in the permeate flux. The permeation is also related to the molecular interaction with other species in the gas mixture. Research done by Shiguang et al [124] reveals a significant decline in CO_2 permeation on the SAPO-34 membrane in the presence of water. This can be related to competitive adsorption. Otherwise, the gaseous diffusion was enhanced upon temperature increase. It is relevant from these observations that the investigated range of temperature exhibits a reflection point where the gaseous diffusion starts to take place in the permeation process as a functional mechanism. For pressure change, the effect is oppositely different from temperature. The surface diffusion increase with pressure, while the gaseous diffusion remains constant at all range of study. In fact, low mobility can happen when we deal with large interactions between molecules at high pressure. At this point, the profile of permeation is strongly associated with the affinity of molecules to the surface. This can be a good explanation of the observed relation of surface diffusion to the pressure. A parametric investigation was applied in the following section for a better understanding pressure effect on the separation process. Considering the obtained results, it can be said that is more appropriate to define the permeation through the silicalite-1 membrane using only surface diffusion as a dominant model.

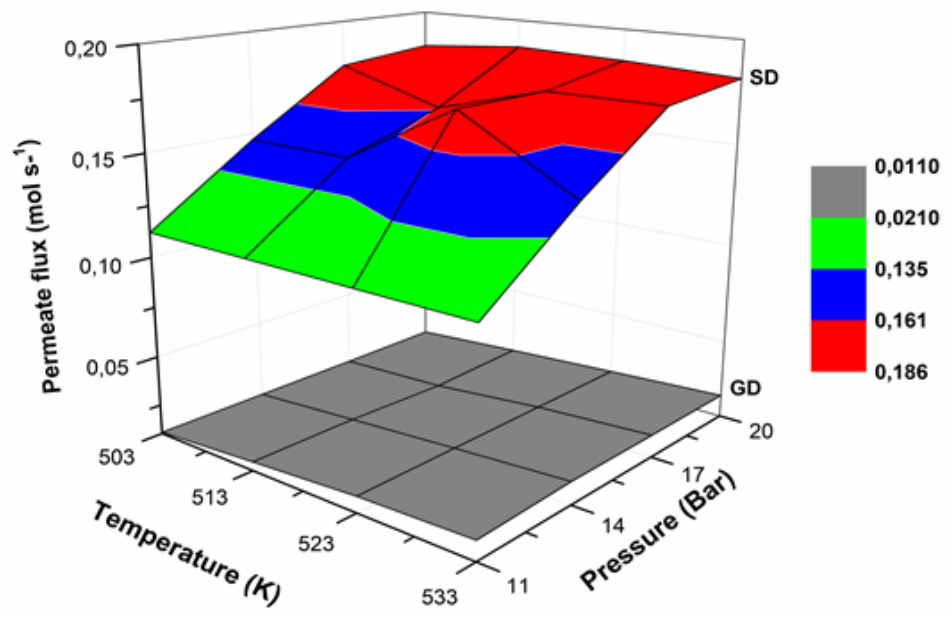


Figure IV.1: Contribution of surface diffusion (SD) and gaseous diffusion (GD) on the total permeation under simultaneous variation of initial temperature and total pressure.

IV.3. Pressure effect on CO_2 permeselectivity

After performing the overall permeation using two different mechanisms, we can say that based on our findings we will use surface diffusion as a representative permeation mechanism for all mixture. The majority of the reported separations on zeolite lie on mainly surface diffusion and sometimes capillary condensation due to the high affinity of organic material to the mineral surfaces. This assumption is applied for further investigations. To have more details about the process behavior, the flux of produced paraffins, olefins, syngas, water and carbon dioxide molar flow rates along the reactor at a temperature of 533K and a total pressure of 11bar are predicted and presented in Figure IV.2. It should be noted that at these operating temperatures and pressure the surface diffusion mechanism appears as the major process as discussed in the above section. So, in the following only surface diffusion was considered to quantify the permeation of different components through the silicalite-1 membrane. It is clear from the presented

results that the permeate fluxes of most hydrocarbons follow a nonlinear deviation along the reactor length, in which no measurable value of permeation was recorded at the first one-third region of the reactor followed by a slight increase in the permeate flux. For ethylene, the evolution of the permeation presents an exceptional case, in which no delayed enhancement in the permeate flux was observed. This intriguing trend has positively affected the overall permeation of ethene. Actually, the outlet permeates flux for ethene is relatively larger than that of other hydrocarbons. As supporting evidence, it is clearly seen through the variation of the residual flux along the reactor length that the flux of ethene tends to reach the minimum value of 1.71×10^{-4} mol s^{-1}. In general cases, the following sequence in the permeate flux was perceived: $C_2H_4 > CH_4 > C_3H_6 > C_4H_8 > C_2H_6 > C_5H_{10} > C_3H_8 > C_4H_{10} > C_5H_{12}$. Considering the obtained similarity between this sequence and the one related to the reaction flux, it is relevant that the distinctive variation in the permeate flux is mainly due to the fact that the concentration of studied species in the reaction side influences the surface diffusion. This could be attributed to the increase in driving force across the membrane layer. Raising the concentration will result in a higher pressure gradient between the reaction and the permeate sides. However, it was reported in the literature that the surface diffusion coefficient is inversely proportional to the kinetic diameter [124]. These results fit well with our findings but only when we perform a comparison between the same kinds of hydrocarbons including paraffin or olefins separately. The olefins diffuse more intensely than their corresponding paraffin even they are characterized by greater kinetic diameter [125]. This factor is critical for describing the inhibition effect only if large size molecules compared to pores diameter is investigated.

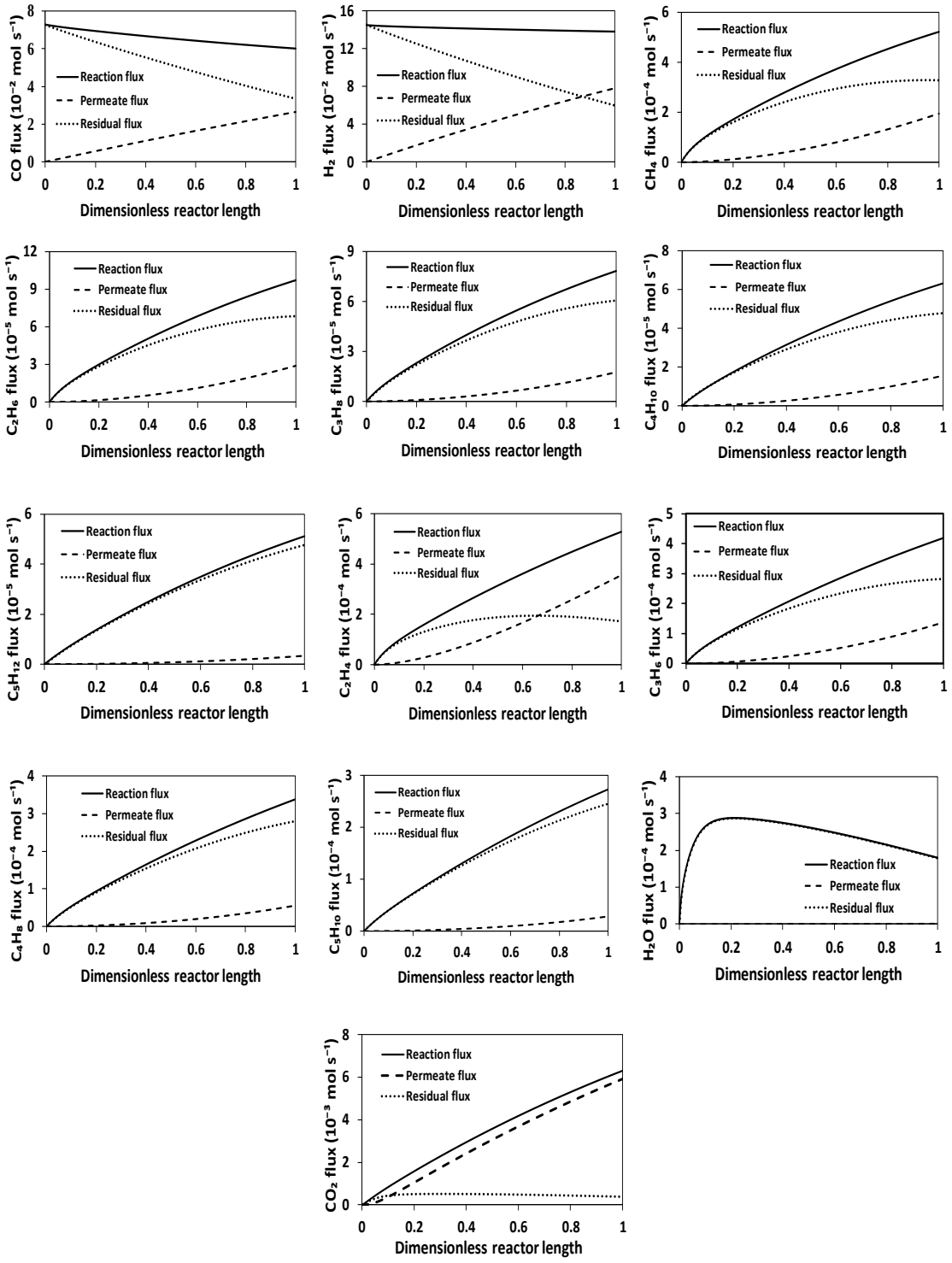


Figure IV.2: Evolution of reaction flux along the reactor at an initial pressure of 11bar.

According to the reported data in Chapter II about the difference in adsorption energy of studied species, the adsorption is proportional to the molecular weight. This means that

heavier hydrocarbons tend to have remarkable adsorption on the surface of the membrane. At the experimental level, this was explained by the expected interaction between hydrocarbons molecules and the surface nearby the pore opening as we expect a high affinity of heavier hydrocarbons to the surface and the larger size due to the high molecular weight will conduct the heavy hydrocarbons to be stuck to the wall of the pore and thus a sharp reduction in the mobility. Besides, we can also observe that paraffins are more likely to be absorbed on the silicalite-1 surface compared to olefins but this has no positive addition that can cause a preferable permeation of paraffin. This indicates that at high levels of operating temperature which are similar to our case, the surface diffusion mechanism becomes dominated by defusing either than the enhanced adsorption becomes an adversative metric to the overall permeation as the heavier hydrocarbons are subjected to great adsorption. Hence, a decline in the absorbed amount will exhibit a major influence on the permeation of heavier hydrocarbons compared to light hydrocarbons. Similar behavior represents a plausible reason for the obtainment of higher olefins and light paraffin permeation through the membrane. In fact, the deviation of surface diffusion is determined in terms of a combination between molecular adsorption and diffusivity. At higher temperatures, at which the adsorption is minimal, the permeation is shifted to become more relevant to the diffusivity. At this point, the strongly adsorbed components will be exposed to higher regression which is caused by the relative reduction of adsorption in the shade of the modest increase in diffusivity. Thus, lower permeation was observed for pentane compared to that of hydrocarbons with smaller chain lengths. According to Figure IV.2, the permeate flux of the carbon monoxide and the hydrogen lies around 2.65×10^{-2} mol s^{-1} and 7.82×10^{-2} mol s^{-1}, respectively. This corresponds to relatively higher permeation compared to the recorded conversions. From the plot of the

residual flux as a function of dimensionless reactor length, it is clear that 46% of carbon monoxide remained at the reactor outlet against only 41% for hydrogen. These findings indicate that the H_2 has the greatest diffusion through the silicalite-1 membrane. By taking into account this difference in the permeation between the H_2 and the CO, the distribution of hydrocarbons will probably be oriented according to the evolution of the molar ratio that corresponds to this syngas. At the given pressure, as expected, no permeation was observed for water. This is due to the nature of the used MFI membrane. However, it was reported in Chapter II that the low content of aluminum in the silicalite-1 structure gives it a hydrophobic character. Thus, the water will diffuse slowly through the membrane because of the low molecular occupancy. On the other side, carbon dioxide exhibits an optimal permeation, where 94% of the reaction flux was permeated along the reactor length. In fact, the high selective separation of carbon dioxide supports the assumption that considers the negligible permeance of other components. As was seen herein (Figure IV.1), the surface diffusion is more sensitive to pressure change and quite independent on temperature. However, several studies [87,92,104] reported that the diffusion through MFI membranes is highly sensitive to the molecular adsorption and thus a decline in species permeation was observed at high temperatures.

For a more illustrative explanation of the pressure effect on the permeation process, in which separative quantification of surface diffusion is used to judge the difference between components permeation. This further investigation was performed on determining the evolution of the reaction flux, the residual flux and the permeate flux of permeate at different values of pressure: 14bar, 17bar and 20bar (Figures IV.3, IV.4 and IV.5). The quantification of mass transport in function of temperature is quite delicate due to the presence of many parameters that describe the permeation model was assumed

constant while it's dependable on temperature change. This includes the activation energy of diffusion and the heat of adsorption. According to what was seen through the depicted results, the following common behavior was perceived as a function of the pressure. The reaction flux of products tends to reach a maximum value with pressure increase from 14 to 20bar as the increase in pressure will boost the reaction rate of FT synthesis. The initial pressure constitutes the partial pressure of hydrogen and carbon monoxide and by raising it we expect to have a higher portion of the partial pressure of reactants that can occupy more active sites on the catalyst surface and thus ensuring higher reaction activity and production yield. The increase in the reaction flux was also observed for the variation of permeate flux. This is has resulted in a relative decrease in the residual flux along the reactor. The produced amount of permeate is subjected to a spontaneous vanish from the reaction side a relatively higher pressure, in which the permeate flux is remarkably increased to reach the point where it becomes comparable to the reaction flux. Further increase in pressure will conduct constant reaction flux after crossing about 80% of the reactor length (Figure IV.5). Hence, a total permeation of H_2 and CO could be obtained. This effect shows a valuable enhancement in the permeation upon pressure raise. At an efficient stage, it can be said that the utilization of the silicalite-1 membrane has granted a big separation of carbon dioxide among the FT mixture. However, the use of Slicallite-1 will eliminate the water effect on CO_2 permeation due to the hydrophobic character of the membrane. Contrary to water, other species such as CH_4 and H_2 can permeate through Sillicalite-1 with different ratios according to change in the molecular structure an affinity to the membrane surface. As can be seen, the permeation of CH_4 and H_2 can be neglected against CO_2 permeation at all ranges of pressure variation.

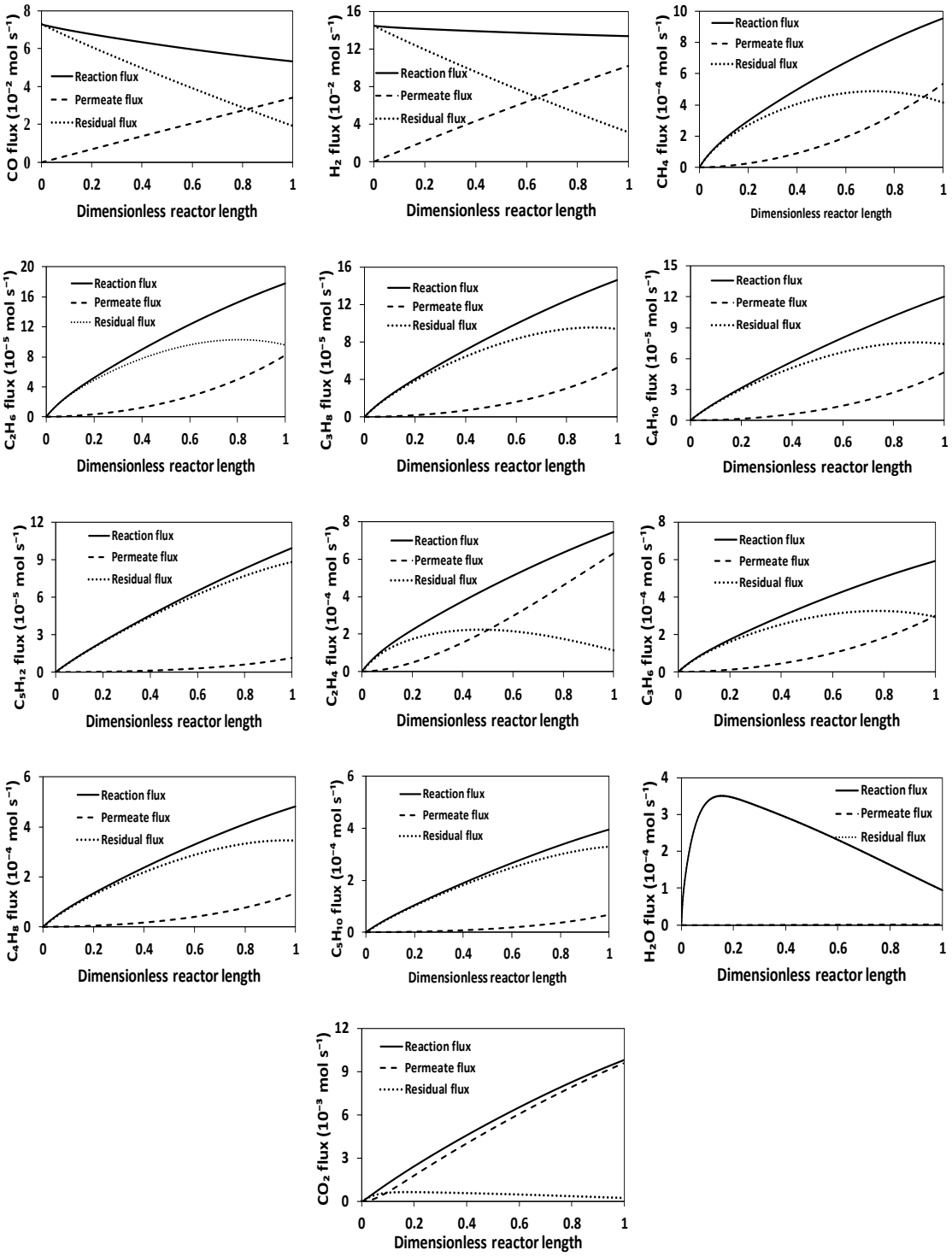


Figure IV.3: Evolution of reaction flux along the reactor at an initial pressure of 14bar.

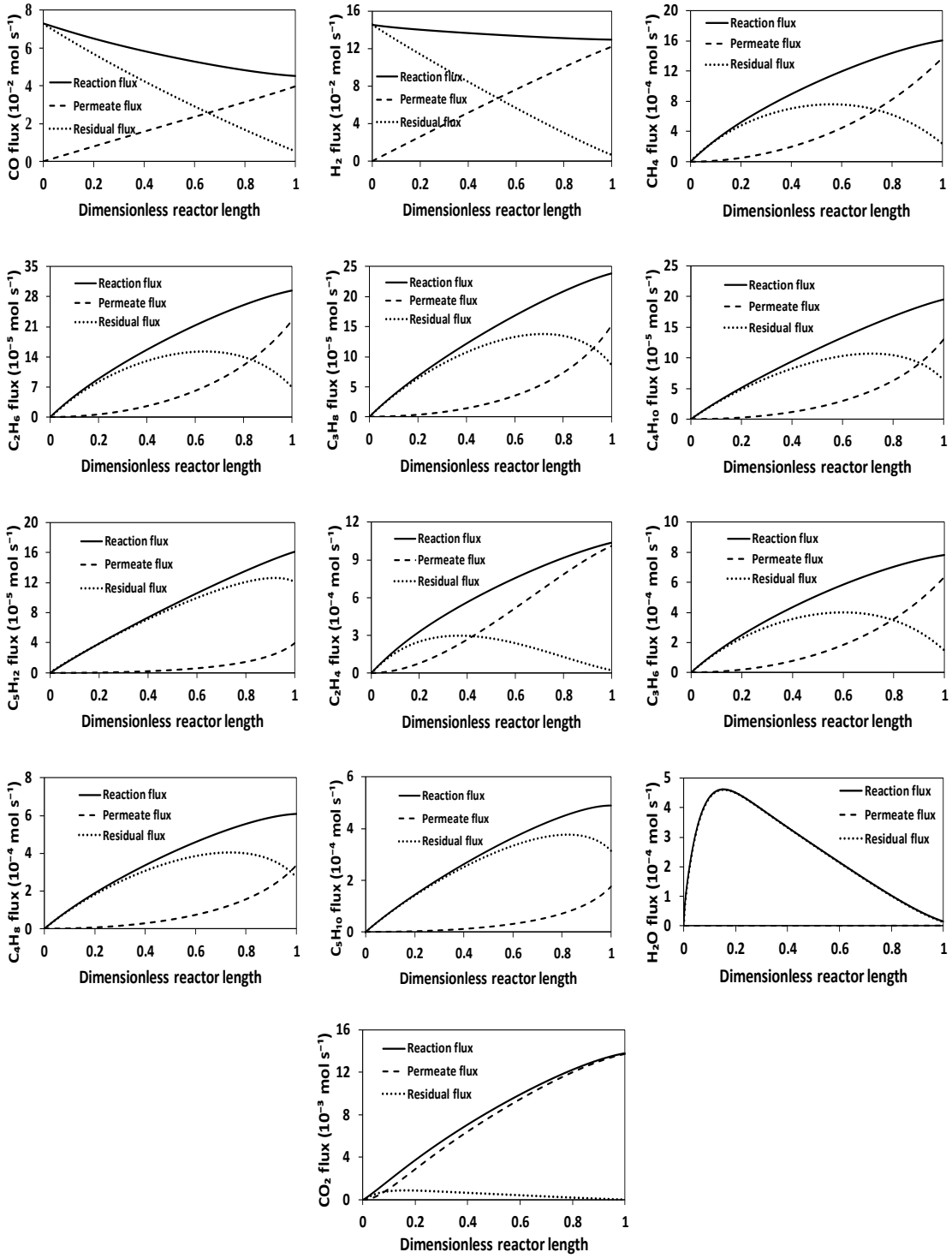


Figure IV.4: Evolution of reaction flux along the reactor at an initial pressure of 17bar.

As the variation of overall permeation was found to be less likely to change as a function of temperature (Figure IV.1), we did not investigate the effect of temperature on the component's diffusion through the silicalite-1 membrane. Also, assuming independent

diffusion parameters on the temperature at a small scale of variation (10°C) can be misleading in the determination of an accurate model. An experiment done by Poshusta et al [103] on binary gas mixture permeation has shown that CO_2/CH_4 selectivity is equal to 5.5 at room temperature and can decrease upon temperature increase. The same behavior was observed in farther studies [92,101,102]. In order to ensure a deep proceeding in the efficiency of the silicalite-1 membrane, the permeation of different species was restricted to be independent on the reaction flux. In this case, a permeation factor was basically used instead of permeate flux to define the efficiency of the membrane. Figure IV.6 displays the variation of the permeation factor as a function of pressure. Regarding the variation of this new metric, it can be concluded that raising pressure will boost the overall permeation, at which desirable separation properties were obtained. At 20bar, the permeation factor of all components goes through an optimal value of 1. This means that a total permeation of reaction flux has occurred. For water, the increase in the permeation factor does not indicate that there is an improvement in the separation efficiency upon pressure raise. Otherwise, it is mainly due to the observed decline in the reaction flux. The water is produced during the FT reaction and then consumed by the secondary equilibrium water gas shift reaction in order to produce hydrogen and carbon dioxide. So, pressure raise will positively affect the global rate of FT reactions in the way that most of the produced water is highly reacted with carbon monoxide. At a low range of investigation, the permeate flux of water becomes relatively comparable to the corresponding reaction flux. Even though, high pressures can guarantee a very slight increase in the permeate flux of water. According to the applied mathematical model, the initial pressure has a direct influence on the partial pressure of permeates. This particular enhancement in the permeation factor is due to the increase in

the pressure gradient. In fact, similar results were obtained from permeation experiments [92].

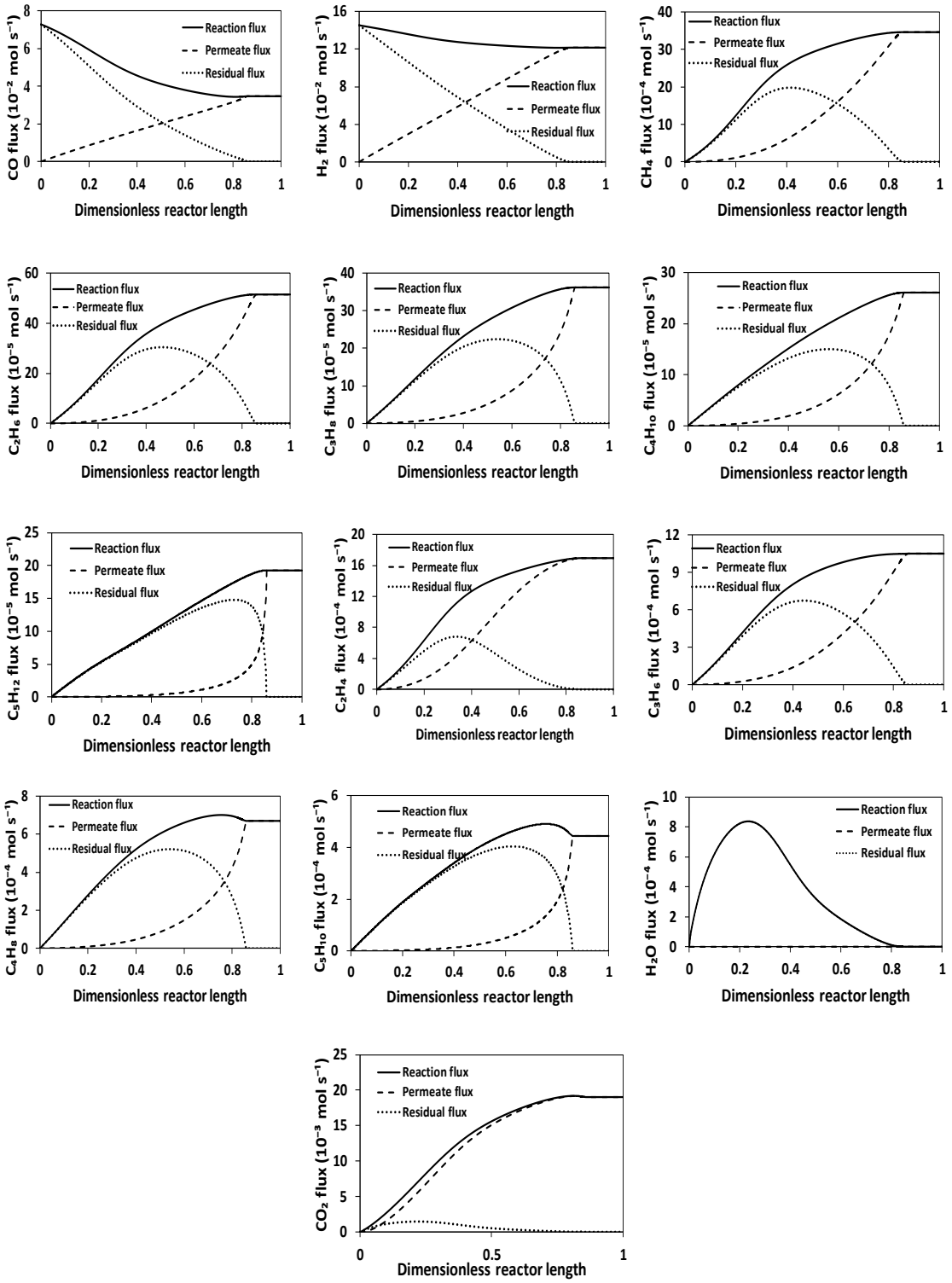


Figure IV.5: Evolution of reaction flux along the reactor at an initial pressure of 20bar.

At a comparative state, the permeation factor of the different species exhibits the following sequence: $CO_2 > C_2H_4 > H_2 > CO > CH_4 > C_3H_6 > C_4H_8 > C_2H_6 > C_4H_{10} > C_3H_8 > C_4H_8 > C_5H_{10} > C_5H_{12} > H_2O$. Symmetric order could be attributed to the differential diffusivity of permeates through the membrane and not concentration-dependent.

Regarding the results presented in Figure IV.7, the selective separation of carbon dioxide over the other components has shown a maximum for pentane by a factor of 13.75 and a minimum for ethene by a factor of 1.39 at a given pressure of 11bar. By increasing pressure, the selectivity intensely decreases in the shade of preserving the original order of magnitude. No selective separation was obtained for carbon dioxide at 20bar. Some experiments reported that the permeation of gas mixture decrease with pressure but the selective permeation of CO_2 improves [87,103]. There is some explanation indicates that this is happened because of the increase in CO_2 adsorption. This is not true because the increase in pressure can not eliminate the temperature effect on CO_2 loading. At high temperatures, the surface coverage is low to be compensated by pressure. Also, if the adsorption increase then the ratio of CO_2/CH_4 flux would rather increase. Hence, it is widely accepted that the decrease in the selective permeation of CO_2 is due to the increase in other components permeation. At high pressures, the adsorption of hydrocarbons and other FT species the Sillicalite-1 surface becomes important. From this point of view, it is relevant that the selective permeation of CO_2 can be reduced relative to the amount of other species permeation. The outlet olefins to paraffin ratio were measured and compared to the case where only carbon dioxide was assumed to be permeable through the silicalite-1 membrane. At 11bar, the O/P molar ratio is around 1.78 which is slightly lower than the obtained ratio for one component permeation (1.85). This was caused by the high permeation of olefins over paraffin. In the shade of these results, remarkable enhancement

in the production of olefins was observed. By comparing the variation of syngas molar ratio in the reaction side, it can be concluded that the higher production of olefins is related to the remarkable decline in the partial pressure of hydrogen compared to that of carbon monoxide, as the molar ratio decreased from an initial value of 2 to 1.79 at the reactor outlet. This trend in syngas composition will favor the formation of unsaturated hydrocarbons including olefins. These results fit well with the investigated reaction rates of permeate. It can be so recorded from the results that the reaction rate of propene is about $0.86x10^{-4}$ mol Kg^{-1} s^{-1}. This is 6 times higher than that of the corresponding paraffin. Assuming syngas permeable through the silicalite-1 membrane can shift the distribution of hydrocarbons towards a selective production of olefins. These findings support the results of the previous Chapter where the silicalite-1 membrane can be applied for favoring the production of olefins.

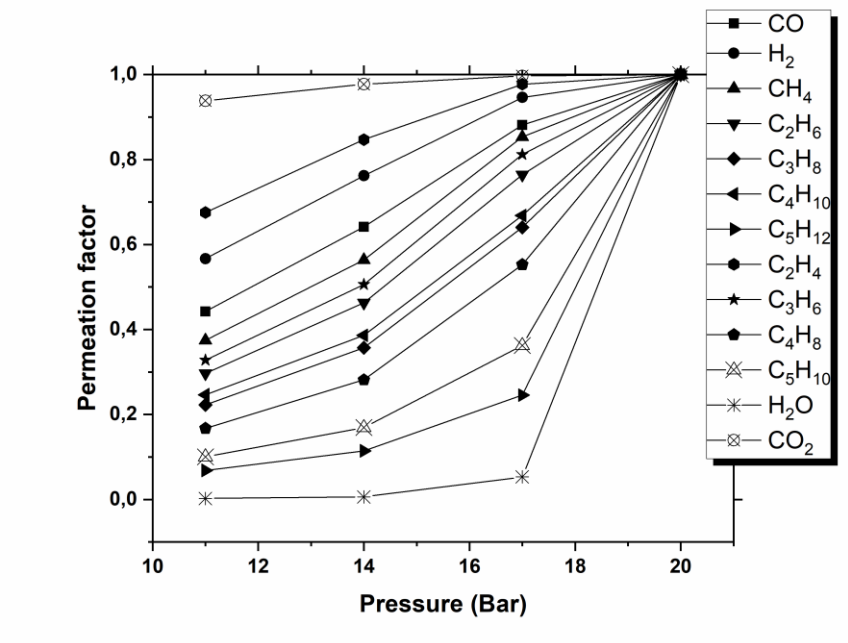


Figure IV.6: Variation of the permeation factor as a function of initial pressure.

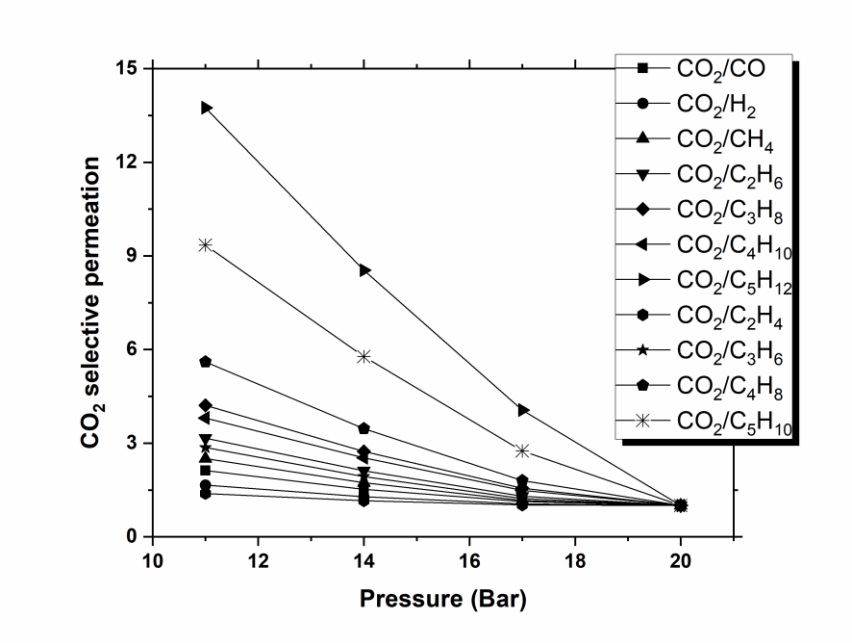


Figure IV.7: Variation of the CO_2 selective permeation as a function of initial pressure.

General Conclusions

The work reported in this thesis consisted of: a) critical literature review on the general concept of FT synthesis, the kinetic mechanisms and models and the applied industrial configuration of reactors (Chapter I), b) reactor modeling based on building a mathematical model with MATLAB software that can perform the anticipated variation in hydrocarbons selectivities (Chapter II) and c) theoretical investigation of ideal and non-ideal permeation effect on hydrocarbons distribution (Chapters III and IV). Data related to the mathematical models were taken from literature under similar applied operating conditions. A new concept of reactor design has been theoretically investigated and proposed for control of the composition of clean hydrocarbons towards a selective formation of paraffin or olefin produced by FT synthesis in membrane reactors. This study allowed concluding that the main results show that:

- The use of the membrane reactors configurations is able to remove water or carbon dioxide from the reaction zone and consequently affecting reactants concentrations. This offers the possibility to influence *in-situ* the molar composition of the H_2/CO ratio and consequently the composition of the product mixture. The H_2/CO ratio increased along the reactor in the case of carbon dioxide removal and decreased in the case of water removal, which resulted in a distinctive deviation of hydrocarbons distribution compared to the conventional reactor.
- The evolution of the H_2/CO molar ratio during the reaction caused by the removal of water or carbon dioxide through the membranes could orient the composition of the hydrocarbons and so, the O/P ratio can be controlled and therefore achieving the desired distribution.
- The advantage that should be highlighted here is the evacuation of water and CO_2 from the product mixture could be achieved completely using a large amount of

the sweep gas, which makes that the range of the obtained hydrocarbons clean and exempt from water or CO_2.

- However, these results refer to an ideal permeselectivity and cannot represent real-world separation. This is why an additional investigation was performed to observe the plausible application of the ideal approach without having a big effect on hydrocarbons distribution. This was done using the previous concept under similar reaction conditions but at this time we assume that the whole mixture of FT species can permeate through the membrane.
- The pressure effect was conducted on the permeation to get a more comprehensive deviation in hydrocarbons composition. So, pressure increase has resulted in a considerable increase in the permeate flux. Actually, the observed improvement in the reaction flux can mislead the obtained results. Thus, a permeation factor was calculated and used to define the permeation instead of the permeate flux in order to get a better analysis of membrane efficiency dependence on the pressure gradient.
- The silicalite-1 is more efficient for the separation of light components and the permeation enhances upon pressure raise. This behavior could be attributed to the increase in pressure gradient between the reaction side and the permeate side, which allows better diffusion of permeates.
- The higher diffusivity of small-sized molecules can make the observed difference in components permeation. These results can be pictured through the variation of the selective separation of carbon dioxide. Poor separation of carbon dioxide was achieved at high pressures.

- Operating under low levels of pressure is highly recommended to ensure a productive and easy control of hydrocarbons distribution through the elimination of carbon dioxide.

Finally, it can be concluded that the olefins to paraffins ratio obtained under the investigated conditions is approximately the same one obtained when assuming only carbon dioxide permeation. This leads to the conclusion that even we consider other components permeation, the final distribution of hydrocarbons still favorable for olefins.

References

[1] D. Karimipourfard, N. Nemati, S. Bahrani, M.R. Rahimpour, Simultaneous increase of H2 and gasoline production by optimizing thermally coupled methanol steam reforming with Fischer-Tropsch synthesis, Chem. Prod. Process Model. 13 (2018).

[2] M. Martinelli, M.K. Gnanamani, B. Demirel, S. LeViness, G. Jacobs, W.D. Shafer, An Overview of Fischer Tropsch Process: Catalysts, Reactors and XtL Processes, Appl. Catal. Gen. (2020) 117740.

[3] S.F. Rasmussen, Implementation of Fischer-Tropsch Jet Fuel Production in the Danish Energy System, (2019).

[4] D. Liuzzi, E. Fernandez, S. Perez, E. Ipiñazar, A. Arteche, J.L.G. Fierro, J.L. Viviente, D.A. Pacheco Tanaka, S. Rojas, Advances in membranes and membrane reactors for the Fischer-Tropsch synthesis process for biofuel production, Rev. Chem. Eng. Advance online publication, (2020).

[5] G.P. van der Laan, Kinetics, selectivity and scale up of the Fischer-Tropsch synthesis, PhD thesis, University of Groningen, Groningen, Netherlands, 1999.

[6] G. Bruni, C. Rizzello, A. Santucci, D. Alique, M. Incelli, S. Tosti, On the energy efficiency of hydrogen production processes via steam reforming using membrane reactors, Int. J. Hydrog. Energy. 44 (2019) 988–999.

[7] V.S. Sikarwar, M. Zhao, P.S. Fennell, N. Shah, E.J. Anthony, Progress in biofuel production from gasification, Prog. Energy Combust. Sci. 61 (2017) 189–248.

[8] F. Botes, J. Niemantsverdriet, J. Van De Loosdrecht, A comparison of cobalt and iron based slurry phase Fischer–Tropsch synthesis, Catal. Today. 215 (2013) 112–120.

[9] M.P. Rohde, D. Unruh, G. Schaub, Membrane application in Fischer–Tropsch synthesis reactors—Overview of concepts, Catal. Today. 106 (2005) 143–148.

[10] D.M. del Monte, A. Vizcaíno, J. Dufour, C. Martos, Effect of K, Co and Mo addition in Fe-based catalysts for aviation biofuels production by Fischer-Tropsch synthesis, Fuel Process. Technol. 194 (2019) 106102.

[11] M.K. Gnanamani, H.H. Hamdeh, W.D. Shafer, D.E. Sparks, B.H. Davis, Fischer–Tropsch Synthesis: Effect of Potassium on Activity and Selectivity for Oxide and Carbide Fe Catalysts, Catal. Lett. 143 (2013) 1123–1131.

[12] V.R.R. Pendyala, U.M. Graham, G. Jacobs, H.H. Hamdeh, B.H. Davis, Fischer–Tropsch Synthesis: Deactivation as a Function of Potassium Promoter Loading for Precipitated Iron Catalyst, Catal. Lett. 144 (2014) 1704–1716.

[13] A.Y. Khodakov, W. Chu, P. Fongarland, Advances in the development of novel cobalt Fischer− Tropsch catalysts for synthesis of long-chain hydrocarbons and clean fuels, Chem. Rev. 107 (2007) 1692–1744.

[14] S. Storsæter, Ø. Borg, E.A. Blekkan, B. Tøtdal, A. Holmen, Fischer–Tropsch synthesis over Re-promoted Co supported on Al2O3, SiO2 and TiO2: Effect of water, Catal. Today. 100 (2005) 343–347.

[15] A. Haghtalab, J. Shariati, A. Mosayebi, Experimental and kinetic modeling of Fischer–Tropsch synthesis over nano structure catalyst of Co–Ru/carbon nanotube, React. Kinet. Mech. Catal. 126 (2019) 1003–1026.

[16] N. Moazami, H. Mahmoudi, P. Panahifar, K. Rahbar, A. Tsolakis, M.L. Wyszynski, Mathematical Modeling and Performance Study of Fischer-tropsch Synthesis of Liquid Fuel over Cobalt-silica, Energy Procedia. 75 (2015) 62–71.

[17] H.C. Butterman, M.J. Castaldi, CO_2 as a carbon neutral fuel source via enhanced biomass gasification, Environ. Sci. Technol. 43 (2009) 9030–9037.

[18] S. Hafeez, S. Al-Salem, A. Constantinou, Membrane Reactors for Renewable Fuel Production and Their Environmental Benefits, in: Membr. Environ. Appl., Springer, 2020: pp. 383–411.

[19] D. Chakrabarti, M.K. Gnanamani, W.D. Shafer, M.C. Ribeiro, D.E. Sparks, V. Prasad, A. de Klerk, B.H. Davis, Fischer–Tropsch mechanism: 13C18O tracer studies on a ceria–silica supported cobalt catalyst and a doubly promoted iron catalyst, Ind. Eng. Chem. Res. 54 (2015) 6438–6453.

[20] J. Cheng, P. Hu, P. Ellis, S. French, G. Kelly, C.M. Lok, Chain growth mechanism in Fischer− Tropsch synthesis: A DFT study of C− C coupling over Ru, Fe, Rh, and Re surfaces, J. Phys. Chem. C. 112 (2008) 6082–6086.

[21] J. Gaube, H.-F. Klein, Further support for the two-mechanisms hypothesis of Fischer–Tropsch synthesis, Appl. Catal. Gen. 374 (2010) 120–125.

[22] S.-H. Kwack, M.-J. Park, J.W. Bae, K.-S. Ha, K.-W. Jun, Development of a kinetic model of the Fischer–Tropsch synthesis reaction with a cobalt-based catalyst, React. Kinet. Mech. Catal. 104 (2011) 483–502.

[23] H. Atashi, F. Siami, A.A. Mirzaei, M. Sarkari, Kinetic study of Fischer–Tropsch process on titania-supported cobalt–manganese catalyst, J. Ind. Eng. Chem. 16 (2010) 952–961.

[24] Tejas Bhatelia, Wenping Ma, Burton Davis, Gary Jacobs, Dragomir Bukur, Kinetics of the fischer-tropsch reaction over a ru promoted co/Al_2O_3 catalyst, Chem. Eng. Trans. 25 (2011) 707–712.

[25] M. Rahmati, M. Mehdi, M. Bargah-Soleimani, Rate equations for the fischer-tropsch reaction on a promoted iron catalyst, Can. J. Chem. Eng. 79 (2001) 800–804.

[26] G.P. Van der Laan, A.A. Beenackers, Intrinsic kinetics of the gas–solid Fischer–Tropsch and water gas shift reactions over a precipitated iron catalyst, Appl. Catal. Gen. 193 (2000) 39–53.

[27] E.S. Lox, G.F. Froment, Kinetics of the Fischer-Tropsch reaction on a precipitated promoted iron catalyst. 2. Kinetic modeling, Ind. Eng. Chem. Res. 32 (1993) 71–82.

[28] H. Schulz, Short history and present trends of Fischer–Tropsch synthesis, Appl. Catal. Gen. 186 (1999) 3–12.

[29] D. Bianchi, S. Borcar, F. Teule-Gay, C. Bennett, Evolution of surface and bulk compositions of an iron catalyst in relation to catalytic activity for the Fischer-Tropsch reaction, J. Catal. 82 (1983) 442–456.

[30] J.M. Gracia, F.F. Prinsloo, J. Niemantsverdriet, Mars-van Krevelen-like mechanism of CO hydrogenation on an iron carbide surface, Catal. Lett. 133 (2009) 257.

[31] R. Guettel, U. Kunz, T. Turek, Reactors for Fischer-Tropsch Synthesis, Chem. Eng. Technol. 31 (2008) 746–754.

[32] R.B. Anderson, Catalysts for the Fischer-Tropsch synthesis, Catalysis. 4 (1956) 29–255.

[33] M.E. Dry, Advances in fishcher-tropsch chemistry, Ind. Eng. Chem. Prod. Res. Dev. 15 (1976) 282–286.

[34] G.A. Huff Jr, C.N. Satterfield, Intrinsic kinetics of the Fischer-Tropsch synthesis on a reduced fused-magnetite catalyst, Ind. Eng. Chem. Process Des. Dev. 23 (1984) 696–705.

[35] M. Dry, T. Shingles, L. Boshoff, Rate of the Fischer-Tropsch reaction over iron catalysts, J. Catal. 25 (1972) 99–104.

[36] W.H. Zimmerman, D.B. Bukur, Reaction kinetics over iron catalysts used for the fischer-tropsch synthesis, Can. J. Chem. Eng. 68 (1990) 292–301.

[37] H.E. Atwood, C.O. Bennett, Kinetics of the Fischer-Tropsch reaction over iron, Ind. Eng. Chem. Process Des. Dev. 18 (1979) 163–170.

[38] W. Shen, J. Zhou, B. Zhang, Kinetics of Fischer-Tropsch synthesis over precipitated iron catalyst, J Nat Gas Chem. 4 (1994) 385–400.

[39] W.D. Deckwer, R. Kokuun, E. Sanders, S. Ledakowicz, Kinetic studies of Fischer-Tropsch synthesis on suspended iron/potassium catalyst-rate inhibition by carbon dioxide and water, Ind. Eng. Chem. Process Des. Dev. 25 (1986) 643–649.

[40] M. Dry, T. Shingles, L. Boshoff, G. Oosthuizen, Heats of chemisorption on promoted iron surfaces and the role of alkali in Fischer-Tropsch synthesis, J. Catal. 15 (1969) 190–199.

[41] S. Ledakowicz, H. Nettelhoff, R. Kokuun, W.D. Deckwer, Kinetics of the Fischer-Tropsch synthesis in the slurry phase on a potassium promoted iron catalyst, Ind. Eng. Chem. Process Des. Dev. 24 (1985) 1043–1049.

[42] G. Graaf, J. Winkelman, E. Stamhuis, A. Beenackers, Kinetics of the three phase methanol synthesis, in: Elsevier, 1988: pp. 2161–2168.

[43] R.A. Dictor, A.T. Bell, Fischer-Tropsch synthesis over reduced and unreduced iron oxide catalysts, J. Catal. 97 (1986) 121–136.

[44] L. Mazzone, F. Fernandes, Modeling of Fischer-Tropsch synthesis in a tubular reactor, Lat. Am. Appl. Res. 36 (2006) 141–148.

[45] F.A. Fernandes, Polymerization kinetics of Fischer-Tropsch reaction on iron based catalysts and product grade optimization, Chem. Eng. Technol. Ind. Chem. Equipment-Process Eng. 28 (2005) 930–938.

[46] D.C. Sorescu, Plane-wave density functional theory investigations of the adsorption and activation of CO on Fe_5C_2 surfaces, J. Phys. Chem. C. 113 (2009) 9256–9274.

[47] M.A. Petersen, P.J. Steynberg, J.-A. van den Berg, W.J. van Rensburg, PHYS 127-Structure-dependence of the mechanism of CO activation on Hagg iron carbide (chi-Fe_5C_2) surfaces, in: AMER CHEMICAL SOC 1155 16TH ST, NW, WASHINGTON, DC 20036 USA, 2009.

[48] P. Steynberg, J. Van den Berg, W.J. van Rensburg, Bulk and surface analysis of Hägg Fe carbide (Fe_5C_2): a density functional theory study, J. Phys. Condens. Matter. 20 (2008) 064238.

[49] M. Ojeda, R. Nabar, A.U. Nilekar, A. Ishikawa, M. Mavrikakis, E. Iglesia, CO activation pathways and the mechanism of Fischer–Tropsch synthesis, J. Catal. 272 (2010) 287–297.

[50] A. Haghtalab, M. Nabipoor, S. Farzad, Kinetic modeling of the Fischer–Tropsch synthesis in a slurry phase bubble column reactor using Langmuir–Freundlich isotherm, Fuel Process. Technol. 104 (2012) 73–79.

[51] T.J. Donnelly, I.C. Yates, C.N. Satterfield, Analysis and prediction of product distributions of the Fischer-Tropsch synthesis, Energy Fuels. 2 (1988) 734–739.

[52] A.N. Pour, H. Khodabandeh, M. Izadyar, M.R. Housaindokht, Detailed kinetics of Fischer–Tropsch synthesis on a precipitated iron catalyst, React. Kinet. Mech. Catal. 111 (2014) 29–44.

[53] A.T. Bell, Catalytic synthesis of hydrocarbons over group VIII metals. A discussion of the reaction mechanism, Catal. Rev. Eng. 23 (1981) 203–232.

[54] B. Wojciechowski, The kinetics of the Fischer-Tropsch synthesis, Catal. Rev. Sci. Eng. 30 (1988) 629–702.

[55] B. Sarup, B. Wojciechowski, Studies of the fischer-tropsch synthesis on a colbalt catalyst. III. mechanistic formulation of the kinetics of selectivity for higher hydrocarbon formation, Can. J. Chem. Eng. 67 (1989) 620–627.

[56] C. Boyer, J. Gazarian, V. Lecocq, S. Maury, A. Forret, J.M. Schweitzer, V. Souchon, Development of the Fischer-Tropsch Process: From the Reaction Concept to the Process Book, Oil Gas Sci. Technol. – Rev. D'IFP Energ. Nouv. 71 (2016) 44.

[57] K.T. Knutsen, Modelling and optimization of a Gas-to-Liquid plant, (2013).

[58] I.C. Yates, C.N. Satterfield, Intrinsic kinetics of the Fischer-Tropsch synthesis on a cobalt catalyst, Energy Fuels. 5 (1991) 168–173.

[59] H.P. Withers Jr, K.F. Eliezer, J.W. Mitchell, Slurry-phase Fischer-Tropsch synthesis and kinetic studies over supported cobalt carbonyl derived catalysts, Ind. Eng. Chem. Res. 29 (1990) 1807–1814.

[60] N.P. Ali, F. Riyahi, M.R. Housaindokht, M. Irani, S.M.K. Shahri, B. Hatami, Hydrocarbon production rates in Fischer-Tropsch synthesis over a Fe/Cu/La/Si catalyst, J. Energy Chem. 22 (2013) 119–129.

[61] B.-T. Teng, J. Chang, C.-H. Zhang, D.-B. Cao, J. Yang, Y. Liu, X.-H. Guo, H.-W. Xiang, Y.-W. Li, A comprehensive kinetics model of Fischer–Tropsch synthesis over an industrial Fe–Mn catalyst, Appl. Catal. Gen. 301 (2006) 39–50.

[62] B. Teng, J. Chang, H. Wan, J. Lu, S. Zheng, Y. Liu, Y. Liu, X. Guo, A Corrected Comprehensive Kinetic Model of Fischer–Tropsch Synthesis, Chin. J. Catal. 28 (2007) 687–695.

[63] X. Guo, Y. Liu, J. Chang, L. Bai, Y. Xu, H. Xiang, Y. Li, Isothermal Kinetics Modelling of the Fischer-Tropsch Synthesis over the Spray-Dried Fe-Cu-K Catalyst, J. Nat. Gas Chem. 15 (2006) 105–114.

[64] C.G. Visconti, E. Tronconi, L. Lietti, R. Zennaro, P. Forzatti, Development of a complete kinetic model for the Fischer–Tropsch synthesis over Co/Al_2O_3 catalysts, Chem. Eng. Sci. 62 (2007) 5338–5343.

[65] R. Jalilzadeh, M. Moqadam, A Comprehensive Kinetic Model of Fischer-Tropsch Synthesis over Supported Cobalt Catalyst, Preprints. (2017).

[66] A. Mosayebi, R. Abedini, Detailed kinetic study of Fischer–Tropsch synthesis for gasoline production over CoNi/HZSM-5 nano-structure catalyst, Int. J. Hydrog. Energy. 42 (2017) 27013–27023.

[67] A. Alipour-Dehkordi, M.H. Khademi, Use of a micro-porous membrane multi-tubular fixed-bed reactor for tri-reforming of methane to syngas: CO_2, H_2O or O_2 side-feeding, Int. J. Hydrog. Energy. 44 (2019) 32066–32079.

[68] S. Sie, R. Krishna, Fundamentals and selection of advanced Fischer–Tropsch reactors, Appl. Catal. Gen. 186 (1999) 55–70.

[69] A. Bellal, L. Chibane, A new concept for control and orientation of the distribution of clean hydrocarbons produced by Fischer–Tropsch synthesis over an industrial iron catalyst, React. Kinet. Mech. Catal. 129 (2020) 725–742.

[70] B.H. Davis, Fischer–Tropsch synthesis: overview of reactor development and future potentialities, Top. Catal. 32 (2005) 143–168.

[71] S. Sie, M. Senden, H. Van Wechem, Conversion of natural gas to transportation fuels via the shell middle distillate synthesis process (SMDS), Catal. Today. 8 (1991) 371–394.

[72] M.E. Dry, The Fischer–Tropsch process: 1950–2000, Catal. Today. 71 (2002) 227–241.

[73] H. Benson, J. Field, D. Bienstock, H. Storch, Oil Circulation Process for Fischer-Tropsch Synthesis, Ind. Eng. Chem. 46 (1954) 2278–2285.

[74] P. Keith, Gasoline from natural gas, Oil Gas J. (1946).

[75] B. Jager, Developments in Fischer-Tropsch technology, Stud. Surf. Sci. Catal. 119 (1998) 25–34.

[76] H. Kölbel, M. Ralek, The Fischer-Tropsch synthesis in the liquid phase, Catal. Rev. Sci. Eng. 21 (1980) 225–274.

[77] A. Forret, J.M. Schweitzer, T. Gauthier, R. Krishna, D. Schweich, Scale Up of Slurry Bubble Reactors, Oil Gas Sci. Technol. - Rev. IFP. 61 (2006) 443–458.

[78] B. Everett, B. Eisenberg, R. Bauman, Advanced gas conversion technology: A new option for natural gas development, in: 1995.

[79] J. De Swart, R. Van Vliet, R. Krishna, Size, structure and dynamics of “large” bubbles in a two-dimensional slurry bubble column, Chem. Eng. Sci. 51 (1996) 4619–4629.

[80] D.J. Vermeer, R. Krishna, Hydrodynamics and mass transfer in bubble columns in operating in the churn-turbulent regime, Ind. Eng. Chem. Process Des. Dev. 20 (1981) 475–482.

[81] D. Alihellal, L. Chibane, Simulation study of the effect of water removal from Fischer–Tropsch products on the process performance using a hydrophilic membrane reactor, React. Kinet. Mech. Catal. 117 (2016) 605–621.

[82] M.R. Rahimpour, A. Mirvakili, K. Paymooni, B. Moghtaderi, A comparative study between a fluidized-bed and a fixed-bed water perm-selective membrane reactor with in situ H_2O removal for Fischer–Tropsch synthesis of GTL technology, J. Nat. Gas Sci. Eng. 3 (2011) 484–495.

[83] R.L. Espinoza, E. du Toit, J. Santamaria, M. Menendez, J. Coronas, S. Irusta, Use of membranes in fischer-tropsch reactors, in: Stud. Surf. Sci. Catal., Elsevier, 2000: pp. 389–394.

[84] F. Gallucci, E. Fernandez, P. Corengia, M. van Sint Annaland, Recent advances on membranes and membrane reactors for hydrogen production, Chem. Eng. Sci. 92 (2013) 40–66.

[85] L. Meng, T. Tsuru, Hydrogen production from energy carriers by silica-based catalytic membrane reactors, Catal. Today. 268 (2016) 3–11.

[86] M.P. Rohde, In-situ H_2O removal via hydrophilic membranes during Fischer-Tropsch and other fuel-related synthesis reactions, KIT Scientific Publishing, Karlsruhe, 2011.

[87] W. Zhu, P. Hrabanek, L. Gora, F. Kapteijn, J.A. Moulijn, Role of adsorption in the permeation of CH_4 and CO_2 through a silicalite-1 membrane, Ind. Eng. Chem. Res. 45 (2006) 767–776.

[88] C. Algieri, P. Bernardo, G. Golemme, G. Barbieri, E. Drioli, Permeation properties of a thin silicalite-1 (MFI) membrane, J. Membr. Sci. 222 (2003) 181–190.

[89] S. Guo, C. Yu, X. Gu, W. Jin, J. Zhong, C. Chen, Simulation of adsorption, diffusion, and permeability of water and ethanol in NaA zeolite membranes, J. Membr. Sci. 376 (2011) 40–49.

[90] D. Liu, Y. Zhang, J. Jiang, X. Wang, C. Zhang, X. Gu, High-performance NaA zeolite membranes supported on four-channel ceramic hollow fibers for ethanol dehydration, RSC Adv. 5 (2015) 95866–95871.

[91] M. Pera-Titus, C. Fité, V. Sebastián, E. Lorente, J. Llorens, F. Cunill, Modeling pervaporation of ethanol/water mixtures within 'real'zeolite NaA membranes, Ind. Eng. Chem. Res. 47 (2008) 3213–3224.

[92] W.J. Bakker, L.J. Van Den Broeke, F. Kapteijn, J.A. Moulijn, Temperature dependence of one-component permeation through a silicalite-1 membrane, AIChE J. 43 (1997) 2203–2214.

[93] Y.-N. Wang, W.-P. Ma, Y.-J. Lu, J. Yang, Y.-Y. Xu, H.-W. Xiang, Y.-W. Li, Y.-L. Zhao, B.-J. Zhang, Kinetics modelling of Fischer–Tropsch synthesis over an industrial Fe–Cu–K catalyst, Fuel. 82 (2003) 195–213.

[94] Z. Rui, H. Ji, Y. Lin, Modeling and analysis of ceramic–carbonate dual-phase membrane reactor for carbon dioxide reforming with methane, Int. J. Hydrog. Energy. 36 (2011) 8292–8300.

[95] M.R. Rahimpour, H. Elekaei, Optimization of a novel combination of fixed and fluidized-bed hydrogen-permselective membrane reactors for Fischer–Tropsch synthesis in GTL technology, Chem. Eng. J. 152 (2009) 543–555.

[96] L.A. Díaz-Trujillo, G. Toledo-Chávez, G. Jiménez-García, H. Hernández-Escoto, R. Maya-Yescas, Modelling Laboratory Fischer-Tropsch Synthesis Using Cobalt Catalysts, Int. J. Chem. React. Eng. 16 (2018).

[97] M. Zhuo, K.F. Tan, A. Borgna, M. Saeys, Density Functional Theory Study of the CO Insertion Mechanism for Fischer−Tropsch Synthesis over Co Catalysts, J. Phys. Chem. C. 113 (2009) 8357–8365.

[98] B.H. Davis, Fischer–Tropsch synthesis: current mechanism and futuristic needs, Fuel Process. Technol. 71 (2001) 157–166.

[99] W. Zhu, L. Gora, A. Van den Berg, F. Kapteijn, J. Jansen, J. Moulijn, Water vapour separation from permanent gases by a zeolite-4A membrane, J. Membr. Sci. 253 (2005) 57–66.

[100] J.C. Poshusta, R.D. Noble, J.L. Falconer, Characterization of SAPO-34 membranes by water adsorption, J. Membr. Sci. 186 (2001) 25–40.

[101] M.C. Lovallo, A. Gouzinis, M. Tsapatsis, Synthesis and characterization of oriented MFI membranes prepared by secondary growth, AIChE J. 44 (1998) 1903–1913.

[102] A.J. Burggraaf, Z.A.E.P. Vroon, K. Keizer, H. Verweij, Permeation of single gases in thin zeolite MFI membranes, J. Membr. Sci. 144 (1998) 77–86.

[103] J.C. Poshusta, R.D. Noble, J.L. Falconer, Temperature and pressure effects on CO2 and CH4 permeation through MFI zeolite membranes, J. Membr. Sci. 160 (1999) 115–125.

[104] S.K. Wirawan, D. Creaser, J. Lindmark, J. Hedlund, I.M. Bendiyasa, W.B. Sediawan, H_2/CO_2 permeation through a silicalite-1 composite membrane, J. Membr. Sci. 375 (2011) 313–322.

[105] J. van den Bergh, A. Tihaya, F. Kapteijn, High temperature permeation and separation characteristics of an all-silica DDR zeolite membrane, Microporous Mesoporous Mater. 132 (2010) 137–147.

[106] J. van den Bergh, W. Zhu, J.C. Groen, F. Kapteijn, J.A. Moulijn, K. Yajima, K. Nakayama, T. Tomita, S. Yoshida, Natural gas purification with a DDR zeolite membrane; permeation modelling with maxwell-stefan equations, in: Stud. Surf. Sci. Catal., Elsevier, 2007: pp. 1021–1027.

[107] R. Nagumo, H. Takaba, S. Nakao, Prediction of Ideal Permeability of Hydrocarbons through an MFI-Type Zeolite Membrane by a Combined Method Using Molecular Simulation Techniques and Permeation Theory, J. Phys. Chem. B. 107 (2003) 14422–14428.

[108] J. Xiao, J. Wei, Diffusion mechanism of hydrocarbons in zeolites—I. Theory, Chem. Eng. Sci. 47 (1992) 1123–1141.

[109] A. Farzaneh, M. Zhou, E. Potapova, Z. Bacsik, L. Ohlin, A. Holmgren, J. Hedlund, M. Grahn, Adsorption of Water and Butanol in Silicalite-1 Film Studied with *in Situ* Attenuated Total Reflectance–Fourier Transform Infrared Spectroscopy, Langmuir. 31 (2015) 4887–4894.

[110] O. Talu, M.S. Sun, D.B. Shah, Diffusivities ofn-alkanes in silicalite by steady-state single-crystal membrane technique, AIChE J. 44 (1998) 681–694.

[111] C. Bläker, C. Pasel, M. Luckas, F. Dreisbach, D. Bathen, Investigation of load-dependent heat of adsorption of alkanes and alkenes on zeolites and activated carbon, Microporous Mesoporous Mater. 241 (2017) 1–10.

[112] I.C. Arik, J.F. Denayer, G.V. Baron, High-temperature adsorption of n-alkanes on ZSM-5 zeolites: influence of the Si/Al ratio and the synthesis method on the low-coverage adsorption properties, Microporous Mesoporous Mater. 60 (2003) 111–124.

[113] F. Kapteijn, W.J.W. Bakker, G. Zheng, J. Poppe, J.A. Moulijn, Permeation and separation of light hydrocarbons through a silicalite-1 membrane, Chem. Eng. J. Biochem. Eng. J. 57 (1995) 145–153.

[114] S. Jakobtorweihen, N. Hansen, F.J. Keil, Molecular simulation of alkene adsorption in zeolites, Mol. Phys. 103 (2005) 471–489.

[115] T. Leppäjärvi, I. Malinen, D. Korelskiy, J. Hedlund, J. Tanskanen, Maxwell–Stefan Modeling of Ethanol and Water Unary Pervaporation through a High-Silica MFI Zeolite Membrane, Ind. Eng. Chem. Res. 53 (2014) 323–332.

[116] A.O. Koriabkina, Diffusion of alkanes in MFI-type zeolites., (2003).

[117] C. Wang, B. Li, Y. Wang, Z. Xie, Insight into the topology effect on the diffusion of ethene and propene in zeolites: A molecular dynamics simulation study, J. Energy Chem. 22 (2013) 914–918.

[118] F. Jousse, L. Leherte, D.P. Vercauteren, Energetics and diffusion of butene isomers in channel zeolites from molecular dynamics simulations, J. Mol. Catal. Chem. 119 (1997) 165–176.

[119] N. Dvoyashkina, D. Freude, A.G. Stepanov, W. Böhlmann, R. Krishna, J. Kärger, J. Haase, Alkane/alkene mixture diffusion in silicalite-1 studied by MAS PFG NMR, Microporous Mesoporous Mater. 257 (2018) 128–134.

[120] J.Z. Yang, Q.L. Liu, H.T. Wang, Analyzing adsorption and diffusion behaviors of ethanol/water through silicalite membranes by molecular simulation, J. Membr. Sci. 291 (2007) 1–9.

[121] A. Bellal, L. Chibane, On the Effect of the Inlet Hydrogen Amount on Hydrocarbons Distribution Produced via Fischer-Tropsch Synthesis, in: Adv. Renew. Hydrog. Sustain. Energy Carr., Springer, n.d.: pp. 451–458.

[122] L. Yu, S. Fouladvand, M. Grahn, J. Hedlund, Ultra-thin MFI membranes with different Si/Al ratios for CO2/CH4 separation, Microporous Mesoporous Mater. 284 (2019) 258–264.

[123] L. Sandström, E. Sjöberg, J. Hedlund, Very high flux MFI membrane for CO_2 separation, J. Membr. Sci. 380 (2011) 232–240.

[124] S. Li, SAPO-34 membranes for CO_2/CH_4 separation, J. Membr. Sci. 241 (2004) 121–135.

[125] W.J. Bakker, F. Kapteijn, J. Poppe, J.A. Moulijn, Permeation characteristics of a metal-supported silicalite-1 zeolite membrane, J. Membr. Sci. 117 (1996) 57–78.